URBAN HEAT ISLANDS IN SANTA CLARA, CALIFORNIA: A HUMAN-ENVIRONMENT INTERACTION STUDY

By

Ana Lucrecia Rivera Rivera

A DISSERTATION

Submitted to
Michigan State University
in partial fulfillment of the requirements
for the degree of

Geography – Doctor of Philosophy

2023

ABSTRACT

Population growth increases urbanization, impacting surface albedos and altering surface energy balances, including the reduction of urban evaporative cooling, thus forming surface urban heat islands (SUHIs). Neighborhoods with higher vegetative densities, therefore, tend to have lower temperatures than those with sparse vegetation. In the United States, racially and ethnically segregated neighborhoods have limited green infrastructure, exposing populations to higher ambient temperatures. The increase in the number and quality of urban forests has become popular to reduce intra-urban tree-canopy inequality and mitigate urban heat. The effectiveness of trees in heat mitigation is highly site-dependent. Different mitigation interventions thus must be evaluated with the use of numerical microscale models, which could facilitate decision-making.

This study determined seasonal daytime and nighttime land surface temperature (LST) trends and distributions in Santa Clara County (SCC), California. It then related these results to vegetation (NDVI) and evapotranspiration (ET) values, as well as to census tract-level median household income, percentage of Hispanic/Latino populations, and the built environment per the Local Climate Zone (LCZ) classification framework. The level of segregation and socioeconomic status (SES) between Hispanics and non-Hispanic Whites and among Hispanic/Latinos was further explored and related to temperature exposures and health outcomes. In response to the findings, the ENVI-Met software was used to evaluate urban heat mitigation measures. The combination of these assessments comprised a comprehensive human-environment approach for health exposure evaluation emphasizing differences among Hispanics by the origin of birth by which to define environmental injustice.

Results show upward trends in daytime summer (0.10°C per year) and winter (0.11°C per year) mean LST and weak nighttime trends (0.03 and 0.04°C per year, respectively). Winter NDVI and LST values exhibit positive correlations, but negative correlations are found for summer NDVI and LST values, which are stronger during daytime hours, indicating that the cooling effects of vegetation occur primarily during the daytime. Maximum LSTs occur in low-income neighborhoods characterized by scarce vegetation with a high percentage of Hispanic/Latino populations, particularly of Mexican origin. Mexicans live in highly segregated neighborhoods with low and very low SES and report low health insurance coverage rates. Evaluation of mitigation strategies suggests a non-linear relationship between tree coverage percentage and air temperature changes, with a threshold cooling effect associated with increasing tree coverage.

TABLE OF CONTENTS

LIST OF ABBREVIATIONS

A/C: Air Conditioning

AUHI: Air Urban Heat Islands

BLUHI: Boundary-Layer UHI

CLUHI: Canopy-Layer UHI

CDC: Center for Disease Control and Prevention

CSI: Composite Socioeconomic Index

ECOSTRESS: ECOsystem Spaceborne Thermal Radiometer Experiment

ET: Evapotranspiration

HVIs Heat Vulnerability Indices

HW: Heat waves

ISS: International Space Station

LAD: Leaf Area Density

LAI: Leaf Area Index

LST: Land Surface Temperature

MRFs: Measure Review Frameworks

NWS: National Weather Service

PSD: Public Space Design

SCC: Santa Clara County

SES: Socioeconomic Status

SUHI: Surface Urban Heat Island

T_a: 2-m Height Air Temperature

T_s: Radiative Surface Temperature

TI: Thermal Inertia

UHI: Urban Heat Island

UHII: Urban Heat Island Intensity

WMO: World Meteorological Organization

CHAPTER 1. INTRODUCTION

Heat waves (HWs) are extreme weather events during which unusually high temperatures last several consecutive days (Center for Disease Control and Prevention-CDC, 2013). HWs can reduce human thermal comfort, exacerbate symptoms for individuals with preexisting diseases and medical conditions, and cause sudden and premature death (Basu & Samet, 2002), even in high-income countries with high-quality healthcare services (Martínez-Austria et al., 2016). The risk of premature mortality during HWs is highest among people aged 65 years or older (Hajat & Kosatky, 2010), those who live in urban areas, vulnerable communities (e.g., low-income populations), and individuals who may experience high heat exposure due to their occupation. During the August 2003 European HW, 70,000 excess deaths were attributed to extreme heat exposure (Robine et al., 2008). Most of those deaths occurred in the elderly who lived alone (Vandentorren et al., 2006). This HW occurred after an unusually warm June, with temperatures 4-5°C above monthly means averages. In the United States, deaths attributable to natural heat exposure, although generally considered preventable, represent a continuing public health concern. An average of 702 heat-related deaths occurred annually in the US from 2004-2018 (Vaidyanathan et al., 2020).

The direct effects of high ambient heat on human physiology and susceptibility are mediated by indirect factors (e.g., socioeconomic and the built environment). The impact of HWs, for example, may be exacerbated for residents who live in high-vulnerability areas (e.g., low-income urban areas with few amenities, high-population density, and poorly ventilated housing; Grineski et al., 2015; Shonkoff et al., 2011), with no in-home air-conditioning (A/C) units, or where energy is unaffordable (Hajat & Kosatky, 2010). In the United States, segregated racial and ethnic minority populations of low socioeconomic status will likely experience higher heat exposure (Mitchell & Chakraborty, 2018), partly because of the paucity of vegetated areas. In Phoenix, Arizona, for example, Mexican-Americans living in unvegetated dense downtown neighborhoods have been shown to have higher numbers of heat distress calls into the 911 system. In contrast, Anglo-American populations living in low-density suburban neighborhoods with vegetated areas experience lower vulnerability to extreme heat (Uejio et al., 2011).

Urban areas are less vegetated than their rural and suburban surroundings; they store heat during the day and slowly release it at night, resulting in higher ambient temperatures that contribute to a phenomenon known as Urban Heat Island (UHI; Rosenfeld et al., 1995). In UHIs, city centers are 1-2°C warmer than their surroundings, and during calm, clear nights, this difference

can be up to 12°C (Voogt, 2007). The urban-rural temperature difference defines the UHI intensity (UHII; Zhao et al., 2018) of Air Urban Heat Islands (AUHIs), as exhibited in measurements of 2-m height air temperature (T_a), and Surface Urban Heat Islands (SUHIs), based on radiative surface temperature (T_s) measurements (Li et al., 2017).

Spatial variability in vulnerability within UHIs results from the non-uniform distributions of built environmental features and social factors (e.g., elders living alone and/or urban crime rates; Huang et al., 2011). Some factors that may explain variations in vulnerability include anthropogenic heat from residential, commercial, and industrial activities (Ching et al., 2018). Neighborhood instability also influences heat mortality through the disinvestment of protective amenities (e.g., fewer parks) and reduced ability to maintain social networks, thus increasing heat-related mortality rates (Semenza et al., 1996; Smoyer, 1998). In Philadelphia (1999) and Phoenix (2005), high vacancy rates resulted in weak social networks and higher social isolation, which led to an increase in heat distress calls and higher heat mortality probability (Uejio et al., 2011).

Urban Climate

The UHI term was introduced to English-language literature in 1947. Balchin & Pye (1947) found that warmer temperatures in the center of Bath resembled a "heat island within a built-up area." The isotherm maps showed concentric rings around the central city area, where temperatures were highest in the city center in proportion to building density and decreased with distance to the peripheral rural lands (Sundborg, 1950). UHIs are complex phenomena (Peterson, 1969) as each one displays different characteristics and is controlled by unique energy exchange processes (Arnfield, 2003). UHIs result from particular aspects of urban morphology (form and function) and anthropogenic heat emissions (Priyadarsini et al., 2008) and are influenced by topography, solar radiation, wind speed, and cloud cover (Sundborg, 1950; Voogt, 2007; Giovannini et al., 2013). Their temperatures also vary horizontally and vertically (Duckworth & Sandberg, 1954). UHIs also exhibit seasonal, daytime, and nighttime variations (Rivera et al., 2017; Deilami et al., 2018;). The results from UHI analyses, therefore, vary by scale, from regional to city to building to pedestrian levels (Mirzaei, 2015). Studies of UHIs are generally classified into three categories (Voogt, 2007; Deilami et al., 2018):

1. Boundary-Layer UHI (BLUHI): The planetary boundary layer lies over the canopy layer (rooftop) and can extend upwards to 1 km or more during the day and hundreds of meters or less at night (Deilami et al., 2018). The BLUHI is generally used for mesoscale studies.

Temperature data are acquired with direct measurements obtained by sensors mounted on aircraft, radiosondes, and tall towers or indirectly via Sonic Detection Ranging (Sodar), Light Detection and Ranging (LiDAR), and Radio Acoustic Sounding System (RASS; Oke et al., 2017);

2. Canopy-Layer UHI (CLUHI): Closest to the city surface, the canopy layer extends above the mean building height (rooftop). The urban morphology, land uses, and available vegetation regulate the canopy layer temperature (T_a) distribution (Mills et al., 2010). The CLUHI intensity is, therefore, weak or negative during the day in areas with extensive shading created by high-rise buildings or irrigation. The CLUHI is best suited for microscale studies. Temperature measurements are made with the use of fixed or mobile sensors at 2-m height (Oke et al., 2017). Measurements of CUHIs are, however, limited by network densities, so some studies use satellite-derived estimates to measure UHIs distributions.
3. Surface UHI (SUHI): SUHIs are measured with thermal infrared (TIR) sensors onboard satellites (e.g., Landsat, ASTER, and MODIS), which measure the 'skin' temperature (T_s) or land surface temperature (LST) of urban surfaces. LST values depend on satellite view angle, solar elevation angle, and surface radiative properties, e.g., emissivity ε (Voogt & Oke, 2003).

The spatial and temporal variability of UHIs interacts with the spatial variability of vulnerable populations, as they result from non-uniform distributions of social factors (e.g., elders living alone and/or urban crime rates; Huang et al., 2011), demographics (e.g., population size and age-structure; Tran et al., 2006), cultural and behavioral factors, environmental factors (e.g., urban morphology and land use; Johnson & Wilson, 2009) which further complicates the identification of at-heat risk areas.

Heat Vulnerability

Population vulnerability to UHIs results from complex human-environment interactions. It can result from marginalization, discrimination, psycho-social or economic breakdowns, and/or risky behaviors pertaining to the environment (Rosenberg, 2017). Heat vulnerability indices (HVIs) have been constructed with the use of census data to identify populations at risk during HWs and the placement of cooling centers (Bradford et al., 2015). Socio-demographic characteristics have often proved to be a heat vulnerability predictor, as they position an individual or group within a power hierarchy with the use of objective indicators, such as education, occupation, income, and wealth (Diemer et al., 2013). Socioeconomic status also influences the

ability of populations to protect themselves during extreme heat events because of the potential for reduced access to amenities, such as air conditioning or parks, and access to health care resources (Browning et al., 2006).

Discrepancies in socioeconomic variables that determine heat-related morbidity and premature mortality are due to differences in study areas, study designs, and/or the local and dynamic processes that change the spatial location(s) of vulnerable populations over short periods (Gronlund, 2014). Demographic and economic variables may also complement remotely sensed LST values to identify vulnerable populations (Johnson et al., 2009; Uejio et al., 2011; Bradford et al., 2015). For example, urban slum forms (e.g., overcrowded housing, impervious land cover, poor housing conditions) are associated with high LST values that make these areas more vulnerable to heat during heat waves (Tomlinson et al., 2011; Rosenthal et al., 2014). In the United States, the built environment may vary by race, ethnicity, and income, reflecting historic racial residential segregation; (e.g., Whites reside in detached dwelling neighborhoods surrounded by vegetation, while African Americans reside in contained single- and multi-family housing; Smoyer, 1998).

The increase in the number and quality of urban forests has become popular to reduce intra-urban tree-canopy inequality and mitigate the UHI. There is, however, variability in the effectiveness of trees in reducing the UHI, which results from the combination of design factors (e.g., type of vegetation, area size, fragmentation, arrangement of trees, dominant winds) and local environmental conditions.

Urban Heat Mitigation

Heat mitigation strategies involve the modification of the built-up environment (e.g., increased vegetation), replacement of low albedo surfaces with highly reflective materials, placement of water elements (e.g., roof pond, roof spray cooling, moving water), shades, and increasing ventilation (Memon et al., 2008). City governments implement heat mitigation strategies that increase the number and quality of urban forests, like the Million Trees NYC initiative (Webb, 2017), combined with albedo-based changes like the NYC CoolRoofs program (City of New York, 2023). The use of green infrastructure at both the pedestrian and roof levels significantly reduced air temperature more than highly reflective surfaces (Rosenzweig et al., 2006). The percentage of tree coverage and height of the vegetation, however, influence urban temperatures (Li et al., 2018; Yu et al., 2018). Larger and well-connected green areas, for example, relate to lower LSTs (Kim et al., 2016; Park et al., 2017) and consequently decrease human heat

exposure (Uejio et al., 2011). The question of maximizing the benefits of urban green areas through design (e.g., size, orientation, and spacing), however, still needs to be answered for most cities.

Trees can absorb a high amount of heat and, if well-watered, moderate their leaf temperature via transpiration, thus cooling the surroundings (Oke et al., 1989). Trees provide shade, attenuating radiant energy flows through absorption and reflection, further cooling the surface and near-surface temperature (Declet-Barreto et al., 2013). With moderate winds, the cooling effects can extend beyond the vegetated areas into adjacent, non-vegetated surfaces (Declet-Barerto et al., 2012). The extension of the cooling effects will depend on the arrangement of trees and wind direction, e.g., trees must be placed along dominant wind paths to maximize their cooling potential (Tan et al., 2016). Wind velocity, however, decreases with an increasing green coverage ratio (0.9 m/s), which could significantly affect outdoor thermal comfort (Yuan et al., 2017).

The type of vegetation (species) will also determine the cooling potential. Some plants require the regular opening of leaf pores (stomata) and transpire significant volumes of water, which could provide higher cooling effects than trees with low transpiration (Gunawardena et al., 2017). Evapotranspiration rates, however, vary among species and within individuals of the same species, depending on the environmental conditions (Ballinas & Barradas, 2015).

Tree density, crown diameter (horizontal canopy area), vertical canopy area, leaf area index (LAI), and leaf area density (LAD) are additional characteristics that determine the cooling potential of urban forests (Ballinas & Barradas, 2015). A tree with LAD of 1.0 m2/m3 and LAI of 5 can reduce T_a and T_s values by 1.3°C and 14.7°C, respectively. A tree with a LAD of 1.8 m2/m3 and an LAI of 3 can intercept 84% of free horizontal solar direct radiation, thus reducing temperatures by providing shade (Tan et al., 2016). Microclimate simulations show that temperature values in intensively vegetated areas do not change with the addition of trees, which suggests a threshold in the maximum number of trees to ensure cooling capacity (Makido et al., 2019). In those scenarios, designers should consider additional strategies to improve thermal comfort (Taleghani et al., 2016).

The application of bioclimatic architecture principles can create a climate-conscious design of outdoor spaces with the use of natural components to reduce and enhance their climatic and social benefits (Gaitani et al., 2007). Santos Nouri et al. (2018) constructed four Measure Review Frameworks (MRFs) to describe the application of different types of Public Space Design (PSD)

measures as a bottom-up adaptation response to existing and future climate systems at a local scale: 1) Green – urban vegetation: 2) Sun – shelter canopies; 3) Surface – materials; and 4) Blue – water or misting systems. A public space is, therefore, one that alleviates the impacts of increasing temperatures and enhances its use; these benefits, however, further require the establishment of quantitative and qualitative criteria for its evaluation (Santos Nouri & Costa, 2017).

Gap in Literature

Urban Climate. Since Luke Howard published "The Climate of London" in 1833, significant advances have been made in urban climate studies. The study of urban exposure, however, involves multi-temporal and multi-spatial human and environmental processes. Meso-scale analyses can expand over larger regions but do not have enough accuracy at a microscale level to provide essential information to decision-makers (Mirzaei, 2015). LST distributions do not correlate to 2-m air temperature measurements (Rivera et al., 2017) and only provide limited spatial coverage. Whereas T_a can be measured hourly, T_s can be measured daily (e.g., MODIS) at a low-spatial resolution or on a 16-day basis (e.g., Landsat) at a higher spatial resolution.

Heat Vulnerability. Besides inconsistencies in socioeconomic variables, HVIs use a limited number of satellite images to calculate LSTs. Urban heat-related morbidity and premature mortality studies, additionally, show contradictory findings due to the nature of the study area, study designs, and variables involved. Some variables, for example, exhibit strong multicollinearity, e.g., no high school diploma correlates with low mean household income, while age and occupation are associated with homeownership (Hattis et al., 2012). Age, race, and socioeconomic status alone do not predict heat risk consistently (Xu et al., 2013). Some indices give variables an equal weight, even when not all variables are equally important, and their significance will vary by study (Chow et al., 2012).

Urban Heat Adaptation. The identification of areas at high risk of heat stress facilitates the targeting of public health programs and other mitigation strategies, such as the increase of urban vegetation (Weber et al., 2015). In the US, local governments establish cooling centers, typically with air-conditioning (A/C), providing a cool environment for vulnerable individuals, thereby preventing heat-related illnesses (Widerynski et al., 2017). The use of A/C, however, increases energy demand and could enhance street air temperatures, further exacerbating the potential of adverse health outcomes (De Munck et al., 2013). Urban adaptation for current and future HWs

requires critical thinking of optimal design and suitable location of public spaces that provide temporary shelter from heat for local populations.

These studies demonstrate the variability of the intensity and spatial distribution of UHIs as they result from urban morphology (land use, land cover, building form, and materials) and anthropogenic heat emissions (Priyadarsini et al., 2008) and are influenced by topography, solar radiation, wind speed, and cloud cover, and soil moisture. Given the complexity of physical and socio-demographic factors, a multidisciplinary perspective is necessary to understand the physical processes of UHIs and the population groups most vulnerable to heat-related morbidity and premature death due to urban heat exposures. This dissertation, therefore, is conducted within the discipline of Geography, which is multifaceted, with four prominent research areas: Physical Geography, Urban Geography, and Human-Environment Interactions, which includes Health Geography and Geospatial Technologies.

Purpose of Study

This dissertation addresses the gap between the subdisciplines of Geography: physical, urban, and health geography to perform a multi-scale and multi-temporal analysis of SUHIs, their impacts on susceptible populations and vulnerable communities, and evaluate adaptation strategies for current and future climate scenarios for Santa Clara County (SCC), California. This dissertation research aims to advance our understanding of temporal and spatial variations of the SUHI response to evapotranspiration and its impacts on public health outcomes in a large urban area of the United States. Spatio-temporal variations in SUHI and human health relationships will inform the optimal location of a landscape intervention that considers an increase in the number of trees to reduce the adverse effects of current and projected LST values. Three research objectives are conducted to achieve the goal of this study.

In Chapter 1 (Objective 1), the urban climate analysis determined annual summer daytime and nighttime SUHI temporal trends and spatial distributions with the use of geospatial technologies (e.g., geographic information systems and remote sensing imagery). MODIS datasets aided the long-term temporal analysis for 2000-2020, while ECOSTRESS, on board the ISS, assisted in the spatial analysis for 2018-2022. The Local Climate Zone (LCZ) framework was then used to analyze urban morphology, its relationship with land surface temperature (LST) and evapotranspiration (ET) distributions, as well as to describe the built environment of Hispanic/Latino neighborhoods. In Chapter 2 (Objective 2), heat vulnerability and population

susceptibility were measured with the use of timely census datasets for the same study period to characterize their socioeconomic status and race/ethnicity, which, combined with health data records, resulted in the identification of at-high-risk heat stress populations. In response to the findings from the urban climate and heat vulnerability analyses, urban heat adaptation measures were proposed and evaluated in Chapter 3 (Objective 3) via the ENVI-Met software to measure the potential cooling effect of trees in Reid-Hillview Airport, located in east SCC. Figure 1 shows the overall proposed methodology to fulfill the research objectives.

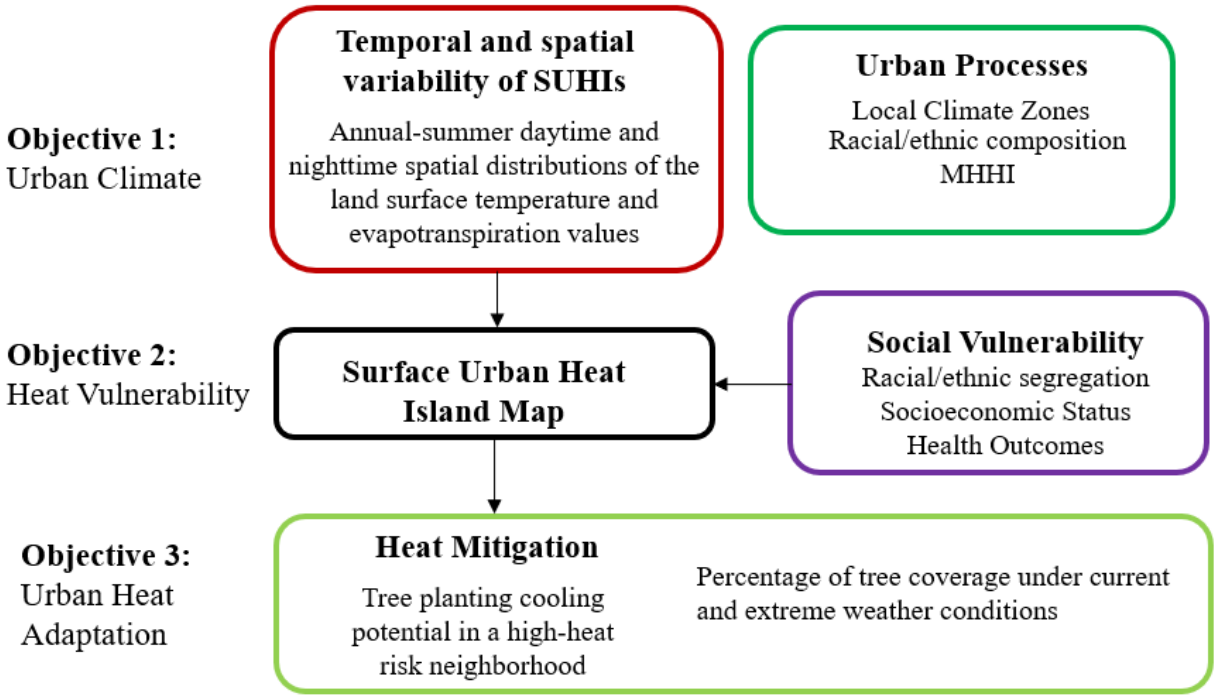

Figure 1. A conceptual framework to fulfill the research goal and objectives.

Theoretical Framework

Geography is a unique discipline that bridges the physical and social sciences, offering the multidisciplinarity necessary to study urban heat. Since the quantitative revolution, *physical* geographers- meteorologists and climatologists- have focused on chemical and biological principles using statistical and mathematical analysis, models, remote sensing, GIS, and field data collection to empirical formulas and theory formulation (Aspinall, 2010). The first and third objectives of this dissertation, therefore, use a positivist theory to investigate urban temperature distributions and heat mitigation, respectively. Through the lens of positivist theory—the spatial and temporal data used in these analyses were studied for their order and patterns to maximize spatial associations to best understand underlying causation in relationships. Urban heat

vulnerability studies explore the causes (alteration of the built environment) and the effects (population morbidity and mortality). As with physical geography, they are also marked by positivism and environmental determinism (e.g., an individual's class status or income, behavioral and genetic adaptation to determine environmental exposure; Emch et al., 2017). The second objective of this dissertation, borrowed from the field of *human* geography, uses a structuralism theory to investigate urban heat vulnerability. This research focused on the higher-level "upstream" structures of society, particularly those that impact how individuals live, work, and recreate, through the lens of structuralism. The spatial distribution of vulnerable populations was explored in relation to socioeconomic status and racial residential segregation, thus uncovering underlying patterns of poverty and racial injustice.

Study Area

The study site is SCC (Figure 2), located in the San Francisco Bay Area (37°18'23"N, 121°54'46"W). SCC has 3,400 square kilometers of land surrounded by water from the San Francisco Bay to the North, the Santa Cruz Mountains to the southwest, and the Diablo Range to the northeast. According to the National Land Cover Dataset (NLCD; Dewitz and USGS, 2021), 25% of SCC was classified as urban developed. The rest of the study area was comprised of forest (31%), shrubland (24%), and herbaceous vegetation (14%). Only 2% of the non-developed area was classified as planted or cultivated. The remaining area was comprised of water (2%), wetlands (<1%), or barren land (<1%).

SCC has experienced, from 1950 to 2010, a surge in heat wave events, which are also projected to intensify in the future (Gershunov & Guirguis, 2012). The mean daily apparent temperature in SCC during the warm season (May 1 to September 30), calculated from meteorological data from 1999 to 2006, was 18.2°C with a range of 9.1 to 32.8°C (Basu & Malig, 2011). Within SCC, San Jose had the highest increase in temperature values, with an average rise of 0.32°C per decade (Lebassi et al., 2009).

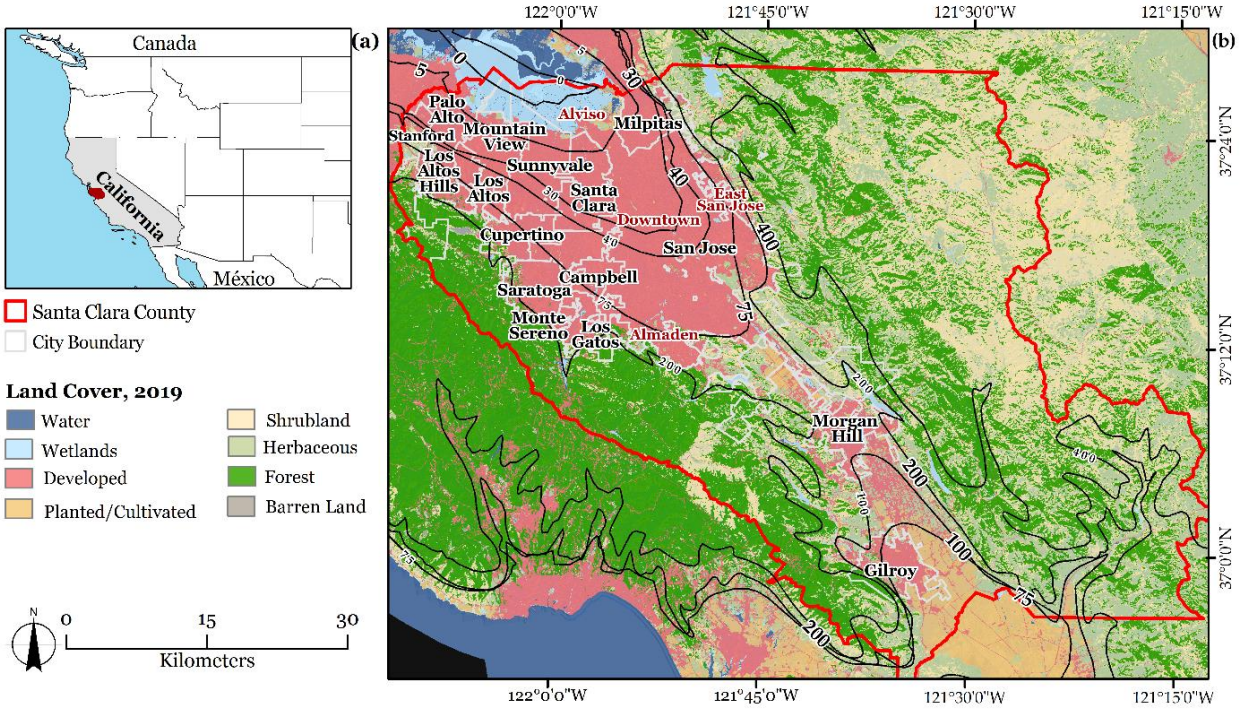

Figure 2. Location of Santa Clara County (SCC): (a) in Northern California (red area), and (b) its land cover (USGS, 2021), 15 cities, and historic neighborhoods of Alviso, East San Jose, and Almaden, as well as topographic contours (m, MSL).

The US Census Bureau (2021) reports a population in SCC of 1.9 million, an increase of 0.15 million from 2010. SCC is a multiracial, multilingual, multicultural society. Of its total population (1,911,226), 32% (622,266) is non-Hispanic White, 26% (498,253) is Hispanic/Latino, of which 85% (420,559) is Mexican, 6% (29,464) Central American, and 3% (15,104) South American (US Census Bureau, 2018). The increased population and intensive droughts have further strained water reservoirs, which could impact water availability that, coupled with rising temperatures, could result in increased health risks, especially for vulnerable groups (e.g., low-income populations). The Hispanic population, as of 2016, was the most significant ethnic or racial minority in the United States, and by 2060, they will represent 27.5% of the total population (Vespa et al., 2020). The findings from this study inform other coastal as well as inland cities with high Hispanic populations on the variability of temperature exposure and health outcomes.

CHAPTER 2. SURFACE URBAN HEAT ISLAND SPATIAL AND TEMPORAL TRENDS IN SANTA CLARA, CALIFORNIA: MODERATING EFFECTS OF THE HUMAN ENVIRONMENT

Introduction

Population growth has driven an increase in anthropogenic greenhouse gas emissions into the atmosphere through the combustion of fossil fuels (IPCC, 2014). These also affect local climate conditions in cities, where anthropogenic releases of heat, moisture, and pollutants and changes in surface properties are some of the leading causes of modified urban climates (Oke, 1987). Heat exchange between the surface and air depends on the thermal properties of the surface and atmospheric conditions (Oke, 1982). Urbanization impacts surface albedos and evapotranspiration (ET) rates, altering surface energy balances and thus creating distinctive local urban climates, including the formation of urban heat islands (UHIs; Oke et al., 2017). UHIs negatively impact energy use, air quality, and human thermal comfort and health (He, 2018). Children, the elderly, low-income groups, and people with preexisting respiratory and cerebrovascular conditions are most vulnerable to these effects (McMichael, 2000). In the United States, racial and ethnic minorities tend to live in neighborhoods with higher heat exposure, which increases heat-related deaths (Jesdale et al., 2013).

UHIs are stronger at the surface (Duckworth & Sandberg, 1954; Bornstein, 1968) under calm wind and clear sky conditions, and they decrease in magnitude outward from the urban core (Raj et al., 2020). Their intensity, defined as the difference between urban and rural temperatures (ΔT_{u-r}), exhibits temporal variations due to several factors (Peng et al., 2012), including differences between urban and rural vegetation, resulting in differing ET cooling rates (Jauregui, 1997). The thermal inertia (TI), the degree of slowness with which the temperature of a body approaches that of its surroundings (Ng et al., 2011), is higher for wet rural areas than for urban environments, and thus wet-rural areas (vs. urban areas) warm more slowly during daytime hours and cool more slowly during evening hours (Swaid, 1991); the reverse is true for dry rural soil areas. Daytime UHIs are thus, in theory, stronger, and nighttime values are weaker for cities surrounded by wet rural environments; the reverse is thus true for cities surrounded by dry rural soils (Imamura,1991; Bornstein et al., 2012; Dou et al., 2015).

UHIs can be estimated via 2-m air temperatures measured by fixed or mobile sensors, producing Canopy UHI values. Measurements of CUHIs are, however, limited by network

densities, so some studies use satellite-derived land surface temperature (LSTs) to estimate Surface Urban Heat Islands (SUHIs) magnitudes and distributions (Voogt, 2007; Stewart & Mill, 2021). Previous results from the Moderate Resolution Imaging Spectroradiometer (MODIS) sensor report negative annual-mean daytime MODIS SUHI intensity trends over 2003-2016 were found in arid Lima, Peru (Wu et al., 2019), as rural regional-warming rates were larger than in urban areas. Positive trends in the extent and intensity of SUHI over 17 years were found in tropical-wet Chennai, India (Raj et al., 2020). A similar positive annual trend was also found in Pune, India, which means its wet season trend is stronger than its dry season value. Negative trends in nighttime values were observed in tropical-wet Lucknow, India (Siddiqui et al., 2021). The same study also reported negative daytime trends, contrary to the generalization of Swaid (1991). Another contradictory study is from tropical-wet Cali, Colombia, which showed increased annual nighttime SUHI intensity from 2003-2016 (Wu et al., 2019).

An analysis by Li et al. (2020) of large cities in various climates showed 2003-2013 MODIS-derived daytime SUHIs amplified by increased wet seasonal precipitation while corresponding nighttime values were reduced or became negative, as wet season rural moisture is greater than urban values. Other examples include MODIS-derived weak or negative daytime SUHIs in dry conditions, e.g., during the 2001-2018 dry season periods in Pune, India (Siddiqui et al., 2021) and from irrigated urban parks in arid Phoenix, Arizona, USA, during 2003-2005 (Imhoff et al., 2010). In Mediterranean climates (e.g., Csa in the Köppen classification system), daytime SUHI intensity peaks in late spring and early summer and decreases as precipitation declines (Sismanidis et al., 2022). As rural vegetation dries due to reduced precipitation, ET decreases, and so does the SUHI intensity. The UHI intensity is, therefore, directly linked to local precipitation (Manoli et al., 2020).

The reduction of evaporative cooling is an important factor contributing to UHIs, as urban moisture content is lower than in nonurban areas, allowing urban areas to warm faster than their vegetated surroundings (Taha, 2017). Droughts, however, can intensify UHIs as insufficient soil moisture in urban areas leads to less latent heat by evapotranspiration (Dong et al., 2018). During the 2012-2016 drought in Los Angeles County, USA, ET values, measured with the combination of Landsat and MODIS, declined from 29.3% in 2011 to 24.6% in 2016, and annual mean daytime LST increased from 34.4 to 37.1°C as the cooling effect from grasses was reduced due to physiological responses, irrigation changes, and losses of green vegetation cover (Allen et al.,

2021). The Normalized Difference Vegetation Index (NDVI), a measure of vegetation cover, has been used to monitor drought conditions and to extract information on soil moisture (Thanabalan et al., 2023). NDVI values range from -1 to 1, with negative values indicating water, positive values near zero indicating bare soil, and higher positive values ranging from sparse vegetation (0.1 - 0.5) to dense green vegetation (0.6 and above). In Los Angeles, CA, MODIS/ASTER-derived NDVI and LST exhibit strong negative correlations, showing that the availability of vegetation may enhance local cooling (Tayyebi & Darrel Jenerette, 2016).

As droughts continue to impact the State of California, limits to outdoor watering will reduce ET rates in urban areas, decreasing their cooling capacity and increasing UHI intensities. Within urban areas, however, outdoor watering varies significantly. High-income areas, for example, are strongly correlated with highly irrigated areas, as high-income households are willing to pay for irrigation despite irrigation limits (Miller et al., 2022). In Los Angeles, higher income was related to greener landscapes, whereas less green landscapes were related to higher percentages of Hispanic or Latino residents (Mini et al., 2014). There is a need to further understand the role of ET and its relation to SUHI intensity, particularly in areas where spatial variations in ET may partly depend on water usage differences among residents of varying income levels.

UHIs have shown significant intra-city variability due to the heterogeneity of urban areas (e.g., differences in the intensity of human activities, amount of green space, and amount and properties of built-up materials), suggesting higher temperatures located in neighborhoods inhabited by low-income populations (Chakraborty et al., 2020). Intra-urban SUHI variability also exhibited seasonal and spatial variations resulting in higher intensity during summer days and within high-density zones (Wang et al., 2023). The intensity of SUHIs has high temporal and spatial variability (Rivera et al., 2017), rendering some sensors insufficient to understand these variabilities, e.g., MODIS has a high-temporal (1-2 days) but a low-spatial resolution (1 km), while Landsat 8 has a high-spatial (100 m) but a low-temporal resolution (16 days). ECOsystem Spaceborne Thermal Radiometer Experiment on Space Station (ECOSTRESS), aboard the International Space Station (ISS), provides daily coverage (superior to Landsat) at a 38 by 69-meter resolution (superior to MODIS), with higher latitude areas measured multiple times per day.

ECOSTRESS data can provide daily LST and ET values; the latter is a valuable indicator of consumptive water use, as it results from the direct evaporation of water and plant transpiration

(Cawse-Nicholson et al., 2021), allowing for the understanding of ET and LST response at the intraurban level. An analysis with the use of ECOSTRESS by Coleman et al. (2020) in Los Angeles shows that LSTs for irrigated and non-irrigated areas were similar in the morning (8-11 a.m.) when atmospheric conditions favor stomatal conductance in both areas. LST values were, however, different in the afternoon (1-3 p.m.), as high temperatures can cause heat stress in non-irrigated areas as soil moisture is insufficient to meet atmospheric demands (Coleman et al., 2020). ECOSTRESS data, therefore, provide the capacity to analyze SUHI variations at high temporal and spatial resolution (Chang et al., 2022). The analysis of long-term LST trends, however, requires large data sets, which limits the number of thermal images that can be analyzed (Ermida et al., 2020). Additional problems arise from inconsistent definitions for land-use and land cover classes, a challenge for comparison studies.

The Local Climate Zones (LCZs) classification system (Stewart & Oke, 2012) was developed to standardize urban morphology classes. It recognizes 10 urban and seven nonurban LCZ areas with uniform surface cover, structure, construction materials, and human activity. LSTs vary broadly by LCZ class, with maximum LST usually recorded for compact and heavy industry areas (Cai et al., 2018). In conjunction with related seasonal variations in urban vegetative cover, soil moisture variation can alter the typical LST-LCZ relationships (Ren et al., 2019). High-density urban areas in compact mid- and low-rise classes have high-heat stress zones (Verdonck et al., 2018) due to their high population densities. Even though industrial and paved classes exhibit high LSTs, they produce only minor stress impacts due to their low densities.

Whereas most previous studies have primarily focused on the LST spatial variability among LCZs, few have explored the use of the LCZ framework to analyze thermal inequality. The current study, therefore, uses a combination of remotely sensed data to determine temporal and spatial summer SUHI distributions and trends in Santa Clara County (SCC), California, and its relationship to the human environment. A 20-year summer averaged MODIS data was used to determine annual winter and summer SUHI and NDVI temporal trends. ECOSTRESS-derived LST and ET variability among LCZs was then studied. The association between race and LCZs, as well as income and LCZs, were then explored via multinominal logistic regressions. The results identified Hispanic/Latino and low-income populations at potentially high heat stress risk from a combination of environmental and social factors, which allowed for the investigation of nature-

society relationships: the role of humans in changing the environment and how this changed environment influences humans (Moseley et al., 2013).

Data and Methods

The first step in this framework evaluated the physical environment via the calculation of annual and seasonal daytime and nighttime LSTs and their corresponding NDVI values from MODIS for 2000-2020 to determine temporal trends. A 4-year summer LST and ET ECOSTRESS for 2018-2022 was then calculated to determine spatial trends. The second step evaluated the social environment per the LCZ framework and US Census data to describe the built environment and assess the distribution of Hispanic/Latino and low-income populations across census tracts in SCC. The third step analyzed LST and ET in relation to LCZ and LCZ in relation to socioeconomic factors. The combination of these assessments resulted in a comprehensive human-environment approach to evaluate SUHI intensity in areas of varying levels of MHHI in SCC.

Physical Environment

MODIS. Annual summer and winter LST and NDVI trends were determined from MODIS. A total of 14 303 satellite images from 5 March 2000 to 31 December 2020 were accessed for Santa Clara County to derive 21 daytime (1000-1400 Central Standard Time = GMT-6 h) and 21 nighttime 2200-0200 (Central Standard Time = GMT-6 h) monthly mean LST trends, as well as the corresponding annual mean NDVI values. For seasonal analysis, summer considers June 01 to August 31, whereas winter considers December 1 to February 28. Images were accessed via Earth Engine (code.earthengine.google.com/), which provides free access to satellite datasets (Gorelick et al., 2017), allowing for long-term LST and NDVI trend computations (Budhiraja et al., 2020; Chakraborty & Lee, 2019; M. Wang et al., 2020). Cloud-covered pixels (>0% cloudiness) in MODIS images were first masked by the use of a Quality Assessment (QA) procedure that provides information on pixel quality and allows users to apply pixel-based filters. The National Land Cover Dataset (USGS, 2019) was then used to retrieve pixels corresponding with values classified as urban developed (classes 21-24) for each LST and NDVI satellite product. This process filtered non-developed (rural) areas from developed (urban) locations to better estimate the urban variability of LST values (Rivera et al., 2022).

ECOSTRESS. Approximately 300 ECOSTRESS scenes were retrieved via the NASA Earth Data Cloud web application, also known as AppEEARS (appeears.earthdatacloud.nasa.gov), for the summer months (June to August) of 2018 to 2022. Determination of LST (Level-2) and ET

(Level-3) distributions first involved a per-pixel filter applied to ECOSTRESS images, using its cloud product to mask cloudy and cloud shadow pixels. As with the MODIS products, pixels corresponding with values classified as urban developed (classes 21-24) for each LST and ET satellite product were retrieved. These values were combined to produce summer LST (°C) and ET (W/m^2) distributions for the study area.

Socioeconomic Environment

Local Climate Zones. The built environment of SCC was described in the current study via the LCZ framework of Stewart and Oke (Stewart & Oke, 2012). The LCZ classification system, developed to standardize urban morphology classes, recognizes 10 urban and seven nonurban LCZ areas with uniform surface cover, structure, construction materials, and human activity. This methodology is based on the World Urban Database and Access Portals Tools (WUDAPT) of Ching et al. (2018) and integrates satellite imagery with open-source software (Bechtel et al., 2015). User knowledge of local morphological conditions helped create the minimum required 20 WUDAPT training samples for each LCZ class via Google Earth software, using 20 June 2020 imagery as the base layer. Less than 15 training samples were digitized for LCZ 2 (compact mid-rise) as it is rare in SCC, and no LCZ 1 (compact high-rise) and LCZ 4 (open high-rise) areas exist in the study area. The samples were then used as input to run an LCZ classification algorithm in the LCZ Generator (lcz-generator.rub.de), a web application to create LCZ maps with its corresponding automated accuracy assessment (Demuzere et al., 2021). As with previous datasets, pixels corresponding with values classified as urban developed (classes 21-24) were retrieved.

Neighborhood Demographics. Racial/ethnicity and economic data were acquired at the census tract level for SCC from the US Census Bureau, ACS Five-Year Estimates (2017-2021). Since the Hispanic/Latino population comprises a third of the total population in SCC, this ethnic group was selected to explain the moderating effects of race on environmental outcomes. The Hispanic/Latino (DP05_0071E) variable was divided by the total population variable (DP05_0001E) to estimate the percentage of the Hispanic/Latino (any race) population per census tract. The socioeconomic status of residents was measured with the use of the median household income (MHHI) variable (DP03_0062E). Census Tract 5116.08 was omitted as it represented Stanford University and had no income data.

Human-Environment

The Zonal Statistics tool in ArcGIS Pro© (version 3.0.3) was used to calculate the mean LST and ET values per census tract. The potential association between the LST, ET, and percentage of Hispanic/Latinos, as well as MHHI, was explored with Spearman correlation statistics, as values do not follow a parametric distribution. The relationship between the built environment and race/ethnicity at the census tract level was examined with the use of a multinomial logistic regression. The most frequently occurring LCZ class per census tract was first found with the use of the Zonal Statistic Tool, majority option, and assigned to each spatial unit to define the dependent variable. The independent variable was defined as Hispanic/Latino (percentage) or as MHHI (dollars).

Results

The human-environment conceptual framework allows for the study of the temporal and spatial variation of LSTs related to NDVI and ET values, as well as Hispanic/Latinos in SCC. MODIS-derived LST results show stronger daytime summer (0.10°C per year) and winter (0.11°C per year) means than their corresponding nighttime values (0.03 and 0.04°C per year, respectively). MODIS-derived NDVI results show no strong temporal trends for summer and winter. Positive correlations were, however, found for winter NDVI and LST values, whereas negative correlations were found for corresponding summer values. ECOSTRESS-derived LST values range from 7.4 to 56.1°C and ET values from 0.7 to 500.4 Watts/m^2. The spatial distribution analysis shows an increasing LST with decreasing ET and an increasing percentage of Hispanic/Latino populations (0.02°C per percent increase in Hispanic/Latinos). Hispanic/Latinos in SCC are, therefore, most likely to experience high LST values due to low soil moisture resulting from high-density buildings (compact low-rise) and the prevalence of impervious surfaces in large low-rise areas.

Physical Environment

MODIS. MODIS annual-mean summer LST values (Figure 3) from 2000 to 2020 show a slight upward daytime trend (m = 0.10°C per year, R^2 = 0.52), with a minimum of 37.4°C in 2001 to a peak of 47.8°C in 2020, along with large yearly annual variabilities ($\pm 1\sigma$) ranging from 2.93 to 3.32°C. The corresponding nighttime annual mean-summer values (Figure 2b) show a weak upward trend (m = 0.03°C per year, R^2 = 0.14) with values ranging from 14.6°C in 2011 to 16.3°C in 2017, and smaller annual variabilities (1.10 to 1.44°C). Annual LST variations are slightly larger for daytime (0.39°C) than for nighttime (0.34°C) hours due to daytime turbulence levels. Annual

summer-mean NDVI ranges from 0.32 in 2005 to 0.37 in 2010 and exhibits no trend (*m* = -0.0006 per year). The Spearman correlation between summer annual-mean LST and NDVI shows a negative but moderate relationship for daytime (rho = -0.42, p-value = 0.06) and nighttime (rho = -0.38, p-value = 0.09) values, although nonsignificant.

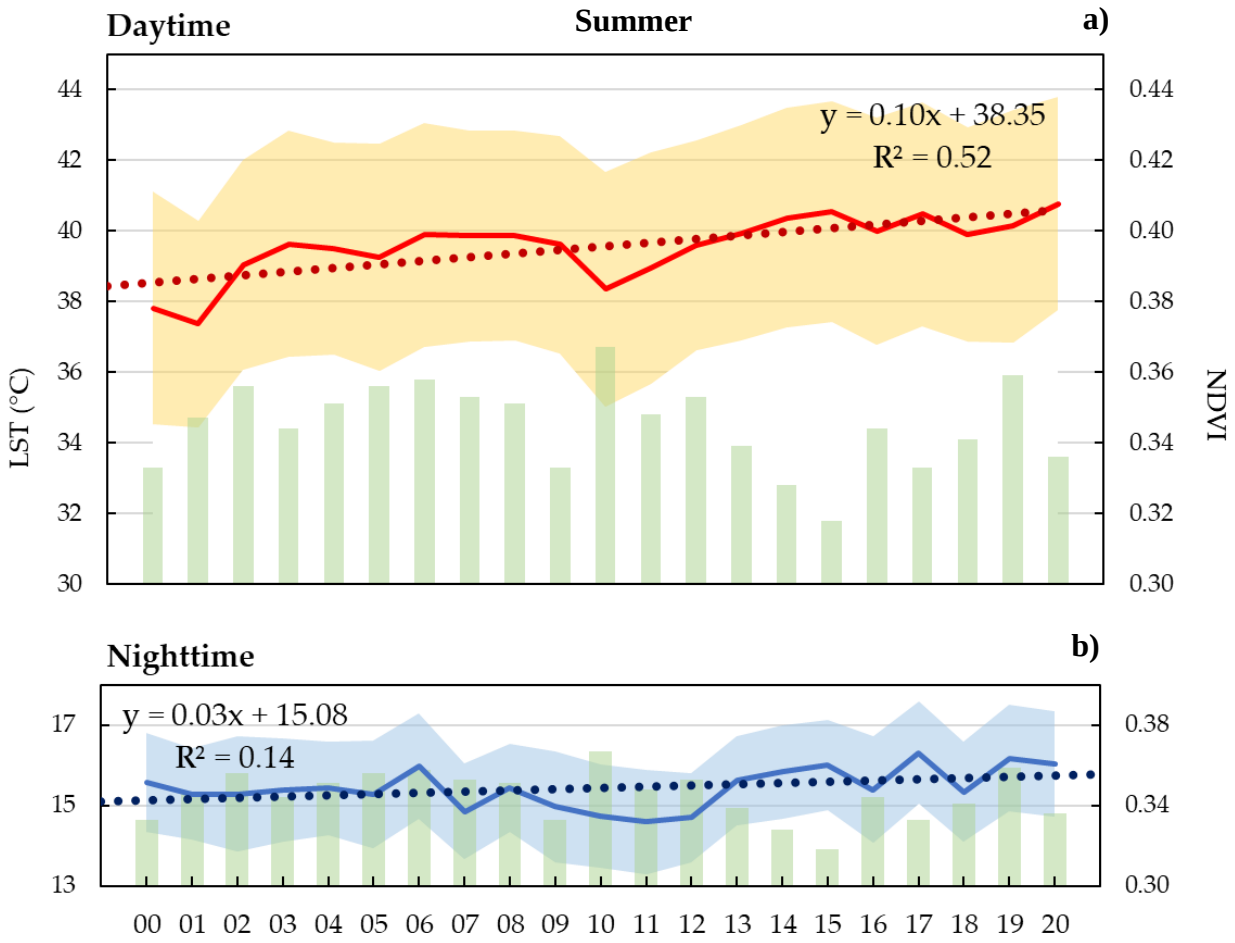

Figure 3. MODIS (2000-2020) summer annual-mean and ± 1σ (color band) variations of a) daytime and b) nighttime LST (°C), as well as annual mean NDVI values.

MODIS annual-mean winter LST values (Figure 4) from 2000 to 2020 show a slight upward daytime trend (*m* = 0.11°C per year, R^2 = 0.28), similar in magnitude to the daytime-summer LST trend. These LST values range from 15.0°C in 2001 to 19.7°C in 2020 and exhibit small yearly annual variabilities (±1σ), ranging from 1.36 to 1.97°C. Corresponding nighttime annual-mean LSTs (Figure 3b) show a weak upward trend (*m* = 0.04°C per year, R^2 = 0.07) with values ranging from 3.18°C in 2006 to 7.15°C in 2014, and very small annual variabilities (0.58 to 1.06°C). Annual LST variations are larger for daytime (0.61°C) than nighttime (0.48°C) hours, and both values are larger than their corresponding summer annual measures. Annual-mean NDVI

ranges from 0.18 in 2009 to 0.37 in 2017, showing a much larger range than summer NDVI values but with an equal maximum value. Winter NDVI exhibits a non-existent trend (*m* = 0.002 per year). The Spearman correlation between winter annual-mean LST and NDVI shows a strong and significant positive relationship for daytime values (rho = 0.60, p-value = 0.00) and a positive but weak relationship with nighttime values (0.11, p-value = 0.65), although nonsignificant.

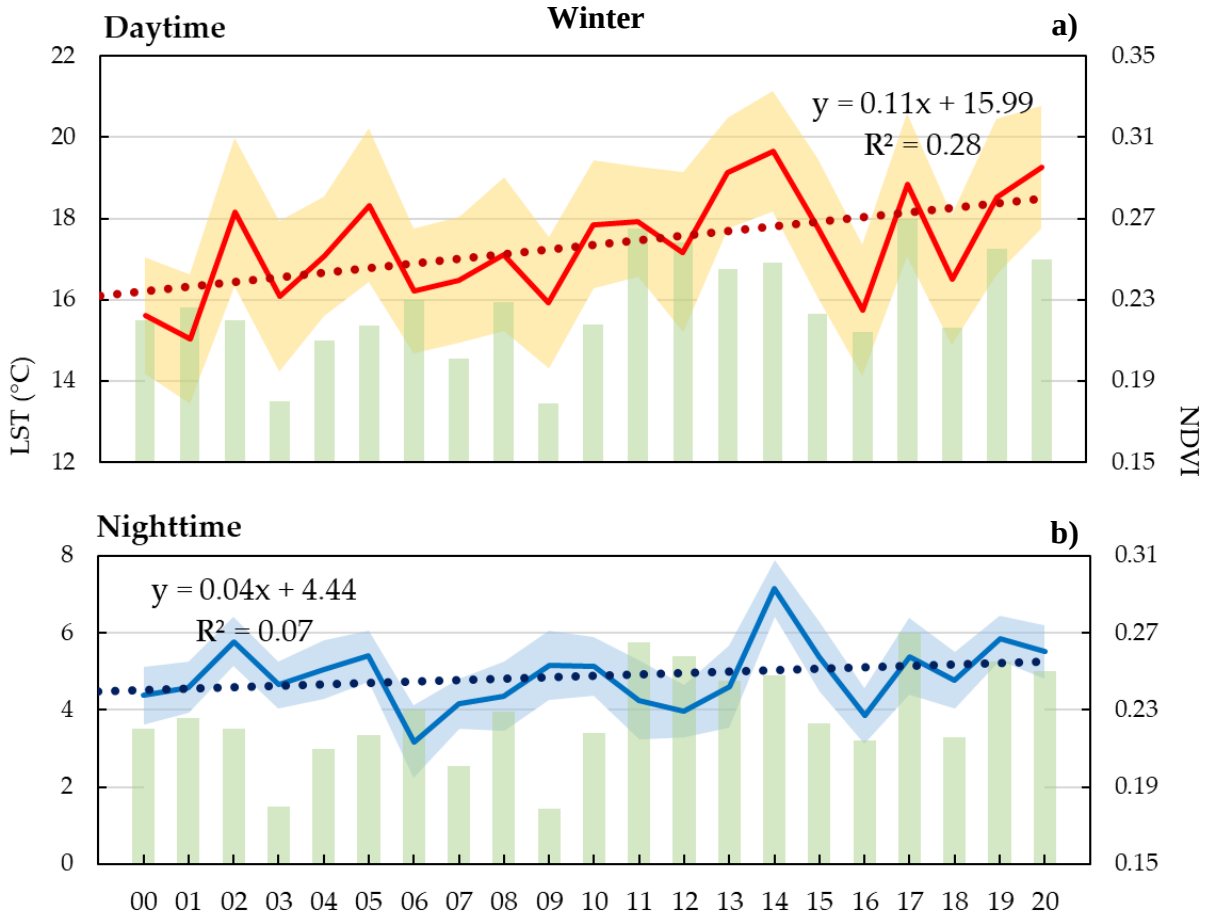

Figure 4. MODIS (2000-2020) winter annual-mean and ± 1σ (color band) variations of a) daytime and b) nighttime LST (°C), as well as annual mean NDVI values.

ECOSTRESS. ECOSTRESS-derived summer 2018-2022 LSTs (Figure 5) for the entire domain range from 7.40 to 56.1°C, with a mean of 26.6°C. The distributions of minimum values are found along the southwest towards the mountain over low-density areas in Saratoga and Los Gatos, while maximum LSTs are found east of San Jose over the Reid-Hillview Airport area. Lower than average values are located west towards Palo Alto and Los Altos Hills, where most of the developed open-space area is located. Sunnyvale and Santa Clara mostly exhibit average LST values over medium-to-high-intensity developed areas corresponding to commercial areas. Major

roads, the San Jose Airport, and the southern part of the City of San Jose have higher-than-average summer LST values.

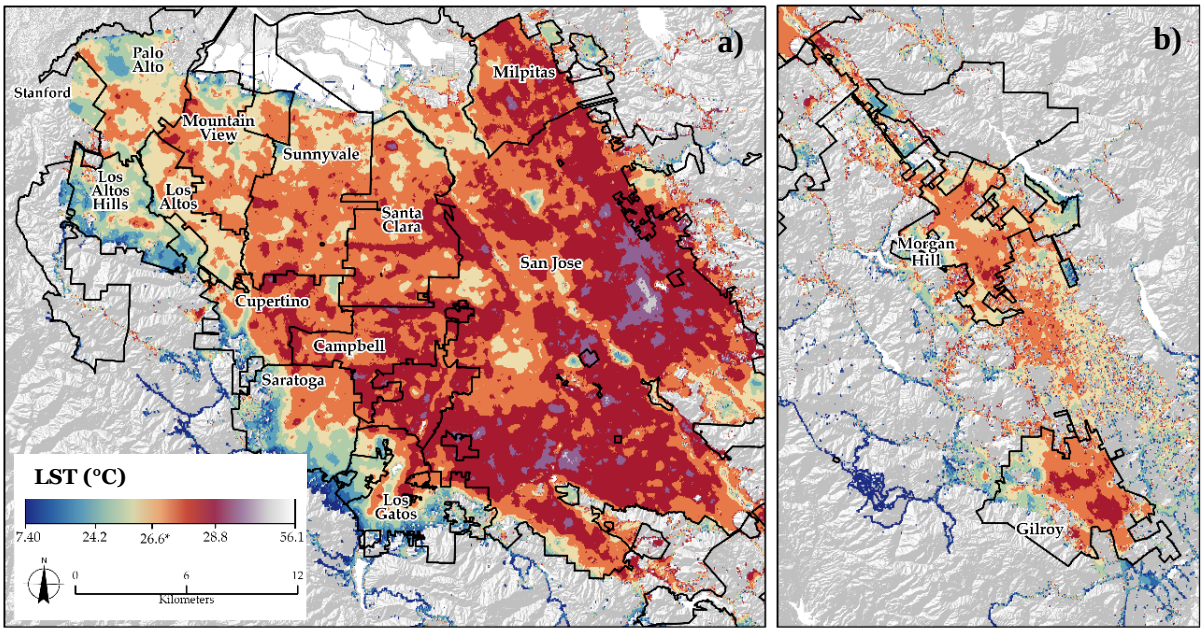

Figure 5. ECOSTRESS (2018-2022) summer (June-August) mean LST (°C) distributions at 70-meter resolution for SCC in its a) central and b) southernmost part.

Summer-mean 2018-2022 ET values for the entire domain range from 0.72 to 500.4 Watts/m^2, with a mean of 130.0 Watts/m^2. The resulting range of values is probably due to the cloud filtering process, where cloud pixels not recognized as clouds were not masked. Another process to remove these undetected cloud pixels includes filtering outliers (e.g., removing pixels below the 8% or above 98% percentile). This process, however, was not done in the current effort to avoid over-filtering pixels. The spatial distributions (Figure 6) show minimum values over the highly impervious Airport and Downtown areas in San Jose and to the southernmost region (6b) in Morgan Hill. Additional minimum ET areas are west in Cupertino, north in Milpitas, and the southernmost part of the study area in Gilroy over high-density and highly impervious areas.

Maximum ET values are to the west in Palo Alto and south of Downtown San Jose over residential areas. Higher-than-average ET values are found in low-density and highly vegetated Los Altos, Saratoga, and Los Gatos. Lower-than-average ET values are primarily located east and south of San Jose over highly-vegetated residential areas. ET and LST values exhibited similar spatial patterns, which thermal inertia can explain; surfaces with low ET values warm faster than their vegetated and well-watered surroundings. The Spearman correlation statistic, therefore,

showed a strong negative and significant relationship between ET and LST values (rho = -0.64, p-value = 0.00).

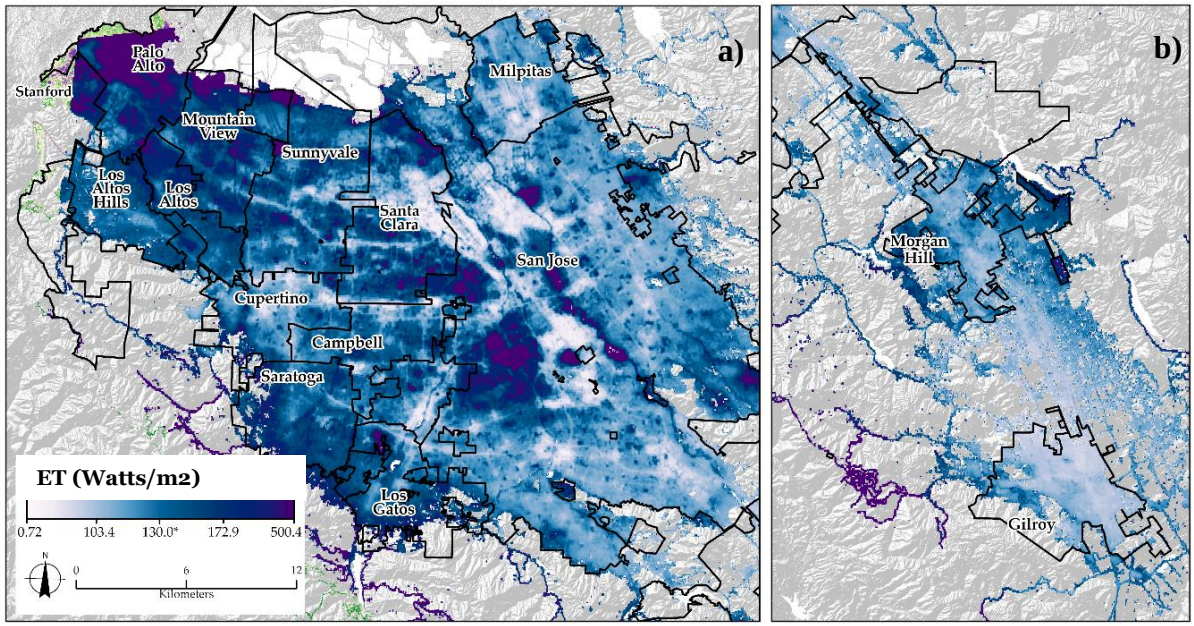

Figure 6. ECOSTRESS (2018-2022) mean-summer (June-August) evapotranspiration (W/m^2) distributions at 70-meter resolution for SCC in its a) central and b) southernmost part.

Socioeconomic Environment

Local Climate Zones. The resulting LCZ classification yielded an overall accuracy of 0.73. The 100-meter LCZ distribution (Figure 7) shows that low-rise urban structures (LCZs 3, 6, 8) comprise most of the urbanized area of SCC. LCZ 3 (compact low-rise) is primarily located within San Jose to its eastern and southernmost parts over highly-density and low-vegetated residential areas, where high LST values were also detected. LCZ 6 (open low-rise), in contrast, is mainly east of the study area over lower-density and highly-vegetated residential areas, while LCZ 8 (large low-rise) is found in the upper part of SCC towards the San Francisco Bay, where most commercial areas are located. LCZ 9 (sparsely built) surrounds the study area and is particularly prevalent in south SCC (Figure 6b) around Morgan Hill, where most agricultural land is located. LCZ A (dense trees), B (scattered trees), and D (low plants) comprised most of the non-urban classes and are primarily found outside city limits.

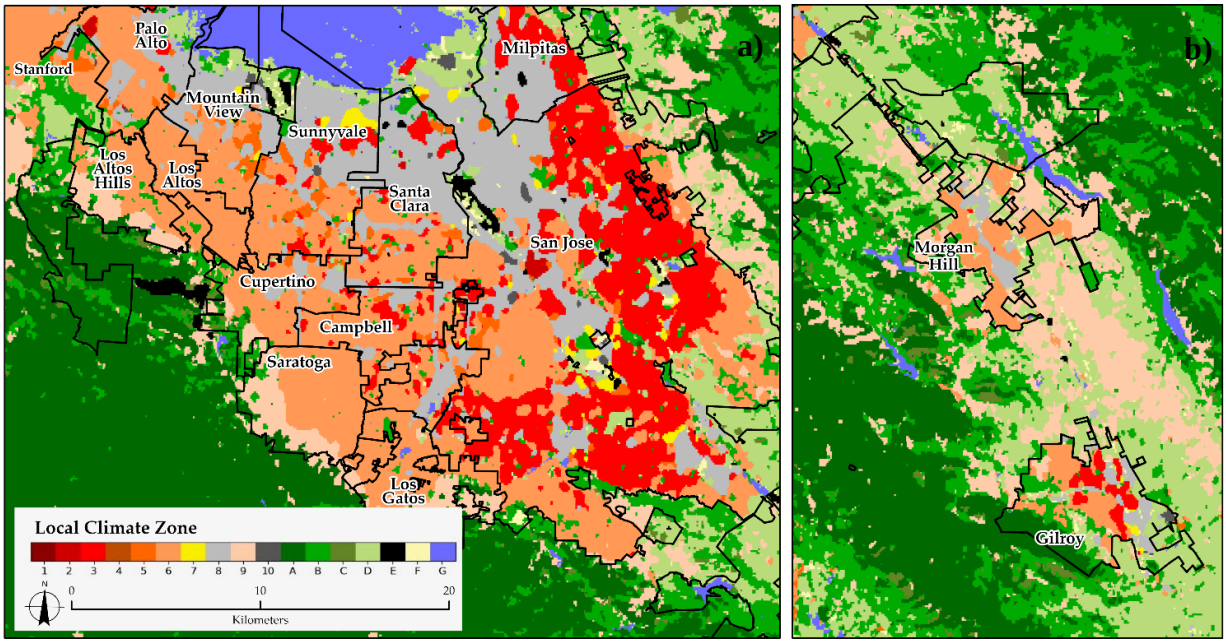

Figure 7. Local Climate Zones (LCZs) distribution at a 100-m resolution for SCC in its a) central and b) southernmost part.

Results of the evaluation between LSTs and LCZs (Figure 8a) show LCZ A (dense trees) had the lowest mean LST of 22.0°C, with values ranging from 16.0 to 27.1°C. Areas comprised of LCZ 3 (compact low-rise) exhibit the highest mean LST (27.7°C) and the smallest range of values from 24.0 to 29.0°C. Maximum ranges of 18.6 to 35.0°C are found for LCZ 9 (sparsely built) due to their spatial variability, reflecting the differences in the surrounding vegetation. For urban LCZ classes, the minimum LST value (26.0°C) is found in LCZ 9 (sparsely built) and the maximum (27.7°C) in LCZ 3 (compact low-rise). Results of the relationships between ET and LCZs (Figure 8b) show that the LCZ A (dense trees) class has the highest mean ET of 204.1 Watts/m^2 with a maximum of 308.6 Watts/m^2, whereas the lowest ET mean (102.6 Watts/m^2) is in LCZ F (bare soil). LZC 9 (large low-rise) exhibits the largest range of values from 60.6 to 263.3 Watts/m^2, with minimum ET in Mountain View and Sunnyvale and maximum in Santa Clara, San Jose, and Milpitas. For urban classes, the minimum ET value (108.7 Watts/m^2) is found in LCZ 10 (heavy industry) and the maximum (123.7 Watts/m^2) in LCZ 6 (open low-rise).

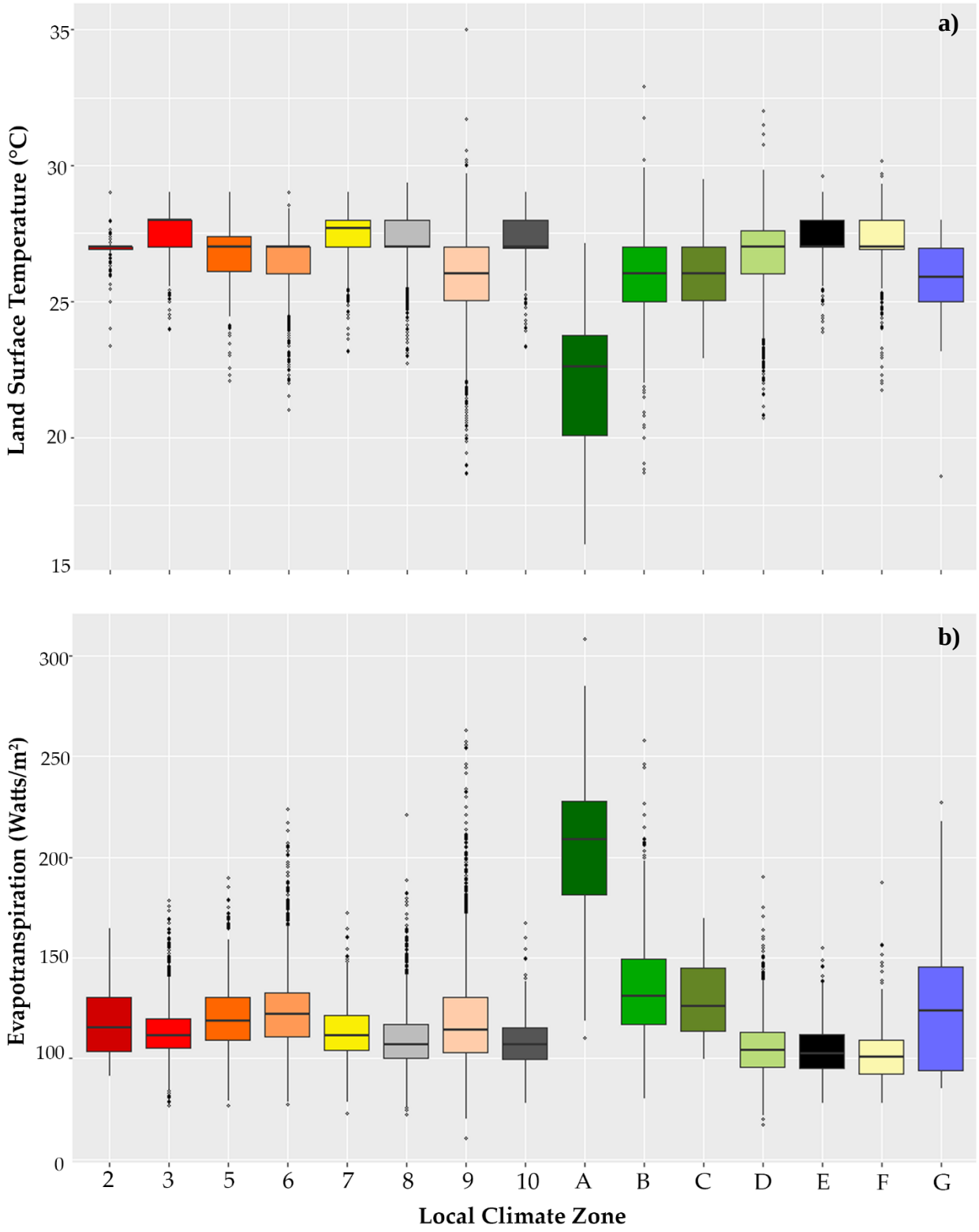

Figure 8. Box plots of a) Land Surface Temperature (°C) and Evapotranspiration (Watts/m^2) values per LCZ class in SCC.

Neighborhood Demographics. In SCC, the percentage of Hispanic/Latinos per census tract varies from 0.38 to 85.6%, with a mean of 25.5%. Resulting distributions (Figure 9) show a maximum concentration (76-86%) of Hispanic/Latino populations in two census tracts in San Jose and two in the southernmost region in Gilroy. These tracts were surrounded by higher-than-average (51-75%) concentrations of Hispanic/Latinos, with an additional census tract to the north in the below-sea level and residential Alviso neighborhood, where most salt marshes out to open waters of the San Francisco Bay are located. A slightly higher-than-average concentration (26-50%) was primarily found east SCC in San Jose and to the south towards Morgan Hill and Gilroy. In the remaining tracts, mostly east of SCC in Palo Alto, Los Altos, and Los Altos Hills, a lower-than-average (0-25%) concentration of Hispanic/Latino populations is found, as well as in the southwest in Los Gatos and Saratoga.

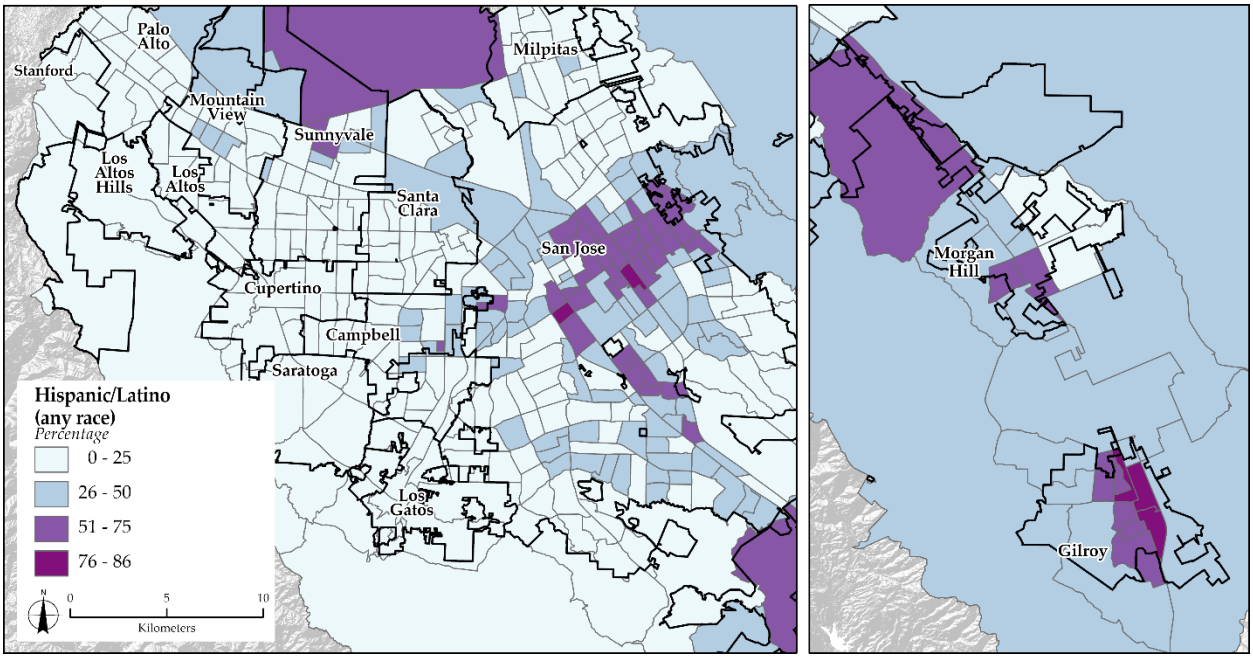

Figure 9. Spatial distribution of Hispanic/Latino population as a percentage per census tract in SCC derived from US Census Bureau American Community Survey (ACS), Five-Year Estimates (2017-2021) data (US Census Bureau, 2022).

In SCC, MHHI values ranged from $34,000 to more than $250,000, with an average value of $145,000. MHHI distributions (Figure 10) show minimum values in the East San Jose neighborhoods and the southernmost region of SCC in Gilroy, coinciding with areas with a maximum concentration of Hispanic/Latino populations. Maximum MMHI values were found to the southwest in Los Gatos, southeast in Los Altos Hills, and east in Palo Alto. Higher-than-

average MHHI census tracts are mostly in Los Altos, Cupertino, and Mountain View, as well as in Campbell and the eastern part of SCC. Lower-than-average values are in the Downtown San Jose Area and some neighborhoods in Santa Clara.

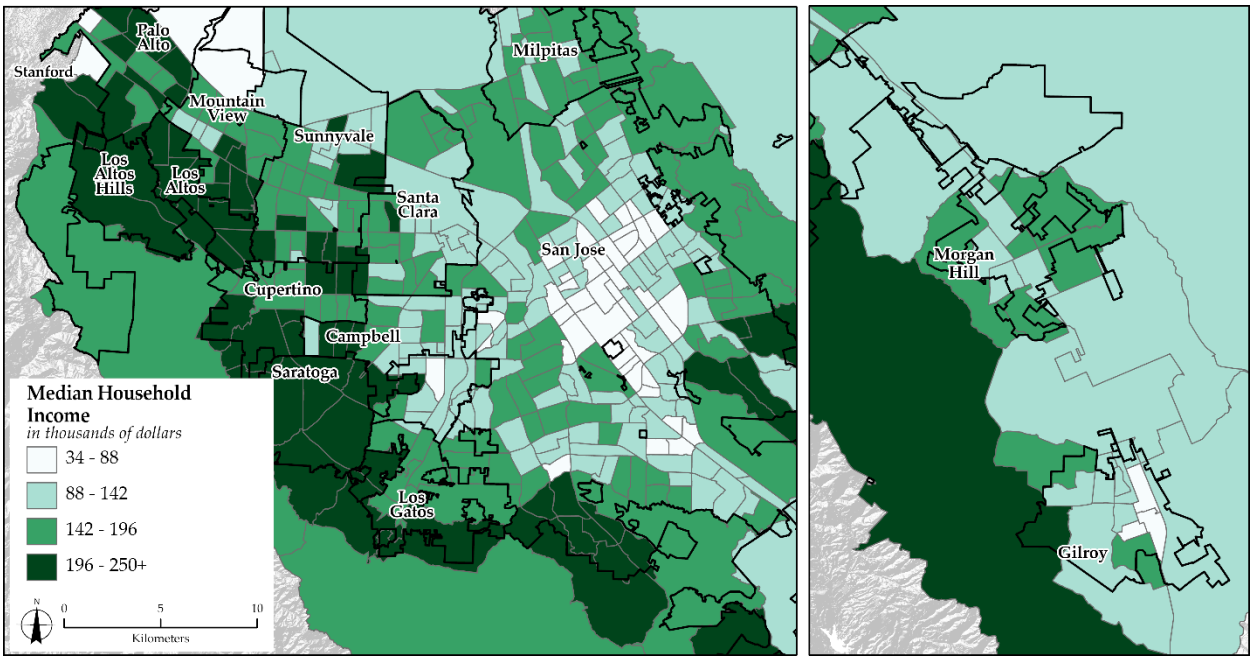

Figure 10. Spatial distribution of median household income (MHHI), in dollars, from the US. Census Bureau American Community Survey (ACS), Five-Year Estimates (2017-2021) data (US Census Bureau, 2022).

Human-Environment

The Zonal Statistic Tool was used to calculate census-tract mean ET and LST to evaluate the human-environment via the relationship of race/ethnicity and physical environment (ET and LST). A Spearman statistic shows that the percentage of Hispanic/Latinos negatively correlates with ET (rho = -0.38, p-value = 0.00) but positively correlates with LST (rho = 0.42, p-value = 0.00). Simple linear regressions were performed to analyze rates of change of ET and LST values by the percentage of the Hispanic/Latino population. Results show a positive LST-Hispanic/Latino trend ($R^2 = 0.15$), with LST values increasing by 0.017°C per percent increase in Hispanic/Latino. A negative trend ($R^2 = 0.13$) is therefore found between ET and Hispanic Latinos, which decreases by 0.52 Watts/m^2 per percent increase in Hispanic/Latino populations.

The most frequently occurring LCZ was assigned to each census tract to analyze the relationship between sociodemographic variables and the built environment per the LCZ classification system. Results of this evaluation (Figure 11) show that neighborhoods comprised

of LCZ 3 (compact low-rise) exhibit the highest mean (38%) and maximum (86%) percentage of Hispanic/Latino populations, followed by LCZ 8 (large low-rise) with 27 and 86%, respectively. The lowest concentration of Hispanic/Latinos (2%) corresponds to LCZ A (dense trees), followed by LCZ 6 (open low-rise) with 16% Hispanic/Latino populations. Open low-rise neighborhoods, however, had a maximum concentration of 66%, reflecting that Latinos are likely to inhabit areas mainly comprised of LCZ 3, LCZ 8, as well as LCZ 6.

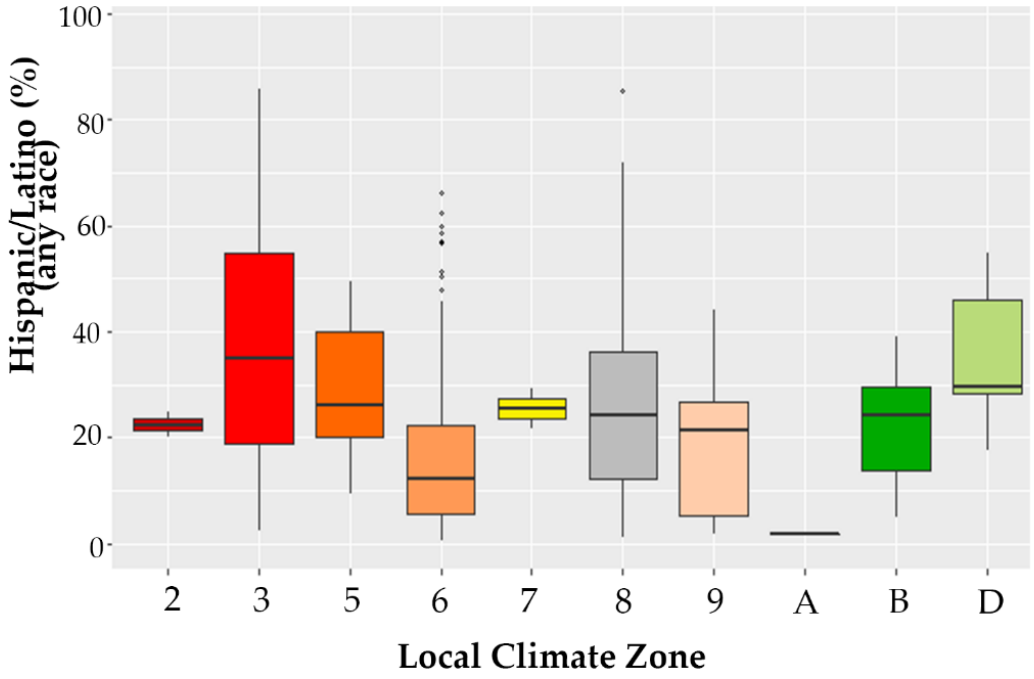

Figure 11. Box plot of Hispanic/Latino populations (percentage) per LCZ class in SCC.

Results of this evaluation (Figure 12) show that neighborhoods comprised of LCZ 2 (compact mid-rise) exhibit the lowest MHHI mean ($115,171), followed by LCZ 3 (compact low-rise) with a MHHI mean of $117,081. Maximum mean MHHI values are in LCZ 9 (sparsely built). LCZ 5 (open mid-rise), 7 (lightweight low-rise), and 8 (large low-rise) lower-than-average MHHI values (<$145,000) ranging from $121000 to $133,000. Higher-than-average MHHI values, in contrast, are found in the rest of the LCZ classes, ranging from $148,000 in LCZ (scattered trees) to $182,000 in LCZ A (dense trees).

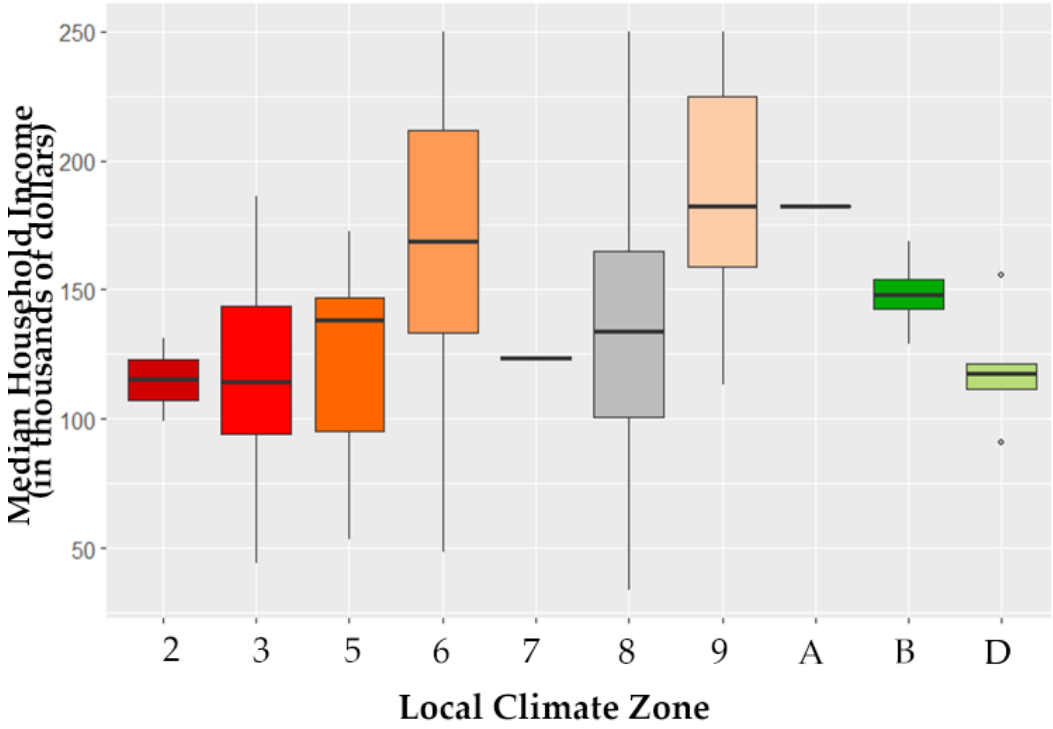

Figure 12. Box plot of Median Household Income (in dollars) per LCZ class in SCC.

Results of the multinomial logistic regression (Table 1) show a negative relationship between the percentage Hispanic/Latinos coefficients and LCZ 6 (open low-rise), 9 (sparsely built), A (dense trees), and B (scattered trees). Coefficients are positive and high for LCZ 3 (compact low-rise) and D (low plants). Still positive coefficients, but not as large, are in LCZ 5 (open mid-rise), 7 (lightweight low-rise), and 8 (large low-rise). The Wald Statistic (z) shows, at an alpha level of 0.05, no significance for all LCZ classes. Although coefficients are not significant, the odds ratio shows large values in LCZ 3 (compact low-rise) and D (low plants), followed by LCZ 5 (open midrise), LCZ 8 (large low-rise), and 7 (lightweight low-rise). Odds of Hispanic/Latino populations are less likely in LCZ B (scattered trees) and 9 (sparsely built). Extremely low odds ratio values are found in LCZ 6 (open low-rise) and A 9 (dense trees).

The multinomial logistic regression results for MHHI show positive coefficients for all LCZ classes, although at different magnitudes. Coefficients are relatively high for LCZ 9 (sparsely built), A (dense trees), and 6 (open low-rise). LCZ B (scattered trees) and 8 (large low-rise) follow with values of 0.019 and 0.11, respectively. Very low coefficients are found for LCZ 7 (lightweight low-rise) and 5 (open mid-rise). Near-zero coefficients are shown for LCZ D (low plants) and 3 (compact low-rise). The Wald Statistic (z) shows, at an alpha level of 0.05, no significance for all LCZ classes except LCZ 6, 9, and A, which also show relatively high odds ratio values ranging

from 1.03 to 1.05. Although not all coefficients are significant, the odds ratio indicates relatively low- values in LCZ 3, 5, 7, and D.

Table 1. Results of multinomial logistic regression between LCZ (majority per census tract) and percentage of Hispanic/Latino (any race) population, as well as Median Household Income (in dollars).

Independent Variable (Y)	LCZ	Coefficient	Standard Error	Wald Statistic	P-value	Odd Ratio
Percentage of Hispanic/Latinos (any race)	3	4.06	4.28	0.95	0.34	57.7
	5	1.78	4.64	0.38	0.70	5.96
	6	-2.92	4.29	-0.68	0.49	0.05
	7	1.03	5.78	0.18	0.86	2.79
	8	1.59	4.29	0.37	0.71	4.89
	9	-1.59	4.59	-0.34	0.72	0.20
	A	-109	90.9	-1.98	0.23	0.00
	B	-0.07	5.04	-0.01	0.98	0.93
	D	3.52	4.76	0.74	0.46	33.7
Median Household Income (in dollars)	3	0.001	0.009	0.15	0.88	1.00
	5	0.004	0.011	0.34	0.74	1.00
	6	0.029	0.008	3.60	0.00	1.03
	7	0.005	0.017	0.30	0.76	1.00
	8	0.011	0.008	1.32	0.19	1.01
	9	0.038	0.009	4.07	0.00	1.04
	A	0.035	0.017	1.98	0.05	1.05
	B	0.019	0.012	1.52	0.13	1.02
	D	0.003	0.013	0.22	0.83	1.00

Discussion

Temporal analysis of SUHI in this study found contrary results to trend analysis reported previously for SCC. An analysis by Lebassi et al. (2009), from summer (June-August) long-term (1970-2005) daily 2-m air temperatures, reported a maximum trend of -0.53°C per decade for SCC, resulting from marine air intrusions, as the air penetrated through a sea-level passage from the northern part of the San Francisco Bay southward towards SCC. As nighttime land surfaces cooled more rapidly than the sea, temperature differences produced maritime airflow. Kueppers et al., 2007 suggested that summer cooling in California resulted from increased irrigation, mainly from agricultural areas. Similarly, vegetation transpiring significant volumes of water within urban areas

could provide higher cooling effects than trees with lower transpiration rates; thus, unirrigated trees or under water stress do not provide sufficient cooling (Ballinas & Barrandas, 2015).

In the urbanized area of SCC, summer LSTs have an upward trend of 0.10°C per year (or 1.00°C per decade), whereas the corresponding nighttime values show no trend of 0.03°C per year (or 0.30 per decade). A higher proportion of the variance is explained for summer daytime (R^2 = 52%) than for corresponding nighttime values daytime (R^2 = 14%). The difference in summer trends between the current effort and those of Lebassi et al. (2009) may be attributed to measurement instruments. While this study uses remotely sensed data to measure LSTs, the latter uses National Climatic Data Center (NCDC) observational sites to measure daily Tmin and Tmax 2-m air temperatures to produce average monthly values.

This difference in trends may also be explained by Simpson's Paradox, which arises because aggregated data supports a trend that disappears or reverses when subgroups are combined (Pearl, 2022). Lebassi et al. (2009) found that from 1970 to 2005, daily mean summer 2-m air temperatures increased by 0.15°C per decade. Observations were then aggregated into inland and coastal subgroups. The former showed an increasing trend of 0.24° per decade, whereas the latter showed a decreasing trend of -0.01°C per decade. The aggregation of spatial data may also result in the Modifiable Areal Unit Problem (MAUP), which arises when data is aggregated according to different zonal systems, causing inconsistent results.

During the summer season, NDVI values exhibit no trend, with a near-zero proportion of variance explained. During summer daytime, high NDVI values from plant growth provide maximum cooling via evapotranspiration, particularly in highly-irrigated areas, allowing them to cool faster. Vegetation also provides shade and absorbs radiation, cooling even over soil and impervious surfaces. A negative relationship consequently exists between summer LST and NDVI values, particularly during daytime hours. The cooling effect of vegetation on LST is, therefore, during the daytime than at nighttime, although most heat-related deaths occur at night. During winter months, there is, however, a positive LST-NDVI relationship. The low photosynthesizing of vegetation provides no cooling and thus does not regulate LST values (Marzban et al., 2017).

During summer, irrigated vegetative cover in urban areas has high evapotranspiration values and warm at a slower rate than those with low evapotranspiration, thus explaining the negative relation. The spatial distribution of summer ET values shows high values in known high-income neighborhoods to the west in Palo Alto and Los Altos. Contrary results were found to the

east in San Jose, where very low-income and majority Hispanic/Latino populations are located. TI may also explain these differences in cooling rates: high-income neighborhoods tend to have high vegetative cover and, thus, warm and cool at slower rates than their impervious counterparts. Trees within high-income communities provide shade, which attenuates radiant energy flows through absorption and reflection, further cooling the surface and near-surface temperature (Declet-Barreto et al., 2013).

In the US, there is substantial evidence that a high proportion of low-income communities, where most racial and ethnic minorities reside, are deprived of green areas that resulted from historical ethno-racial oppression and segregated park system (Wolch et al., 2014). Although the LCZ-Hispanic/Latino multinomial logistic regression results show no statistically significant coefficient (p-value>0.05), the odds of Hispanic/Latino populations are higher in LCZ 3 than in the rest of the urban classes. LCZ 3 exhibits the highest mean LST (27.7°C) and an average ET value of 113.7 W/m^2. The multinomial logistic regression results of LCZ and MHHI show the minimum statistically significant coefficient in LCZ 3, exhibiting a very low MHHI of $117,081. The large but low significant LCZ-Hispanic/Latino vs. the low but significant LCZ-MHHI coefficients may result from 1) different vegetation types within LCZ classes and 2) the aggregation of Hispanic/Latino populations. For the former, results show a wide range of LST and ET values for LCZ 6 (sparsely built), as previous land cover surrounding buildings have different evaporation rates (e.g., low-plants vs. scattered trees). A subclass of LCZ 6 that reflects a difference in surroundings is, therefore, recommended. For the latter, this study does not disaggregate Hispanic/Latinos by origin.

There are socioeconomic differences within Hispanic subgroups, which may expose them to different levels of environmental hazards. Williams et al. (2017) report that Cubans have a college graduation rate three times higher than Mexicans, and Puerto Ricans have higher high school graduation rates than Mexicans (74% vs. 54%), which may contribute to health disparities and risk exposure. Hispanic/Latinos in the US have been treated as a homogenous group, although differences have been reported within this population. Mexicans and Cubans, for example, are less likely to have emergency department visits than non-Hispanic Whites (Weinick et al., 2004), potentially affecting their representation in rates of heat-related emergency room visits. MHHI operates with other characteristics like race, ethnicity, age, and gender. Additional sociodemographic variables, such as employment status, professional occupation, median house

value, education levels, or occupational prestige, should be considered to analyze human-environment relationships. Heat vulnerability studies have documented that minorities are overexposed to environmental hazards, including extreme heat. In California, for example, communities of color have lower MHHIs, and fewer are homeowners (Morello-Frosch et al., 2002). They also have limited access to resources, support, information regarding heat protection actions, and mobility that could reduce their vulnerability (Wolf & McGregor, 2013).

There is, however, a lack of consistency among variables used to measure heat exposure (climatic and built-up environment) and vulnerability (health, demographics, and SES). A heat vulnerability index that considers the nuances of an area (e.g., ethnic/racial differences by origin), including its historical and institutional context (e.g., racial segregation), is required to identify individuals susceptible to extreme heat and that would facilitate place-to-place comparisons. The political and economic forces that lead to that environmental inequality must be examined to understand how institutional discrimination interacts with larger structural forces (Morello-Frosch et al., 2002). Studies that attempt to explain the geographical distribution of heat risk must emphasize the historical roots that caused today's health disparities among communities of color (Ford & Airhihenbuwa, 2010).

There are also different levels of exposure to environmental racism. Thus, the level of heat exposure and perception will vary, to a certain extent, by age, gender, socioeconomic status among races (high-income Hispanic/Latino vs. high-income White), within races (e.g., high-income South American vs. low-income Mexican), immigration status, length of time in the US, health care access, and geographical location (Hispanic/Latino in LA vs. Hispanic/Latino in Vermont). Intersectionality is a theoretical framework suggesting multiple social categories intersect at the individual level (Bowleg, 2012), which may affect their heat vulnerability. The intersection of race and income was studied in the context of fluid intake of individuals (Brooks et al., 2017). Results showed Hispanic/Latino heritage and non-Hispanic Black people in the US are higher than for non-Hispanic Whites, while lower-income adults had a higher risk of inadequate hydration than higher-income adults. Heat studies that consider how differences in the built environment, individual bodies (e.g., children, elderly, people with mobility constraints, pregnant women), and social characteristics (e.g., race, gender, socioeconomic status) intersect are necessary to understand how these moderate heat experiences, including physiologically and behavioral responses (Hamstead, 2021).

Conclusion

As the urban population increases, the built environment expands and replaces natural land cover, human-made surfaces, and heat-emanating activities will continue exacerbating the SUHI formation with deleterious health effects on local populations, particularly among the vulnerable. The spatial identification of these at-risk areas is paramount for implementing effective mitigation and adaptation actions to reduce heat stress. The study of population exposure, however, involves multi-temporal and multi-spatial human and environmental processes and, thus, renders some sensors insufficient to understand these human-environment interactions.

The present study suggests an exploratory methodology to explore the potential association of LST-NDVI/ET values and race/ethnicity-MHHI to evaluate the human-environment spatial relationships between heat exposure and evaporative cooling for each group, as well as differences in the built environment. The physical environment was assessed from a temporal and spatial perspective via the acquisition of MODIS and ECOSTRESS. The built environment was evaluated with the use of the LCZ framework, while the socioeconomic environment was assessed with the use of the MHHI and Hispanic/Latino (any race) variables acquired from the USGS ACS 2017-2021 census data.

Significant results from this effort show that for the urbanized area of SCC, a positive summer-daytime LST trend of 0.11°C per year but a weak LST trend for corresponding nighttime hours (0.04°C per year). A negative relation between summer-daytime LST and NDVI values was found, reflecting the cooling effect of vegetation on LST higher than for nighttime hours. During winter, a positive LST-NDVI relationship was found, particularly for daytime hours, given that the low photosynthesizing of vegetation provides no cooling, thus not regulating LST values. A strong negative relationship was also found for ECOSTRESS-derived summer LST and ET values. The spatial distribution shows minimum LSTs and maximum ET values in high-income communities like Los Altos Hills, Los Altos, and Palo Alto, where a low percentage of Hispanic/Latino populations is found. Maximum ET values and minimum LSTs primarily occurred in low-income neighborhoods of San Jose, with a maximum concentration of Hispanic/Latinos. Low MHHI populations ($117,081) and Hispanic/Latinos most likely exist within LCZ 3, which exhibits the highest mean LST (27.7°C).

Future efforts should overcome some of the limiting assumptions required for the current effort, e.g., the use of monthly mean LSTs instead of hourly 2-m observations. While the latter are

consistent with local government heat warnings, they only provide limited spatial coverage. A technique thus must be developed to combine the 2-m values, satellite-derived LST distributions, and fine-scale 2-m values from Weather Research and Forecasting model simulations. Surrounding vegetation differences within LCZ classes must also be considered to better establish LCZ-LST relationships. Future multidisciplinary efforts should also consider an intersectionality framework for the study of heat vulnerability, as well as differences between and within race/ethnic groups, to predict future heat risks under various climate change scenarios. The identification of areas at high risk of heat stress would facilitate the targeting of public health programs and other mitigation strategies, such as the increase of urban vegetation or the establishment of cooling centers (Widerynski et al., 2017), which could provide a cool environment for vulnerable individuals in Santa Clara County and elsewhere experiencing similar intra-urban human-environment phenomena.

CHAPTER 3. ENVIRONMENTAL INJUSTICE AMONG HISPANICS IN SANTA CLARA, CALIFORNIA: A HUMAN-ENVIRONMENT HEAT VULNERABILITY ASSESSMENT

Introduction

The United Nations projects that by 2030, 60.4% of the world will be urbanized (UN-Habitat, 2020). As cities expand, the urban population will increase energy consumption, greenhouse gas emissions, and environmental degradation. Exposure of cities to weather hazards, like heat waves, will increase and intensify with global warming. Although heat waves are a regional phenomenon, localized heat-stress illnesses (e.g., cramps, heat exhaustion, and heat stroke, leading to thermoregulatory malfunction, organ system failure, and death) are generally observed in urban areas (Grady, 2012). These adverse health outcomes primarily occur in areas with a high concentration of low-income individuals, a majority of racial/ethnic minorities, and those living in poor housing conditions (e.g., inadequate housing materials) and poverty are more likely to suffer from the adverse effects of a changing climate (Rosenthal et al., 2014). Racial and ethnic minorities, who have historically lived in segregated and densely populated neighborhoods, are thus expected to experience higher heat exposure, which will increase heat-related deaths (Jesdale et al., 2013); consequently, the problem is framed as environmental injustice (Mitchell & Chakraborty, 2015).

In the United States, there is substantial evidence that a high proportion of racial and ethnic minorities reside within low-income neighborhoods deprived of green areas and limited access to cooling resources (Gronlund, 2014). On average, non-Hispanic Whites tend to live in census tracts with lower temperatures than census tracts with a majority of people of color, thus reflecting heat exposure as an unevenly distributed environmental burden (Hsu et al., 2021). In Portland, Oregon, mean temperatures during a 2014 heat wave event were negatively correlated with the percentage of non-Hispanic Whites (-0.1515°C for every 10% increase) but positively correlated with the percentage of African Americans and Hispanics (+0.3471°C for every 10% increase), at a US census block group level (Voelkel et al., 2018).

Historical uneven urban development patterns, discriminatory housing realtors, bank loan lending, and zoning practices created racial and ethnic segregated neighborhoods with poor housing conditions and limited green infrastructure, which have persisted and continue to expose them to higher ambient temperatures (Uejio et al., 2011). A study of 108 previously redlined

neighborhoods showed temperatures of almost 7°C higher in redlined areas than in non-redlined ones (Hoffman et al., 2020). In Richmond, Virginia, previously redlined neighborhoods had the highest rates of heat-related emergency room visits, as the number of visits increased by 2.5% for every one-degree increase in ambient temperature (Plumer & Popovich, 2020). In Phoenix, a higher number of heat distress calls have shown to be associated with neighborhoods with a high proportion of Black, Hispanic, linguistically, and socially isolated residents, while in Philadelphia, neighborhoods with high heat mortality were more likely to have low housing values and a higher proportion of Black residents (Uejio et al., 2011).

There is also an association between race, socioeconomic status, and the ability of a population to cope with the heat as it determines their access to mitigating resources (e.g., air conditioning systems). A study performed at a city level indicated that, in four US cities, the prevalence of central air conditioning (A/C) was lower among Black households and likely correlated with socioeconomic characteristics (O'Neill, 2005). In the United States, neighborhoods with a high proportion of minority residents have been associated with low-income status due to institutionalized racism in the form of redlining and zoning ordinances (Gronlund, 2014). In Phoenix, neighborhoods with a high proportion of Hispanic residents, mainly of Mexican origin, were associated with low-income status (Jenerette et al., 2007), low educational attainment, and low use or availability of A/C systems (Harlan et al., 2013).

High levels of segregation result in the isolation of a minority group from amenities, opportunities, and resources that affect social and economic well-being (Massey & Denton, 1989) and, thus, their ability to cope with heat exposure. Highly segregated areas with higher proportions of non-White and low-income residents tend to experience more significant cumulative environmental hazards (e.g., toxic release facilities, noise, heat; Casey et al., 2017; Morello-Frosch et al., 2002). There is, however, a variation in heat-related outcomes by race. During a heat wave in California, Latinos reported increased cardiac-related illnesses, African Americans had acute renal failure and electrolyte imbalance, and Asians had significantly elevated emergency visits for respiratory disorders (Green et al., 2010). Measures of residential segregation are necessary to understand the origins and persistence of environmental health disparities (Morello-Frosch & Lopez, 2006).

Residential segregation is the degree of separation between two or more groups within an urban environment (Massey & Denton, 1988). Residential segregation indices are an objective

measure of racial and economic segregation that could serve as proxies for structural racism (Chambers et al., 2019). There are five key dimensions of residential segregation: evenness, exposure, concentration, centralization, and clustering (Massey & Denton, 1998; US Census Bureau, 2000). The Index of Dissimilarity is a common measure of racial evenness/unevenness across the urban environment and is often used in environmental justice studies. Baxter (2010) used the Index of Dissimilarity (range, 0 to 1) to estimate the degree of ethnic residential segregation in Santa Clara, CA, by block groups in 1990 and 2000. Results showed higher segregation levels between Whites and Hispanics (0.54) than between Whites and Asians (0.45). Comparisons of 1990 and 2000 results showed an increase in residential segregation with fewer White residents in Asian and Hispanic neighborhoods, from 43 to 23% and from 32 to 17%, respectively. The number of White residents in White block groups remained stable (82%). The proportion of Hispanic residents in Asian neighborhoods decreased (16 to 13%), and the proportion of Asians in Hispanic areas increased (12 to 14%). As of 2010, Latinos in Santa Clara County showed the highest levels of segregation (Menendian & Gambhir, 2018).

Levels of segregation, however, vary among Hispanics by origin (Bean & Tienda, 1987). For example, Mexicans tend to live in isolated inner-city ghettos, denying them equal access to schooling, jobs, and health care compared to other Hispanic groups (National Research Council, 2001). The literature is unclear if Hispanics are at higher risk of hospital admissions, which may be related to the differences among Hispanics in socioeconomic status, origin, nativity, and length of time in the United States (Do et al., 2017). Some studies suggest a lower heat health effect, whereas others have found an association between segregation and health outcomes, positioning Hispanics at higher heat risk (Gronlund, 2014). These adverse effects are most likely cardiac-related illnesses, as it has been the primary reported outcome among Latinos (Green et al., 2010).

The differences within Hispanic subgroups may expose them to unique environmental hazards that could contribute to higher morbidity, resulting in widening health disparities. Cubans, for example, have a college graduation rate three times higher than Mexicans, while Puerto Ricans have higher high school graduation rates than Mexicans (Williams et al., 2010). The spatial distribution of land surface temperatures and vegetation, income disparity, the cultural diversity of the population (multiracial, multinational, multilingual, multicultural), and the spatial segregation patterns increase the complexity of assessing heat vulnerability.

The current effort applied existing and fully developed metrics of socioeconomic status and racial segregation to spatially identify heat-vulnerable neighborhoods. It evaluated the relationship between race/ethnicity, the environment (e.g., temperature exposure), socioeconomic status, and health outcomes in Santa Clara County (SCC), CA. The differences among Hispanic/Latinos by origin (Mexican, Central American, and South American) were emphasized. The Hispanic population, as of 2016, was the most significant ethnic or racial minority in the United States, and by 2060, they will represent 27.5% of the total population (Vespa et al., 2020). The findings from this study inform other coastal as well as inland cities with high Hispanic populations on the variability of temperature exposure and health outcomes.

Data and Methods

The current methodology combined Landsat 8 satellite data, the US Census Bureau-American Community Survey (ACS) 2015-2019, Five-Year Estimate, and the PLACES Dataset to determine the distribution of heat-vulnerable populations and health outcomes in SCC. The first step assessed the physical environment via the calculation of the Land Surface Temperature (LST) and Normalized Difference Vegetation Index (NDVI). The second part evaluated the social environment with the use of the Modified Darden-Kamel Composite Socioeconomic Index (CSI) to determine the spatial variability of SES (Darden et al., 2010). The Index of Dissimilarity (D; Massey and Denton, 1988) was calculated to determine levels of segregation within the Hispanic/Latino population. The third part evaluated levels of segregation and SES measures in explaining the variance in the health outcomes among Hispanics, with the use of PLACES data acquired by the Center for Disease Control and Prevention (CDC). The combination of these assessments resulted in a comprehensive human-environment approach for health exposure evaluation by which to define environmental injustice. Details are provided below.

Physical Environment

Heat exposure was determined from LST and NDVI values, calculated from Landsat 8 imagery, accessed via the freely available (Google) Earth Engine website for 2015-2019, in accordance with the ACS (Five-Year Estimates) dataset. Landsat 8, with a time range from 1100-1115 Central Standard Time (CST), has a 30-m spatial resolution in the Visible, Near-Infrared (NIR), and Shortwave Infrared (SWIR) bands and 100-m resolution in the thermal infrared (TIR-1 and TIR-2) bands. The atmospherically corrected TIR and surface reflectance (SR) bands were resampled and made available at a 30-m resolution in Earth Engine. The dataset also included a

Quality Assessment (QA) band, which provides per-pixel cloud, shadow, water, and snow information.

The procedure to retrieve LST and NDVI values first involved a per-pixel filter applied to Landsat 8 images, using its QA band to mask cloudy and cloud shadow pixels from the SR bands. The remaining pixels were then used to calculate LST distributions using the brightness temperature derived from the TIR-1 band. The NIR and Red bands were also utilized to perform an emissivity correction of LST via the calculation of NDVI values (Avdan & Jovanovska, 2016; Weng et al., 2004). The emissivity-corrected LST values were then converted from °K to °C and averaged for the 5-year study period. The averaged values reduce the effects of anomalously wet or dry years and seasonal vegetation and soil moisture changes, which could impact the calculated LST and NDVI values.

The National Land Cover Dataset (USGS, 2019) was used to extract NDVI and LST pixels that corresponded with values classified as developed (21-24), as shown in Figure 1. This process filtered non-populated locations and allowed for the accurate calculation of mean LST and NDVI values per census tract. The extraction of these values reduced the elevation and vegetation effects, especially from the non-developed area of the hills. The ArcGIS Zonal Statistics tool was then used to calculate the mean LST and NDVI values at the census tract level to obtain the mean value per census tract.

Socioeconomic Environment

Socioeconomic and race/ethnicity data used to calculate the Modified Darden-Kamel CSI and the Index of Dissimilarity, respectively, were acquired at the census tract level for SCC from the US Census Bureau, American Community Survey (ACS) 2015-2019 (US Census Bureau, 2020).

*Modified Darden-Kamel CSI***.** The Modified Darden-Kamel CSI measures SES for the entire population in a study area and considers nine variables: 1) percentage of bachelor's degrees, 2) median household income, 3) percentage of managerial and professional status positions, 4) median value of dwelling, 5) median gross-rent of dwelling, 6) percent of homeownership, 7) incidence of low income (-), 8) unemployment rate (-), and 9) percent of households with vehicle (Darden & Rubalcava, 2018). The formula to calculate the Modified Darden-Kamel CSI is:

$$CSI_i = \sum_{j=i}^{k} \frac{V_{ij} - V_{jDMA}}{S(V_{jDMA})} \; ; \qquad (1)$$

where V_{ij} is the jth SES variable for a given census tract *i*, V_{jDMA} is the mean of the *j*th variable in the study area, and *S* (V_{jDMA}) is the standard deviation of the jth variable in the study area. Census tracts with a higher socioeconomic position were assigned a higher score. These scores were then divided into five degrees (or classes) by use of the Dalenius & Hodges (1959) stratification method, which minimizes variation within each group. This process was conducted with the use of the stratification library and implemented in RStudio© (version 4.1.2).

Index of Dissimilarity. The Index of Dissimilarity (D; range 0 to 100) assigns higher values to neighborhoods (census tracts) with a high degree of residential segregation. It was used to evaluate the levels of segregation between non-Hispanic Whites and the Hispanic/Latino population and within Hispanic subgroups, including Mexican, Central American, and South American. It calculates the proportion of Group A that would have to change their neighborhood (or census tract) to achieve an even distribution with Group B (Massey and Denton, 1988, p. 284). High D values reflect a high degree of residential segregation. The formula to calculate D is:

$$D = \left(\frac{1}{2}\sum_{i=1}^{k}|x_i - y_i|\right) \qquad (2)$$

where x_i is the percentage of the total ethnic minority population in SCC (e.g., Hispanic/Latino) in census tract *i*, y_i is the percentage of the total non-minority population in SCC (e.g., non-Hispanic White) living in the same census tract *i*, and k is the total number of tracts in the study area. The absolute differences between these percentages by census tract were then divided into five degrees (or classes) of segregation by use of the Dalenius & Hodges (1959) stratification method to minimize variations within each group, also done in RStudio© with the implementation of the stratification library. This process allowed us to visualize the spatial distribution of Hispanics in the study area. One-half of the sum of these absolute differences results in segregation measurement (D) for the study area.

Health Outcomes. The PLACES 2022 release project data, acquired via the CDC at the census tract level, was used to evaluate health outcomes by SES and segregation levels within Hispanic subgroups (Mexican, Central American, and South American). In partnership with the Robert Wood Johnson Foundation, the CDC provides model-based estimates of health outcomes, unhealthy behaviors, and health prevention measures for urban areas across the United States. Data sources used to generate the 2022 dataset include the Behavioral Risk Factor Surveillance System

(BRFSS) 2020 or 2019 data, Census Bureau 2010 population estimates, and American Community Survey (ACS) 2015–2019 estimates.

Spatial regressions were conducted in the GeoDa software (Anselin et al., 2006) to determine the relationship between environmental and racial measures with chronic health outcomes (e.g., the prevalence of asthma, coronary heart disease) and health status (e.g., current lack of health insurance) for adults (≥18 years) while accounting for spatial effects. The level of LST, segregation, and SES were included as potential predictors of spatial variability in health outcomes. LST was measured on a continuous scale from 7.40 (base) to 56.1°C. The percentage of Hispanic/Latino population per census tract (%) was also measured on a continuous scale from 0 (base) to 100. SES (DK-CSI) was measured on an ordinal scale from VL-SES (base) to VH-SES. A total of 45 models were performed: one per health outcome per racial group assessed.

Human-Environment

Mean LST and NDVI values at the census tract level were overlayed with the Modified Darden-Kamel CSI and Index of Dissimilarity (D) results to evaluate the physical and social environmental risks and study human-environment interactions between heat exposure, socioeconomic status, and race/ethnicity. LST and NDVI values per SES first inform about differences in environmental exposure between the five classes. Mean LST and NDVI values were then compared with the D values to evaluate the differences in environmental exposure by the degree of segregation for each considered race/ethnic group.

The Shapiro-Wilk test (Shapiro & Wilk, 1965) determined LST and NDVI values as non-normal; thus, Kruskal-Wallis tests (Kruskal & Wallis, 1952) were performed to determine how LST and NDVI values differ by SES and ethnicity, with 95% Confidence Intervals. The Univariate Moran's I Index (Anselin, 1995) measured global spatial autocorrelation of the LST and Modified Darden-Kamel CSI values, while the Bivariate Local Moran's I (Anselin et al., 2002) provided a local spatial autocorrelation measure between these two variables. All analyses used first-order Queen contiguity (Anselin & Rey, 2014) to determine neighboring census tracts.

Results

Physical Environment

Landsat 8-derived mean LST distributions (Figure 13) from 2015-2019 for the corresponding developed classes, per the NLCD, show values ranging from 18.2 to 37.9°C, with an average of 28.9°C for the study area. Minima values are mainly found in southeast Los Gatos,

Saratoga, and Los Altos Hills, while maxima values are in East San Jose and South of the Downtown area. Above-average values are found in Santa Clara, Campbell, Cupertino, and Sunnyvale, whereas below-average LSTs are recorded in Palo Alto, Mountain View, Los Altos, and Stanford. Minimum LST values are also along the Guadalupe River and Coyote Creek corridors.

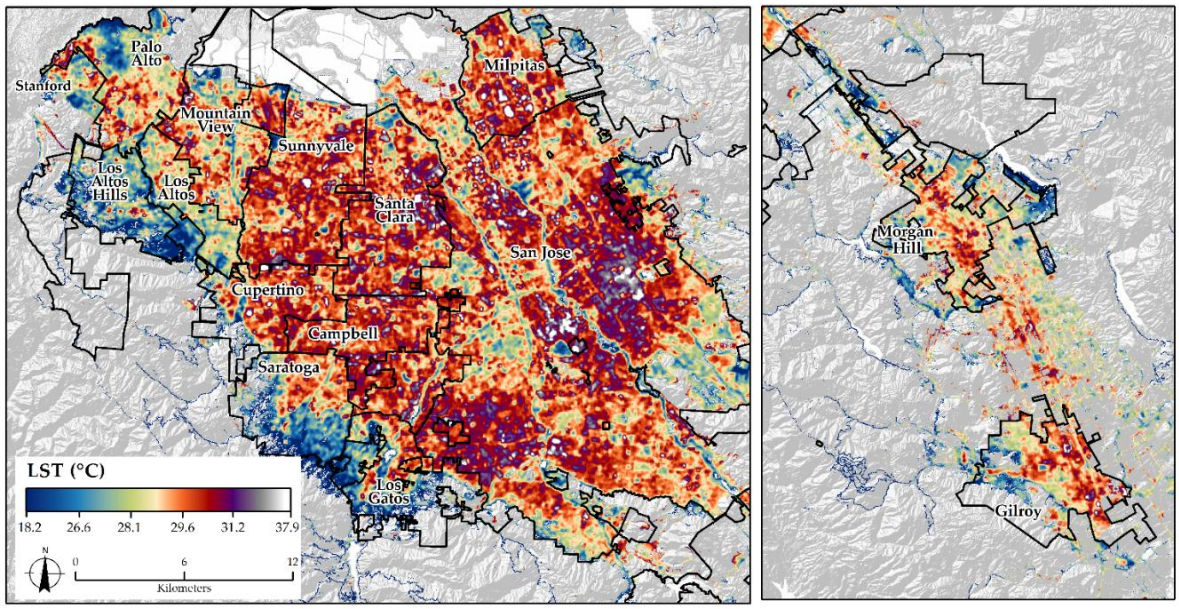

Figure 13. Land Surface Temperature (LST, °C) distribution for 2015-2019.

Landsat 8-derived mean NDVI distributions for 2015-2019 (Figure 14) range from -0.45 to 0.89, where higher values indicate greenness or photosynthetic activity. Maximum values are found in southeast Los Gatos, Saratoga, and Los Altos Hills, corresponding with vegetated mountainous areas and golf courses dispersed throughout the study area. Minimum values are primarily located in the Downtown and northern SCC, corresponding with industrial sites and airports. Below-average values (<0.35) are found in the East San Jose areas and along major transit corridors (e.g., main boulevards and highways). Above-average values (>0.35) are found in Palo Alto, Los Altos, and the southwest San Jose Downtown area.

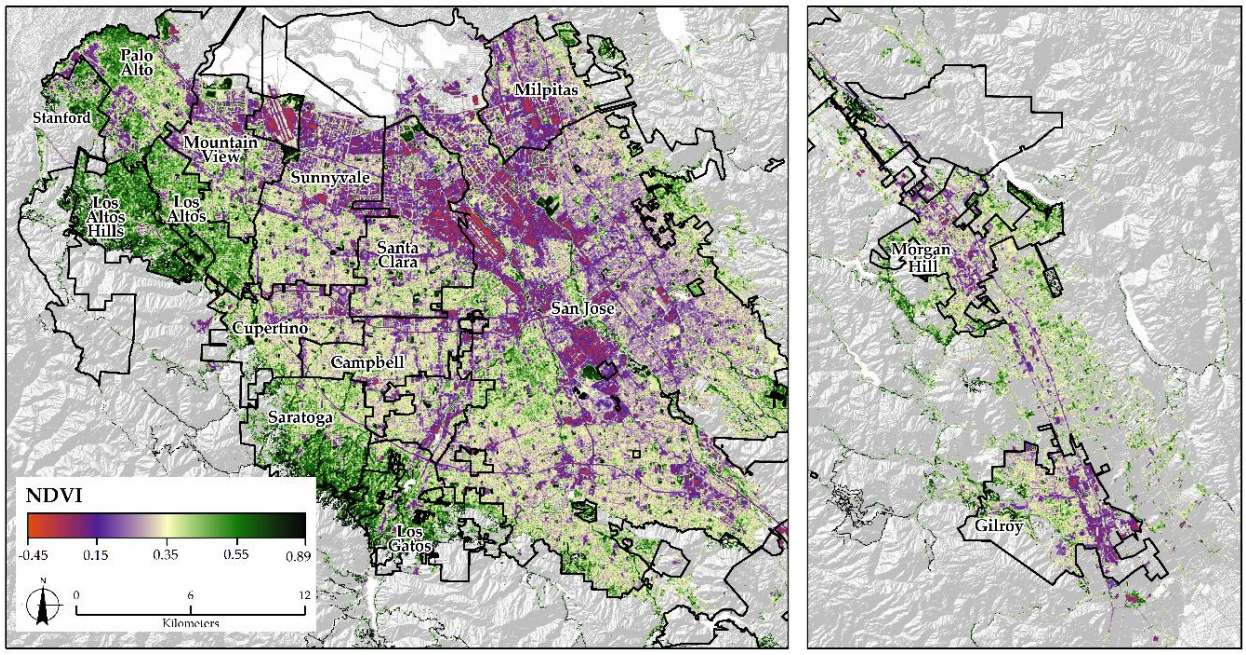

Figure 14. Normalized Difference Vegetation Index (NDVI) distribution for 2015-2019.

Socioeconomic Environment

Modified Darden-Kamel CSI. There are significant disparities between the populations living in Very High-(VH) and Very Low-(VL) socioeconomic status (SES) census tracts in Santa Clara County. Results (Table 2) show a positive linear trend for all variables except for poverty, which increases with decreasing SES, and unemployment, which shows minor variation. The Medium-(M) SES is, however, smaller than the overall mean value in SCC for median household income (MHHI), median house value, and homeownership, suggesting a heavier weight on those variables in the distribution of wealth in SCC.

Neighborhoods with VH-SES have, on average, a median income of $205,06, nearly three times that of neighborhoods with VL-SES, and both higher than the 2019 national median household income of $69,560 (Shrider et al., 2021). VL-SES households spend 28% of their median annual household income on rent ($1,694 per month), almost twice that of VH-SES households ($3,198 per month). Households with a VH-SES are mostly homeowners (82%) with median house values of 1.8 million, further exacerbating the gap between the VH-SES and VL-SES groups. Although vehicle ownership is above 90% for all groups, VH-SES neighborhoods have higher vehicle ownership than VL-SES.

Similar values among groups are found for unemployment, with values that range between 4.1 to 4.3, with minimum ones for VH-SES that increase as SES decreases, except for the M-SES

class, with maximum unemployment of 4.4%. Despite similar unemployment levels, the percentage of families living in poverty in VL-SES is three times that of those with a VH-SES. The percentage of professional and managerial workers is similar to those with bachelor's degrees or higher education, with lower values for VL-SES areas, 28 and 31%, respectively, and increasing with SES to a maximum of 79% (bachelor's degree) and 77.1% (professional and managerial workers) for VH-SES areas.

Table 2. Mean value, as well as its corresponding minimum and maximum (in parentheses), per SES for each considered variable used to calculate the Modified Darden-Kamel (DK) CSI.

SES	VL	L	M	H	VH	Mean SCC
Number of census tracts	62	85	91	84	50	372
DK-CSI	-6.54 (-13.0, -4.7)	-2.87 (-4.5, -1.5)	-0.04 (-1.5, 1.3)	3.06 (1.4, 5.0)	7.92 (5.0, 11.0)	-5.59
Bachelor's degree or higher education (%)	27.9 (8.4, 95.7)	39.8 (7.9, 89.9)	52.4 (10.3, 89.6)	63.7 (29.1, 90.6)	78.9 (56.2, 91.5)	51.5
MHHI (in thousands of $)	73 (26, 116)	102 (31, 141)	125 (45, 167)	158 (98, 240)	205 (110, 250+)	129
Professional and managerial workers (%)	31.2 (10.9, 72.3)	44.3 (17.9, 76.4)	55.4 (15.0, 89.2)	65.5 (35.0, 86.3)	77.1 (57.7, 86.9)	54.0
Median house value (in thousands of $)	647 (122, 1046)	794 (148, 1659)	992 (239, 2000+)	1,280 (655, 2000+)	1,756 (1070, 2000+)	1,060
Median monthly rent ($)	1,694 (686, 2596)	2,038 (810, 3500+)	2,389 (1357, 3303)	2,679 (818, 3500+)	3,198 (1945, 3500+)	2,363
Home-ownership (%)	38.9 (2.0, 80.9)	52.2 (0.0, 89.1)	58 (2.5, 92.4)	67.7 (0.4, 97.3)	82.0 (54.4, 95.3)	58.9
% Poverty	7.8 (0, 27.3)	6.3 (0.8, 37.5)	4.3 (0.0, 14.8)	3.5 (0.0, 12.8)	2.5 (0.0, 9.6)	4.9
Unemployment (%)	4.3 (0.0, 9.3)	4.3 (0.0, 12.5)	4.4 (0.9, 16.2)	4.1 (0.9, 10.0)	4.1 (1.3, 8.2)	4.2
Vehicle ownership (%)	90.3 (66.1, 99.5)	93.9 (61.3, 100)	95.6 (75.5, 100)	96.6 (88.4, 100)	98 (93.5, 100)	94.9

Distributions of the Modified Darden-Kamel CSI results at the census tract level (Figure 15) show neighborhoods with VH-SES in southwest SCC in Palo Alto, Los Altos, Los Altos Hills, Cupertino, Saratoga, Monte Sereno, and Los Gatos, while VL-SES ones are in Downtown and East San Jose, as well as in the southeast cities of Morgan Hill and Gilroy. Stanford University is classified as having a VL-SES and is considered an outlier. Areas with Low (L)-SES surround

those neighborhoods with VL-SES. Almost 25% of the census tracts are classified as areas with M-SES and 23% with H-SES. Of the total population, 12% live within neighborhoods with VH-SES, 24% with H-SES, 25% with M-SES, 22% with L-SES, and 17% with VL-SES.

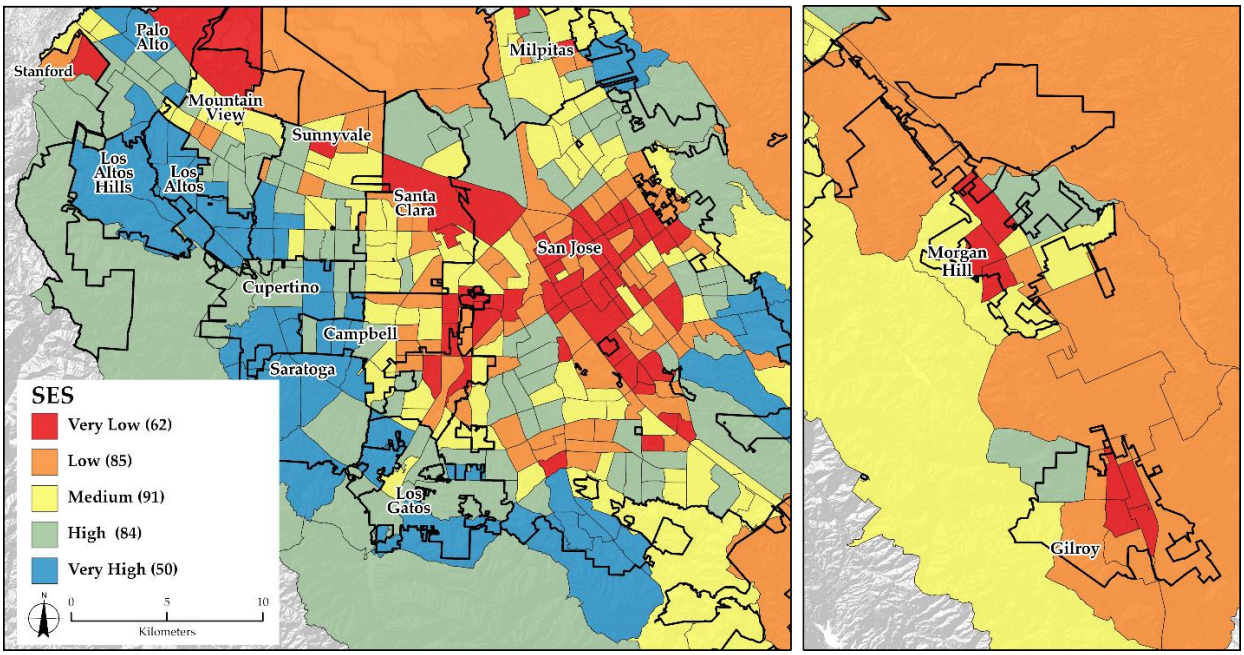

Figure 15. Spatial distribution of socioeconomic status (SES) and number of census tracts per class calculated per the Modified Darden-Kamel Composite Socioeconomic Index (CSI).

The share of the Hispanic/Latino population and within Hispanic subgroups, including Mexican, Central American, and South American, by socioeconomic status in SCC (Table 3) shows an inverse relationship between SES for Hispanic/Latino, Mexican, and Central American groups. A similar proportion of non-Hispanic Whites and South Americans is found for H-, M-, and L-SES. A higher proportion of South Americans is, however, located in the VL-SES group (13.4%) than of non-Hispanic Whites (9.9%). The reverse occurs for VH-SES groups, with 9.1% of South Americans and 16.1% of non-Hispanic Whites belonging to this group. Between subgroups, South Americans show small disparities between VH- and VL-SES (9.1 to 13.4%), followed by Central Americans (3.6-25.3%), with the greatest difference for Mexicans (1.6 to 34.9%).

While 16% of the non-Hispanic White population lives within a VH-SES neighborhood, only 1.6% of the Mexican population lives in a VH-SES area, followed by Central Americans (3.6%) and South Americans (9.1%); these last two with values higher than that of the general Hispanic/Latino population (2.3%). Mexicans are, however, overrepresented in L- and VL-SES

neighborhoods, with 32.6 and 34.9% of their population in these groups, respectively. Central Americans have a lower share of their population in the L- and VL-SES (31.1 and 25.3%). As the SES decreases for all Hispanic/Latino groups, the percentage of the population per class increases, except for South Americans, who have the lowest percentage of their population within an L- and VL-SES neighborhood, a similar trend to that of the non-Hispanic White population.

Table 3. Total population by ethnicity and socioeconomic status.

	Hispanic/ Latino		Mexican		Central American		South American		Non-Hispanic White	
SES	n	%	n	%	n	%	n	%	n	%
VH	11,362	2.3	6,452	1.6	1,084	3.6	1,613	9.1	98,162	16.1
H	60,095	12.2	44,689	11.0	3,788	12.6	4,603	26.0	177,574	29.2
M	104,023	21.2	81,045	19.9	8,235	27.4	4,921	27.8	156,308	25.7
L	155,147	31.6	132,561	32.6	9,350	31.1	4,202	23.7	115,979	19.1
VL	160,351	32.7	142,189	34.9	7,588	25.3	2,383	13.4	59,880	9.9

Index of Dissimilarity. Results of the Index of Dissimilarity (D) by census tract were divided into five classes, per the Dalenius and Hodge stratification method. The descriptive statistics (Table 4) show the mean value, as well as its corresponding minimum and maximum values (in parentheses) per level of segregation between Hispanics and non-Hispanic Whites and among Hispanics/Latinos by origin. The spatial distribution of the results (Figure 16) shows that the highest levels of residential segregation are within the Central American community (Figure 16c), with a D of 52.7. Mexican neighborhoods (Figure 16b) also have high residential segregation (D = 51.4) and are primarily clustered in the East San Jose area. South Americans (Figure 16d) show the least amount of residential segregation (D = 42.0), even lower than the general Hispanic/Latino population (D = 47.4).

Table 4. Mean D value, as well as its corresponding minimum and maximum (in parentheses), per level of segregation, based on the Index of Dissimilarity.

Segregation (D)	Hispanic/Latino	Mexican	Central American	South American
VH	0.72 (0.55, 0.96)	0.92 (0.82, 1.03)	0.96 (0.62, 1.69)	0.87 (0.54, 2.08)
H	0.44 (0.36, 0.54	0.73 (0.62, 0.79)	0.47 (0.39, 0.59)	0.43 (0.34, 0.53)
M	0.28 (0.22, 0.36)	0.49 (0.41, 0.62)	0.31 (0.25, 0.39)	0.26 (0.20, 0.33)
L	0.15 (0.10, 0.22)	0.29 (0.21, 0.40)	0.18 (0.12, 0.25)	0.13 (0.08, 0.20)
VL	0.05 (0.10, 0.22)	0.10 (0.21, 0.40)	0.06 (0.12, 0.25)	0.04 (0.08, 0.20)

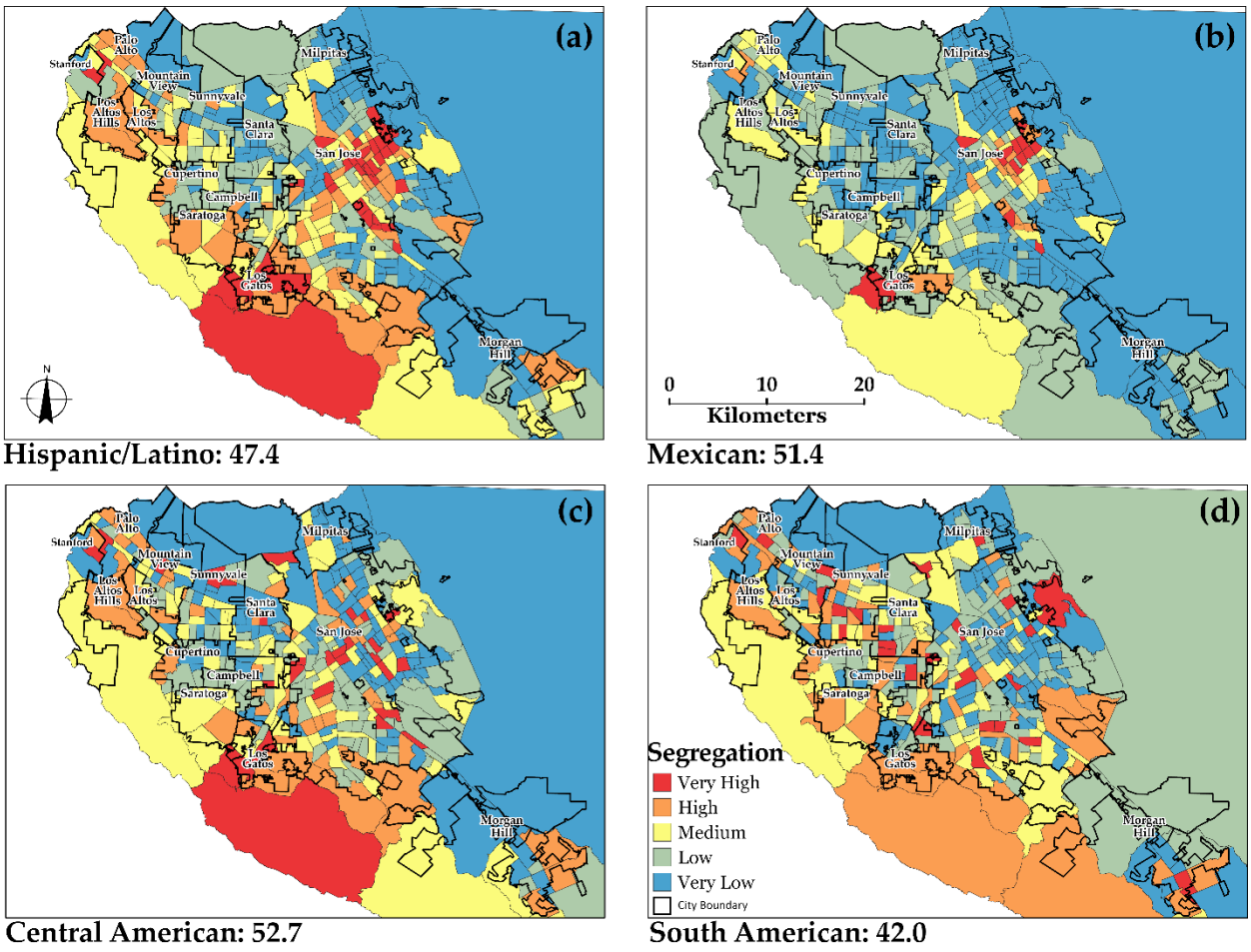

Hispanic/Latino: 47.4 **Mexican: 51.4**

Central American: 52.7 **South American: 42.0**

Figure 16. The spatial distribution and Index of Dissimilarity of (a) Mexicans, (b) Central Americans, (c) South Americans, and (d) the Hispanic/Latino population in Santa Clara County.

Human-Environment

The LST and NDVI relation with SES shows that as SES decreases, mean LST values increase from 28.5 to 29.9°C (Figure 17). The reverse occurs for NDVI values and SES, which decrease from 0.41 to 0.27 as SES decreases. Only VH- and H-SES areas exhibit LSTs lower than the SCC average (29.4°C). VH- and H-SES census tracts exhibit values above the SCC average (0.33). Kruskal-Wallis results show that LST and NDVI values are statistically significantly different for at least one of the groups (H = 53.44, df = 4, p-value = 0.00; H = 117.89, df = 4, p-value = 0.00, respectively). Pairwise comparisons show that LST values vary between groups except between M-and L-SES and L-and VL-SES.

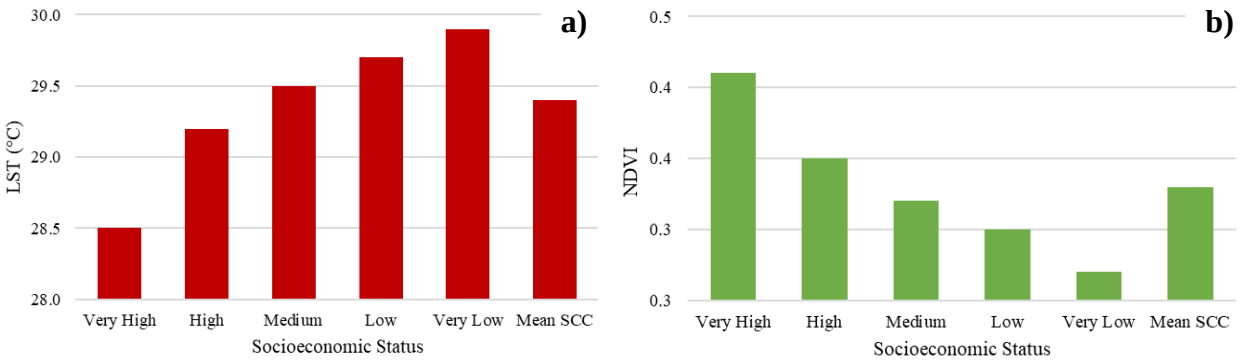

Figure 17. a) Mean LST and b) NDVI by Socioeconomic Status (SES) per the Darden Kamel Composite Socioeconomic Index.

Mean LST and NDVI results combined with stratified D values (Table 5) show a broader range of mean LST values for Mexicans than for non-Hispanic Whites (29.3-30.2°C vs. 29.2-29.5°C). Areas with a VH concentration of the Hispanic/Latino population, particularly Mexicans, have a higher LST than areas with a VL concentration of the Hispanic/Latino population (29.8°C vs. 29.4°C). Minimum LST (28.5°C) and maximum NDVI (0.37) values are observed for areas with an H concentration of South Americans. Minimum NDVI values are observed in areas with a VH concentration of Hispanic/Latino and Mexican populations (0.30 and 0.29, respectively), whereas maximum values are in areas with a H-Hispanic/Latino and M-concentration of Mexican populations (0.37 and 0.36, respectively).

Kruskal-Wallis results show that only LST values are different for at least one group ($H = 14.22$, $df = 4$, p-value = 0.007), while no statistically significant difference is found for NDVI values ($H = 8.221$, $df = 4$, p-value = 0.084). Pairwise comparisons show no statistically significant differences in LST values between areas with a VH-Concentration of South Americans and VH-Concentration of Central Americans and between South Americans and non-Hispanic Whites. Significant differences in LST values are found between Mexicans and South Americans and Mexicans and non-Hispanic Whites.

Table 5. Mean LST, NDVI, and minimum and maximum values (in parentheses) by the level of segregation for Hispanic/Latino, Mexican, Central American, South American, and non-Hispanic Whites.

	Hispanic/Latino		Mexican		Central American		South American		Non-Hispanic White	
Segregation	LST	NDVI	LST	NDVI	LST	NDVI	LST	NDVI	LST	NDVI
VH	29.8 (22.9, 31.4)	0.30 (0.20, 0.67)	30.2 (26.2, 31.4)	0.29 (0.21, 0.54)	29.4 (22.9, 31.3)	0.32 (0.22, 0.67)	29.5 (28.3, 31.4)	0.32 (0.25, 0.42)	29.5 (27.8, 31.1)	0.34 (0.18, 0.67)
H	29.1 (25.4, 31.8)	0.37 (0.17, 0.56)	30.0 (27.8, 31.1)	0.30 (0.20, 0.48)	29.2 (25.4, 31.4)	0.35 (0.17, 0.56)	28.8 (22.9, 30.9)	0.37 (0.16, 0.67)	29.2 (22.9, 31.3)	0.34 (0.17, 0.56)
M	29.3 (24.5, 31.1)	0.35 (0.16, 0.63)	29.1 (22.9, 31.8)	0.36 (0.17, 0.67)	29.2 (24.5, 31.1)	0.34 (0.18, 0.63)	29.4 (24.5, 31.3)	0.33 (0.17, 0.63)	29.3 (24.5, 30.9)	0.33 (0.17, 0.63)
L	29.6 (27.8, 30.9)	0.31 (0.18, 0.44)	29.3 (24.5, 31.1)	0.35 (0.16, 0.63)	29.5 (26.4, 31.8)	0.32 (0.16, 0.53)	29.6 (26.4, 31.1)	0.31 (0.17, 0.53)	29.5 (25.4, 31.8)	0.32 (0.16, 0.46)
VL	29.4 (27.5, 30.8)	0.31 (0.18, 0.46)	29.5 (27.5, 30.9)	0.31 (0.18, 0.46)	29.6 (27.5, 31.1)	0.31 (0.17, 0.46)	29.6 (26.6, 31.8)	0.31 (0.19, 0.51)	29.5 (27.5, 30.8)	0.31 (0.18, 0.44)

The Univariate Moran's I Index results show 0.610 and 0.581 values for the LST and Modified Darden-Kamel CSI measures, respectively, with a p-value < 0.05; thus, values for both variables are clustered. The spatial association between these two variables, explored via the Bivariate Local Moran's I, shows a value of -0.324 (p-value <0.05). Results indicate a negative correlation between LST and SES (Figure 18). High-high clusters of SES and LST values are located within neighborhoods with large low-rise and medium-rise buildings, with a medium concentration of Hispanic/Latinos, specifically South Americans. Low-low clusters of SES and LSTs are mainly located east and southeast of SCC, where the proportion of the Hispanic/Latino population is insignificant (L to VL). Low-high clusters of low SES and high LSTs are in East San Jose, where most of the Hispanic/Latino population resides, where historically, Mexicans have been ghettoized. High-low clusters of high SES and low LSTs are mainly located in the southwest, where most non-Hispanic White and high-income population resides.

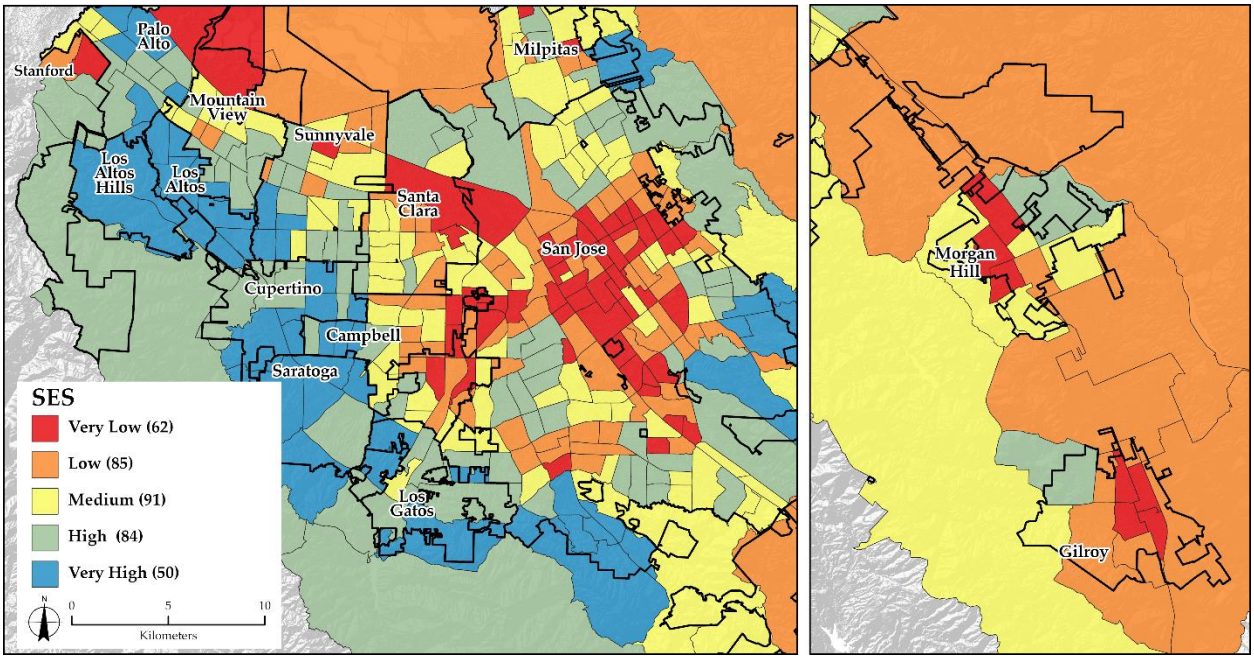

Figure 18. Land Surface Temperature and Modified Darden-Kamel CSI bivariate spatial autocorrelation (p-value <=0.050).

Health Outcomes. A multivariate multiple spatial regression was performed to estimate the prevalence of selected health outcomes and access to health insurance per the PLACES dataset related to the proportion of race/ethnicity, SES, and LST per census tract. Table 6 provides descriptive statistics of the variables used in the analysis. All variables are continuous. Each Health Outcome was defined as an independent variable, and the rest were defined as predictors. A regression was run for each health outcome in combination with each race/ethnicity group, giving a total of 45 multivariate regressions.

Results (Table 7) show that the independent variables account for 23 to 91% of the variance in health outcomes. For all races, high R^2 values (≥70%) are shown in no health insurance, asthma prevalence, and obesity spatial regression models, and moderate R^2 values (40 to 50%) in diagnosed diabetes spatial regression models. The significance of each independent variable, however, varies by race. Although the percentage of the Hispanic/Latino population is positively related to the number of adults with no health insurance, for example, when disaggregated by origin, results show a similar statistically significant high coefficient (18.22) for Mexicans. In contrast, the coefficients for South Americans and non-Hispanic Whites are negative (-40.04 and -6.75, respectively) and statistically significant, whereas the coefficient for Central Americans is insignificant.

The ethnic concentration (%) is positive and statistically significantly explanatory for asthma prevalence, obesity, and diagnosed diabetes for Hispanic/Latinos and Mexicans. Unexpectedly, non-Hispanic Whites also show a positive and significant explanatory value, but only for asthma prevalence and obesity. The South American variables show a significant negative coefficient for diagnosed diabetes, whereas the Central American variable shows no explanatory significance for any health outcome. The spatial regression results from The Darden-Kamel CSI coefficients are negative and significant for the no health insurance and asthma suggesting that with increasing SES no health insurance and asthma prevalence decrease but positive for high cholesterol in all racial/ethnic groups. Although LST has been related to cardiac-related illnesses, results from the model regressions do not show statistically significant coefficients for coronary heart disease and stroke outcomes. LST coefficients, however, are positive and statistically significant for no health insurance (0.44) in the Hispanic/Latino, Mexican, and South American (0.45) groups but negative and statistically significant for obesity (-0.30) in the Hispanic/Latino group. The spatial regression results from The Darden-Kamel CSI coefficients are negative and significant for the no health insurance and asthma variables but positive for high cholesterol in all racial/ethnic groups.

Table 6. Descriptive statistics of variables considered in the multivariate spatial regression.

Variable		Mean	St Dev	Min	Max
Health Outcome (Prevalence)	No Health Insurance	11.67	5.80	4.10	29.20
	Asthma Prevalence	7.61	0.83	5.70	11.00
	Obesity	21.39	3.62	13.80	31.80
	Stroke	2.24	0.47	0.50	4.10
	High Blood Pressure	23.06	3.34	7.00	37.00
	Diagnosed Diabetes	8.47	1.90	1.30	17.40
	High Cholesterol	26.69	3.47	7.90	38.00
	Chronic Kidney Disease	2.27	0.41	0.70	3.80
	Coronary Heart Disease	3.83	0.89	0.70	8.00
Race/Ethnicity (Proportion per census tract)	Hispanic/Latino	0.25	0.20	0.00	0.86
	Mexican	0.21	0.19	0.00	0.83
	Central American	0.02	0.02	0.00	0.10
	South American	0.01	0.01	0.00	0.07
	Non-Hispanic White	0.33	0.20	0.00	0.88
Socioeconomic Status	DK CSI	0.00	4.59	-13.03	11.01
Exposure (°C)	Mean LST	29.43	1.08	22.93	31.78

Table 7. Summary Table of Multivariate Spatial Linear Regression Results by Ethnic Concentration. Coefficients are shown for significance ≤ 0.001.

Ethnicity	Health Outcome (Y)	Spatial Lag	B0	Ethnic Concentration (%)	DK-CSI	LST	R^2
Hispanic/ Latino	No Health Insurance	0.35	-9.77	17.18	-0.12	0.44	0.91
	Asthma Prevalence	0.69	4.62	0.99	-0.03	-0.08	0.71
	Obesity	0.55	16.17	9.32		-0.30	0.81
	Stroke	0.52	2.28				0.24
	High Blood Pressure	0.60	18.10				0.28
	Diagnosed Diabetes	0.68		1.84			0.52
	High Cholesterol	0.64	16.47		0.15		0.43
	Chronic Kidney Disease	0.51	2.09	0.48			0.30
	Coronary Heart Disease	0.53	5.17				0.23
Mexican	No Health Insurance	0.33	-8.99	18.22	-0.15	0.44	0.92
	Asthma Prevalence	0.70	4.51	0.90	-0.03	-0.08	0.71
	Obesity	0.58	15.55	8.79			0.80
	Stroke	0.52	2.32				0.24
	High Blood Pressure	0.60	18.28				0.28
	Diagnosed Diabetes	0.67		2.11			0.52
	High Cholesterol	0.64	16.57		0.16		0.43
	Chronic Kidney Disease	0.51	2.13	0.52			0.30
	Coronary Heart Disease	0.53	5.22	0.39			0.23
Central American	No Health Insurance	0.68			-0.40		0.82
	Asthma Prevalence	0.75	3.85		-0.05		0.70
	Obesity	0.76			-0.20		0.74
	Stroke	0.55					0.24
	High Blood Pressure	0.61	17.96				0.29
	Diagnosed Diabetes	0.73					0.51
	High Cholesterol	0.64	16.42		0.16		0.43
	Chronic Kidney Disease	0.59					0.29
	Coronary Heart Disease	0.55	5.03				0.23
South American	No Health Insurance	0.67		-40.04	-0.43	0.45	0.83
	Asthma Prevalence	0.75	3.84		-0.05		0.70
	Obesity	0.77			-0.21		0.74
	Stroke	0.54	2.29				0.26
	High Blood Pressure	0.60	18.61				0.30
	Diagnosed Diabetes	0.70		-27.68			0.53
	High Cholesterol	0.64	17.04		0.16		0.45
	Chronic Kidney Disease	0.58	1.86				0.30
	Coronary Heart Disease	0.55	5.14				0.25
Non-Hispanic Whites	No Health Insurance	0.57		-6.75	-0.42		0.84
	Asthma Prevalence	0.65		1.08	-0.07		0.72
	Obesity	0.74		2.54	-0.25		0.75
	Stroke	0.55			-0.02		0.25
	High Blood Pressure	0.61					0.29
	Diagnosed Diabetes	0.67					0.51
	High Cholesterol	0.64			0.14		0.44
	Chronic Kidney Disease	0.59			-0.02		0.30
	Coronary Heart Disease	0.53					0.25

Discussion

This study reveals socioeconomic neighborhood inequalities and an uneven spatial distribution of NDVI and LST values across Hispanic communities in SCC. Almost half the Mexican population lives in highly segregated neighborhoods with L- and VL-SES, mainly located in East San Jose, where, historically, they have been ghettoized. Areas with a VH-Concentration of Mexicans show higher LST and lower NDVI values than neighborhoods with a VH-Concentration of Whites. The spatial patterns of residential segregation and environmental and socioeconomic neighborhood inequality reflect high-temperature values and a low amount of green areas available in Mexican neighborhoods, implying possible environmental racism that could have resulted from historical racial/ethnic processes (e.g., racism and discrimination). Results of this study thus suggest that the ethnic composition of a neighborhood is strongly linked to LST values. Mexicans, in general, could be at a higher risk of heat stress and heat mortality during heat waves.

Although the study area is racially diverse, there is an intrinsic ethnic division of labor (Mehrens, 2015), as shown in Table 1. Since the "Factory Valley," when the region dominated the manufacture of semiconductors, thus earning the name Silicon Valley (Cheyre, Kowalski, & Veloso, 2015), around 70-80% of people working in manufacturing jobs were immigrants, women, and people of color, who continued being the backbone of Santa Clara County's economy long after the Gold Rush (Pellow & Park, 2002). For example, Siegel (1995) states that, during the 1970s, most managers were White (88%), and only 4% and 5% were Latino and Asian, respectively. By the 1980s, the number of Asians in managerial positions increased from 5 to 10%, but the percentage of Latinos remained. From the 1970s to the 1980s, however, the percentage of White laborers decreased from 41 to 19%, while the number of Latinos remained almost the same (34 to 36%; Siegel, 1995). In the current tech industry, the ethnic division of labor remains in the top three most profitable companies – Google, Facebook, and Apple – where only 2 to 7% of the workforce is Hispanic/Latino (Mehrens, 2015). Hispanic/Latinos make up 69% of janitorial workers. As shown in this study, only 30% of the population in VL-SES tracts hold a professional or managerial occupation, of which nearly 30% are Hispanic/Latino.

There is a massive disparity between the population living in VHSES and VLSES and high living costs. The median rent in SCC was $2,363 a month, yet the minimum wage in SCC is $15.65/hour. Skyrocketing house prices have forced many people into homelessness, and the area

hosts the largest homeless camp in the continental US (R. Johnson, 2013). Of the 4,350 homeless people, 3,219 were unsheltered. Most homeless individuals are male (70%), and 46% self-identified as Latino; among homeless families with children, 78% were single-mother families, of which 56% were Hispanic/Latino. Approximately 47% of unaccompanied children also identified as Hispanic or Latino (Applied Survey Research, 2017). The Hispanic/Latino population, most living with a median household income of $73,000, although with low levels of unemployment (4.3%), live in poverty and are at risk of eviction and homelessness.

Homeless individuals showed higher rates of preexisting psychiatric illnesses and comorbid conditions (e.g., cancer, cerebrovascular, infectious diseases), which increases their heat mortality risk (Ramin & Svoboda, 2009). Their inability to access drinking water and lack of healthcare make them susceptible to high temperatures and further exacerbate their illnesses (Nicolay et al., 2016). Homelessness and age are critical variables that drive heat-related mortality (Putnam et al., 2018). Homeless populations do not perceive themselves as vulnerable, avoid water distribution routes, and are frequently asked to leave cooled public areas (Benmarhnia et al., 2018).

Inequalities exist within the Hispanic/Latino Population. Although the Hispanic/Latino population is, on average, highly segregated and impoverished, Mexicans represent the highest share of VLSES. Residential segregation in Silicon Valley dates to the late 1800s, during the gold rush. Southwest San Jose became a valuable player with the discovery of a quicksilver mine in the Almaden Valley. Mexicans and Native Americans, considered second and third-class citizens, worked the mines in dangerous conditions. Over time, the area around the Almaden mine would become known as the segregated neighborhood of Mexican workers. According to this study, a high concentration of the Hispanic/Latino population, primarily Central Americans, is located around the Almaden mine and less in the East San Jose area, exhibiting M- to VH-SES but being the most segregated Hispanic subgroup.

By the 1940s, most Latinos lived in the segregated muddy fields on the East Side of San Jose. Nearly 30% of the Mexican population, however, lives in VL-SES and concentrates in East San Jose, also known as “Sal Si Puedes” (get out if you can; Heppler, 2018). Most Central Americans, in contrast, concentrate southwest SCC towards the Almaden neighborhood. South Americans are the least segregated group but do not concentrate in the same areas where Mexicans and Central Americans commonly settle. The percentage of South Americans in VH-SES (9.1%)

is four times higher than that of Mexicans in VH-SES (1.6%). According to results from the Modified Darden-Kamel CSI, most Mexicans (67%) exhibit VL-and L- SES.

Heat disparities within Hispanics. Although areas with a VH concentration of Hispanics have higher LST values than non-Hispanic Whites, Mexicans have the highest LST values (1.2°C higher than non-Hispanic Whites), thus reflecting being overburdened by heat and, as previously discussed, poverty. The most considerable differences in LST values (1.4°C) are shown between the VH-Mexican and H-South American groups. Results also showed the same statistically significant temperature (1.4°C) difference between VH- and VL- SES. The VL-SES group is also 1°C above the mean SCC value.

Epidemiological studies have found that a 1°C increase in maximum temperature can increase ambulance response calls due to heat-related illnesses by 29% (Bassil et al., 2011), heat-related emergency-room visits by 2.5% (Plumer & Popovich, 2020), and heat-related mortality from 1 to 3% (Hajat & Kosatky, 2010). Based on findings from our study, low-income Mexicans would have the highest rates of heat-related outcomes, mainly due to their lack of health insurance (18.22) and comorbidities: obesity (8.79), diagnosed diabetes (2.11), asthma prevalence (0.90), chronic kidney disease (0.52), and coronary heart disease (0.39). Mexicans, therefore, are the primary racial group driving adverse health outcomes. The concentration of Central Americans exhibits no explanatory value of health outcomes, whereas the concentration of South Americans has a negative explanatory value.

Klinenberg (2002) found that suburbs in Chicago composed mainly of African American residents exhibited a higher mortality rate than those primarily consisting of Latino residents. The low heat-related risk among the Hispanic population may be partly explained by the differences in SES between the Hispanic/Latino population and the Hispanic Health Paradox (HPP). HPP indicates that although Hispanic immigrant populations in the US experience high economic deprivation, they tend to have better health outcomes than their native-born counterparts and other racial/ethnic subgroups, including the Anglo-White majority (Kim et al., 2014).

Conclusion

From the Gold Rush to the Apple janitorial strike, Silicon Valley was built by discriminatory practices and policies (Pitti, 2004). The capitalist wage system and the dominance of Euro-American culture helped marginalize non-White groups in California (Almaguer, 2009). Income inequalities emerged in the region because of economic and political policies that resulted

in specific residential patterns. Five-year Landsat 8 satellite and Census Bureau-ACS 2015-2019 data were used to assess the physical and social environment via the calculation of LST, NDVI, Modified Darden-Kamel CSI, and Index of Dissimilarity. This study used the Index of Dissimilarity to estimate the degree of Latino/Hispanic residential segregation and the Darden-Kamel CSI to calculate SES by census tract. The combination of these indicators allowed for the identification of vulnerable communities. Results showed differences in residential segregation, socioeconomic status, and high-temperature exposure (LST and NDVI) among Hispanics by origin. Hispanic/Latinos, primarily Mexicans, live in highly segregated areas and are exposed to high LST and low NDVI values. The Univariate Moran's I Index and Bivariate Local Moran's I results show a statistically significant spatial correlation. These measures allowed for the identification of heat-vulnerable populations, who in SCC are more likely to be Mexicans experiencing comorbidities and living in the historic neighborhood of *Sal Si Puedes*, where institutionalized racist and discriminatory processes have historically segregated them.

Relatively small differences in LSTs by SES and ethnic group may result from the aggregation of mean annual values that could homogenize extreme cold and heat days. Although non-developed areas were filtered to produce a more accurate temperature measurement of populated areas, this study does not consider urban morphology (e.g., land use and building form), which may vary by class and ethnicity, as studies have found higher population densities in Hispanic neighborhoods in the US. Future studies should consider averaging LST values for warm months only (e.g., May – September) and describing the built environment (e.g., population density, building materials), which may vary by SES. Additional variables, such as homelessness, housing characteristics, crime, social cohesion or isolation, collective behaviors, and age-structure differences within the Hispanic population, need to be included in more comprehensive heat-related studies to provide a more robust evaluation of the at-risk population in urban areas, where heat stress is expected to intensify.

Proposed solutions to reduce heat exposure include urban greening projects, shading sidewalks, parking lots, and other paved surfaces, and using trees or additional structures (e.g., sailcloth and solar panels; Rodriquez & Chapman, 2013). Urban greening is a complex affair: it involves major infrastructural, management, maintenance, and watering complexities that impose costs and challenges for low-income communities. Recommendations thus also include promulgating local codes to accelerate the adoption of cooling strategies. This regulatory approach

could be complemented with heat-emergency preparedness plans at the community level and the placement of cooling centers. Local communities must have input in the development of these mitigation and adaptation strategies (Wilhelmi & Hayden, 2010). A multi-scale, multi-stakeholder approach would be the best path to ensure hazard reduction, especially in low-income and racial/ethnic minorities.

CHAPTER 4. EVALUATION OF HEAT MITIGATION STRATEGIES IN SANTA CLARA, CALIFORNIA: A SENSITIVITY ANALYSIS OF URBAN TREES

Introduction

Neighborhoods with higher vegetative densities tend to have lower temperatures, especially during heatwaves, than those with sparse vegetation (Declet-Barreto et al., 2013). Wealthier neighborhoods, however, have more access to healthy green spaces than low-income communities (Wilson & Belonis, 2016). In the United States (US), a high proportion of racial and ethnic minorities reside within racially segregated urban areas and low-income communities deprived of green areas and with scarce vegetative coverage that resulted from historical ethno-racial oppression and segregated park systems (Wolch et al., 2014). In four metropolitan areas in the State of California (Los Angeles, Sacramento, San Diego, and San Francisco), the percentage of impervious surfaces positively correlates to the number of residents of color and the proportion of residents living in poverty (Shonkoff et al., 2011).

Parks in primarily racial and ethnic minority neighborhoods also tend to have less acreage than parks in predominately White communities (Boone et al., 2009). A smaller park size results in a higher pressure on park space (e.g., a higher number of users per unit area), leading to higher park degradation (Wolch et al., 2014). Lack of park maintenance can also increase particulate matter (PM) pollution from dirt lots, as grasses and trees tend to be less irrigated (Declet-Barreto et al., 2013). In Phoenix, for example, Latino neighborhoods tend to have fewer green areas (Wolch et al., 2014) and higher levels of temperature-dependent air pollution (e.g., Nitrogen Dioxixe-NO_2 and $PM_{2.5}$) than their White counterparts (Taha, 2004; Su et al., 2011).

In Los Angeles, more funding is designated for creating and maintaining parks in White-dominated areas than in colored communities (Wolch et al., 2005). In 1996, the City of Los Angeles adopted Proposition K to generate revenue through a real-property tax that would provide enough funding for local communities to increase their green infrastructure. The results showed that funding patterns often exacerbated rather than alleviated existing inequalities in park and open space resource distributions, as resources were unevenly distributed across racial/ethnic communities. Much more funding was allocated to neighborhoods with already accessible parks. Park spending equaled $45.13 per child in predominantly White areas (more than 50% White) and only $26.64 per child in non-White dominant areas (less than 50% White). Access to parks does

not translate into its use, especially if neglected, as they can be perceived as "dangerous, unpleasant, and unwelcoming" and can even serve as crime generators (Boessen & Hipp, 2018).

The provision of ecologically adequate and maintained vegetation is vital for equitable outcomes, especially since neglected parks often create *ecologies of fear* that emphasize legacies of race-based social control and criminalization of environments and their occupants (Brownlow, 2006). The benefits of green areas also extend to public health, as they create *salutogenic* urban environments that can help mitigate human health problems, such as asthma, allergies, obesity, and increased stress. Parks can, therefore, be defined as *therapeutic landscapes* or areas that positively affect an individual's health or have a therapeutic effect (Emch et al., 2017). Low-income communities, however, receive even fewer benefits from green spaces than higher-income neighborhoods and tend to lack other resources (e.g., healthcare and A/C access) that could mediate the detrimental effects.

The increase in the number and quality of urban forests has become popular to reduce intra-urban tree-canopy inequality, enhance community well-being, and mitigate urban heat. Trees provide shade and moderate leaf temperature via transpiration, significantly decreasing air temperatures (Oke et al., 1989; Turner-Skoff & Cavender, 2019). Their shade attenuates radiant energy flows through absorption and reflection, further cooling the surface and near-surface temperature (Declet-Barreto et al., 2013). Tree density, crown diameter (horizontal canopy area), vertical canopy area, leaf area index (LAI), and leaf area density (LAD) are additional characteristics determining the cooling potential of urban forests (Ballinas & Barradas, 2015). A tree with an LAI of 5 and LAD of 1 m^2/m^3 can reduce the air temperature by 1.3°C and the surface temperature by 14.7°C (Tan et al., 2016).

The use of numerical modeling software at the microscale level has become popular among urban climatologists and designers to explore and evaluate the improvement of human thermal comfort through tree planting. ENVI-met, a computational fluid dynamics (CFD) model developed by the Institute for Geography at Ruhr-University in the late 1990s (Taleghani et al., 2016), has been recognized as the most often used model for micro-climate studies (Jänicke et al., 2021). ENVI-met simulates three-dimensional environments at high levels of temporal (1-10 sec) and spatial (0.5-10 m) resolutions (Hebbert & Jankovic, 2013). It, therefore, allows the representation of complex geometries and various vegetation covers (Ali-Toudert & Mayer, 2007). The software consists of five models: 1) an atmospheric model that calculates air movement, temperature, and

humidity; 2) a surface model that calculates long- and short-wave radiation from different surfaces based on shading and solar paths; 3) a vegetation model that calculates foliage using LAD and evaporation rates; 4) a soil model that considers the exchange processes of natural and artificial surfaces, including water bodies; and 5) a biometeorological model, that calculates the energy balance of the human body to determine thermal comfort (Ambrosini et al., 2014).

The model requires two files: the input file (.inx), which describes the physical properties of the simulation area (buildings, surface, vegetation), and the configuration file (.simx), which contains the initial weather data, duration, and time of simulation (Taleghani, 2018). The locations of buildings and rooftops are drawn using the SPACES application, available in the ENVI-met suit, using aerial imagery. The ENVI-met .simx file requires input parameters as initial conditions (i.e., air temperature, wind speed, wind direction, relative humidity) from weather stations, usually located at airports or buildings' rooftops, which may not represent the modeled area. To overcome the limitations of larger-scale processes not modeled by ENVI-met, including the unavailability of atmospheric variables for initialization and validation purposes, ENVI-met can be combined with mesoscale models, like the urbanized version of the Weather Research and Forecasting (uWRF; Mc Rae et al., 2018).

Significant results from ENVI-met show that the benefits of trees for the improvement of thermal comfort come mainly from shading rather than transpiration (Mballo et al., 2021). With moderate winds, the cooling effects can extend beyond the vegetated areas into adjacent, non-vegetated surfaces (Declet-Barreto et al., 2012). The extension of the cooling effects, however, will depend on the arrangement of trees and wind direction. Tan et al. (2016) reported that trees placed along dominant wind paths resulted in maximized cooling effects. Similarly, Ng et al. (2012) used microclimate simulations to analyze different green design strategies to reduce the air temperature in Hong Kong. The increase in green coverage, however, results in decreased wind velocities (0.9 m/s), which could significantly affect outdoor thermal comfort (Yuan et al., 2017). Tree planting is a common and effective mitigation strategy, often less costly than lakes/blue spaces or other evaporative surfaces. During the daytime, the effectiveness of trees in improving thermal comfort reduces with increasing urban density as the shadowing effect of building heights reduces the cooling effects of tree shade (Morakinyo et al., 2017). Microclimate simulation results reported that areas with existing vegetation coverage do not change in temperature when adding more trees (Makido et al., 2019). These results suggest a threshold in the number of trees to

maximize cooling capacity and thermal comfort. The effect of trees on the local environment, however, is highly dependent on the particular characteristics of a place (e.g., surrounding urban morphology); thus, their effects must be analyzed using the most highly spatial resolution available (Garrison, 2021), accounting for different urban forms and climates (Janicke et al., 2021).

The current effort evaluated the potential cooling effect of trees in Reid-Hillview Airport (RHVA), located in east Santa Clara County (SCC), in California, via ENVI-Met simulations. Whereas most previous efforts have primarily focused on the evaluation of multiple mitigation strategies, this study performs a sensitivity analysis to analyze the thermal conditions of the area under current summer and extreme heat conditions after increasing the percentage of tree coverage. Land Surface Temperature in the surrounding neighborhood ranges from 30 to 33°C, with the maximum values at the RHVA (Rivera et al., 2022). Most residents in the area are Hispanics, mainly of Mexican or Central American origin, with a very low to medium socioeconomic status. Most residents are not homeowners, which tree-planting projects within these residential areas, as residents cannot make long-term decisions regarding the property. In August 2021, the SCC Board of Supervisors voted to close the RHV Airport, as elevated blood lead levels were found in children living near the Airport, similar to those found in children tested in Flint, Michigan, during the water crises (Wittenberg, 2023). The RHVA area could be a site of urban renewal where tree coverage can be increased. The current social and environmental conditions, as well as the site's potential for future land uses, thus justified the selected area to perform a sensitivity analysis.

Data and Methods

The current methodology uses satellite imagery from Google Earth and data from OpenStreet Map to localize building footprints and vegetation distributions within the model domain and produce the input files (.inx). Five scenarios were simulated to evaluate the cooling potential of tree coverage in a potentially repurposed RHVA. The first scenario served as a baseline to assess the current thermal conditions of the selected site. The subsequent scenarios evaluated the thermal conditions of the area after increasing tree coverage to 25%, 50%, 75%, and 100%. All scenarios were assessed under typical (9 July 2017) and extreme (1 September 2017) cloudless summer conditions.

Simulation Area. The microclimate analysis was conducted for the RHVA in the East San Jose neighborhood (Figure 19). Satellite imagery shows the Airport has a surface of 0.73 km^2, including a runway of 0.36 km^2. Of the runway area, 0.25 km^2 is covered by pervious surfaces,

primarily grasses. The location of trees was only considered along one section of the runway (in red) within a 0.02 km^2 area. The RHVA is surrounded by high-density housing to the east and north. A small park with a few trees is located to the north, while a water park is located to the west. A large mall is south of the airport area, with impervious surfaces and no trees.

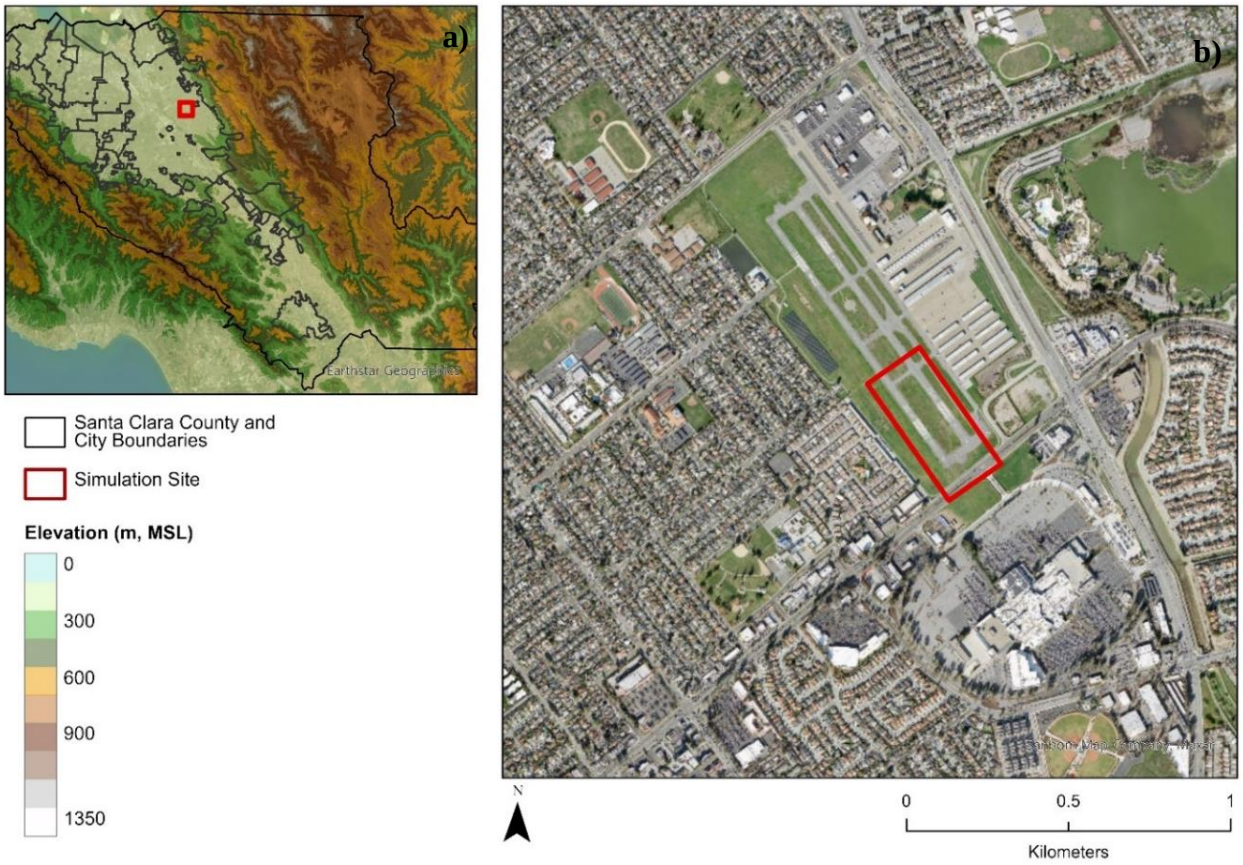

Figure 19. Study area map showing a) elevation (m, MSL) of Santa Clara County and boundaries for its 15 cities, as well as the location of the Reid-Hillview Airport, and b) ENVI-met simulation site (red box) within the Airport.

ENVI-Met Model

The simulation site included a domain area of 120 by 240 meters. A grid spacing of 1.5 meters was used for each 3-D axis to maximize resolution and minimize computational time. The model resulted in 80 by 160 horizontal grids, considering five additional cells at each lateral boundary. The height of the model equaled 30 meters or 20 vertical grids, which is sufficient for this application, given the absence of building structures within the simulation site. The tree species considered for this analysis is an Oak (Quercus spp.) of medium height (13 meters) and crown diameter (8 meters) with deciduous foliage, given they are endemic to the study area. The default properties of the oak, available on the ENVI-met 5 library, define the tree as having a C3

photosynthetic metabolism, which requires the regular opening of leaf pores (stomata), transpiring significant volumes of water (Gunawardena et al., 2017). Default values for foliage short-wave albedo (0.18) and short-wave transmittance (0.30) were maintained for all simulations. To achieve a tree coverage of 25%, 50%, 75%, and 100%, the number of trees placed was 19, 41, 60, and 82, respectively (Figure 20). All were placed with a uniform spacing of 6 meters to minimize crown overlapping.

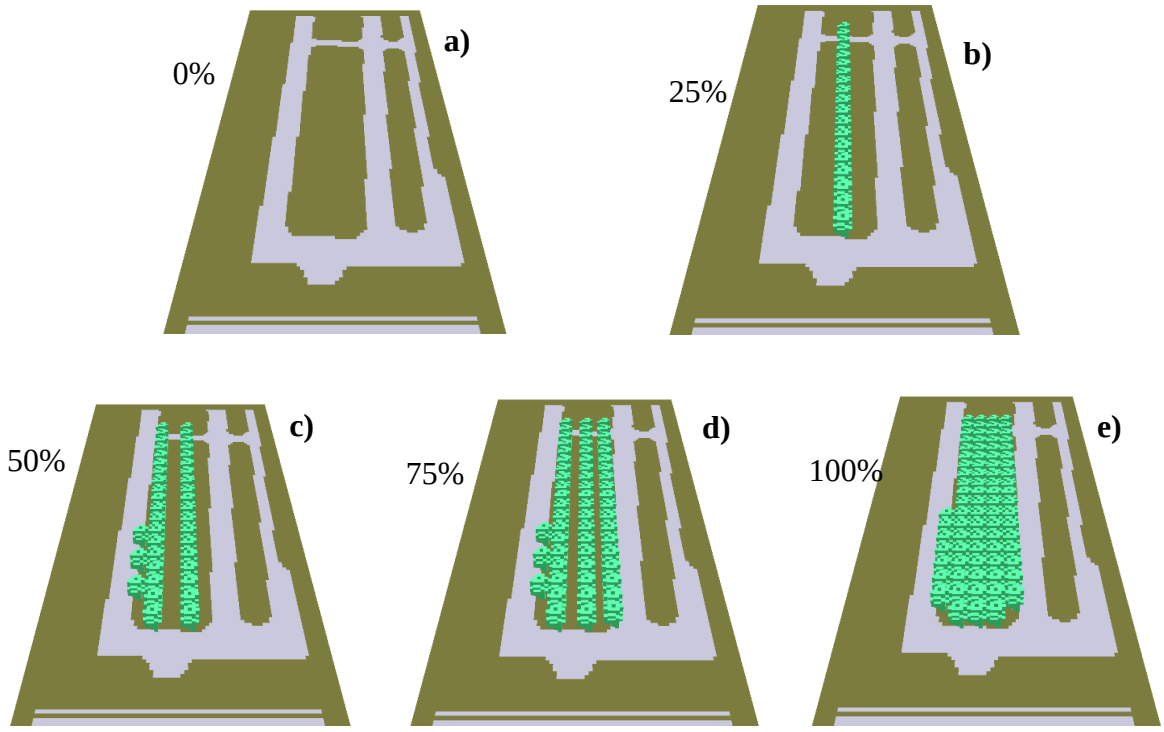

Figure 20. ENVI-Met simulation scenarios for a) existing conditions and after increased tree cover by b) 25%, c) 50%, d) 75%, and e) 100%.

Typical summer simulations started on 9 July 2017 at 0700 Local Standard Time (LST) and were run over a 12-hour period. The first five hours were considered a spin-up period and were not further analyzed. Simulated air temperature results were analyzed for daytime (1200-1800 LST) hours. A similar period was used for extreme conditions, with simulations starting on 1 September 2017. All simulations were run with the use of simple forcing meteorological conditions, which require minimum and maximum air temperature and relative humidity values during a 24-hour cycle, along with their corresponding times of occurrence (Table 8). Model parameters are then computed at each time step. ENVI-Met initialization values were extracted from uWRF simulation results, previously run for the considered dates (McRae et al., 2018). A

constant wind speed value of 1.5 m/s was used for all simulations, given numerical problems reported for higher speeds. The roughness length of the surface was established at 0.010 meters.

Table 8. Meteorological constants for daytime (1200-1800 LST) ENVI-Met simulations.

Input Variable	Typical	Extreme
Date	09 July 2017	01 September 2017
Specific humidity (g/kg)	6.6	5.6
Wind direction (°)	320	307
Air Temperature (°C, hour in LST)	Min: 15, 0700 Max: 31, 1600	Min: 20, 0700 Max: 40, 1500
Relative Humidity (%, hour in LST)	Min: 24, 1300 Max: 79, 0700	Min: 15, 1500 Max: 54, 0700

Results

ENVI-Met simulation results show air temperature reductions (Δ) at a 1-meter street level in the study area. The mean air temperature for the entire domain (Figure 21) shows that during typical summer conditions, a 25% tree coverage reduces mean baseline temperature from -0.03°C at 1500 to -0.08°C at 1800, whereas a 50% tree coverage reduces temperature from -0.07 to -0.18°C during the same hours. A 75% tree coverage reduces baseline mean air temperature from -0.10 to -0.25°, and a 100% reduces values from -0.12 to -0.31°C during the same hours. During extreme heat conditions (Figure 3b), mean air temperature differences from baseline values show the cooling effects of tree planting starting at 1500, with maximum cooling effects at 1800. A 25% tree coverage reduces baseline mean air temperature from -0.04 to -0.14°C at 1500 and 1800 hours, respectively. A 50% tree coverage scenario reduces air temperature from -0.07 to -0.24°C, whereas a 75% tree coverage scenario reduces values from -0.09 to -0.32°C during the same hours. A 100% tree coverage scenario reduces mean air temperature from -0.10°C at 1500 to -0.39°C at 1800.

Hourly rates of change are, however, non-linear during both weather conditions for all scenarios. During typical summer conditions, minimum decreases in hourly air temperature are seen for the 25% tree coverage scenario, ranging from 0.00°C from 1500 to 1600 to 0.03ºC from 1400 to 1500 and 1700 to 1800. Greater temperature changes occur from 1400 to 1500 hours for 50 and 75% of tree coverage scenarios, with -0.06 and -0.08°C reductions, respectively. Lower mean air temperature changes then occur until 1800. For a 100% tree coverage scenario, the temperature is reduced by -0.09°C from 1400 to 1500 and by -0.07°C every hour from 1600 until 1800. During extreme heat conditions, temperatures change at a faster rate than for typical summer

conditions. Minimum decreases in hourly air temperature (from -0.02 to -0.03°C) are also seen for the 25% tree coverage scenario, from 1400 to 1700, with maximum reduction from 1700 to 1800 (-0.05°C). A similar behavior occurs for the 50% tree coverage scenario, with a constant rate of change of -0.05°/hour until 1700, with a -0.08°C change from 1700 to 1800. Higher rates of change from previous hours, particularly from 1700 to 1800, are found for the 75 and 100% tree coverage scenarios, with -0.11 and -0.14°C, respectively.

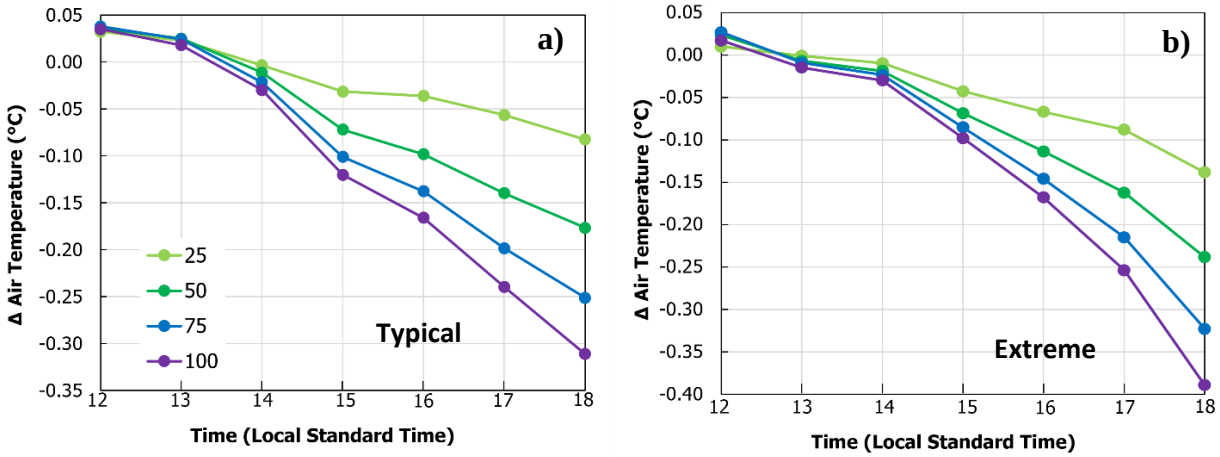

Figure 21. Mean air temperature differences (°C) from the baseline scenario for the entire simulation by the hour (Local Standard Time; LST) during a) typical summer (09 July 2017) and b) extreme heat (01 September 2017) weather conditions.

The non-linear changes in hourly air temperature during both weather conditions for all scenarios thus suggest a threshold in the number of trees to maximize cooling capacity, as additional trees would reduce air temperature minimally. Comparisons of air temperature at a 1-meter street level (Figure 22) during typical summer conditions show that at 1500, the largest difference between 25 and 50% tree coverage scenarios (0.04°C) and the smallest between 75 and 100% tree coverage (0.02°C). A similar pattern is found at 1800 (Figure 22b), with the largest difference between 25 and 50% tree coverage (0.09°C) and the minimum between 75 and 100% tree coverage (0.06°C). For extreme weather conditions, maximum differences are found between baseline and 25% tree coverage scenarios at 1500 (0.04°C) and 1800 (0.014°C), whereas minimum differences are found between 75 and 100% tree coverage scenarios (0.01 at 1500°C and 0.07°C at 1800). As tree coverage increases, differences in mean air temperature between scenarios decrease.

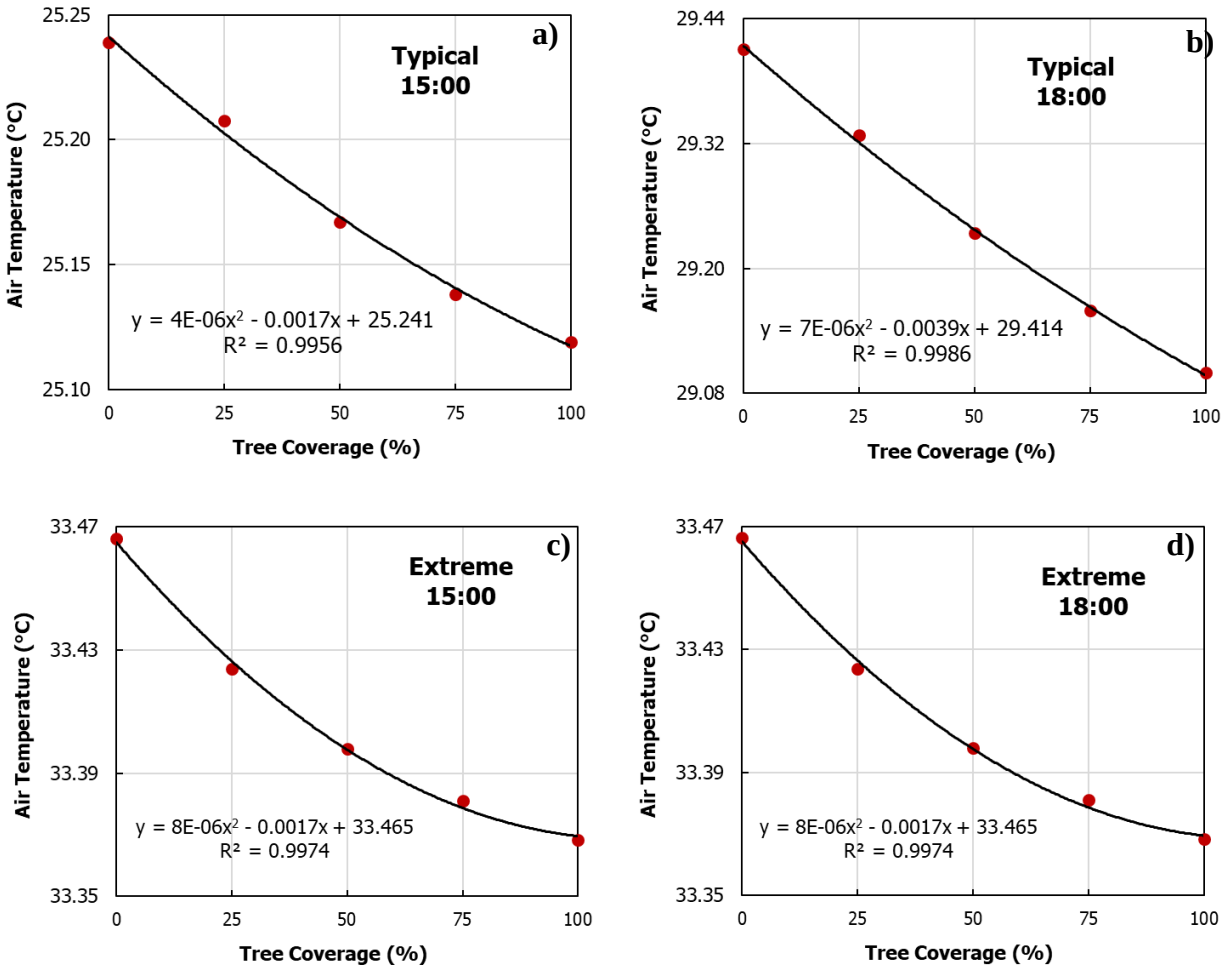

Figure 22. Mean air temperature differences (°C) from the baseline scenario for the entire simulation by the hour (Local Standard Time; LST) during a) typical summer (09 July 2017) and b) extreme heat (01 September 2017) weather conditions.

Distributions of air temperature at 1800 for all scenarios (Figure 23) show that, under typical summer conditions, minimum values decrease with increasing tree coverage from 29.00 to 27.64°C, but maximum values only decrease from 29.95 to 29.88°C. The range of median temperature values, therefore, only range from 29.40 to 29.29°C from 0 to 100% tree coverage, respectively, whereas the mean ranges from 29.41 to 29.10°C. Typical temperature values under 50 to 100% tree coverage scenarios follow a bimodal distribution, with a first peak around the first interquartile range and a second peak around the median. Corresponding values under extreme heat weather conditions minimum values range from 25.90°C for a 0% tree coverage (baseline) scenario to 34.32°C for a 100% tree coverage scenario, while maximum values range from 36.59 to 36.44°C under the same scenarios. The median temperature ranges from 36.09 to 25.86°C and

mean values from 36.13 to 35.14°C. Under extreme conditions, however, values for all mitigation scenarios follow a normal but negatively skewed distribution, with a second but smaller peak for maximum temperatures. As the percentage of tree coverage increases, distributions tend to be platykurtic, meaning fewer values are distributed around the mean.

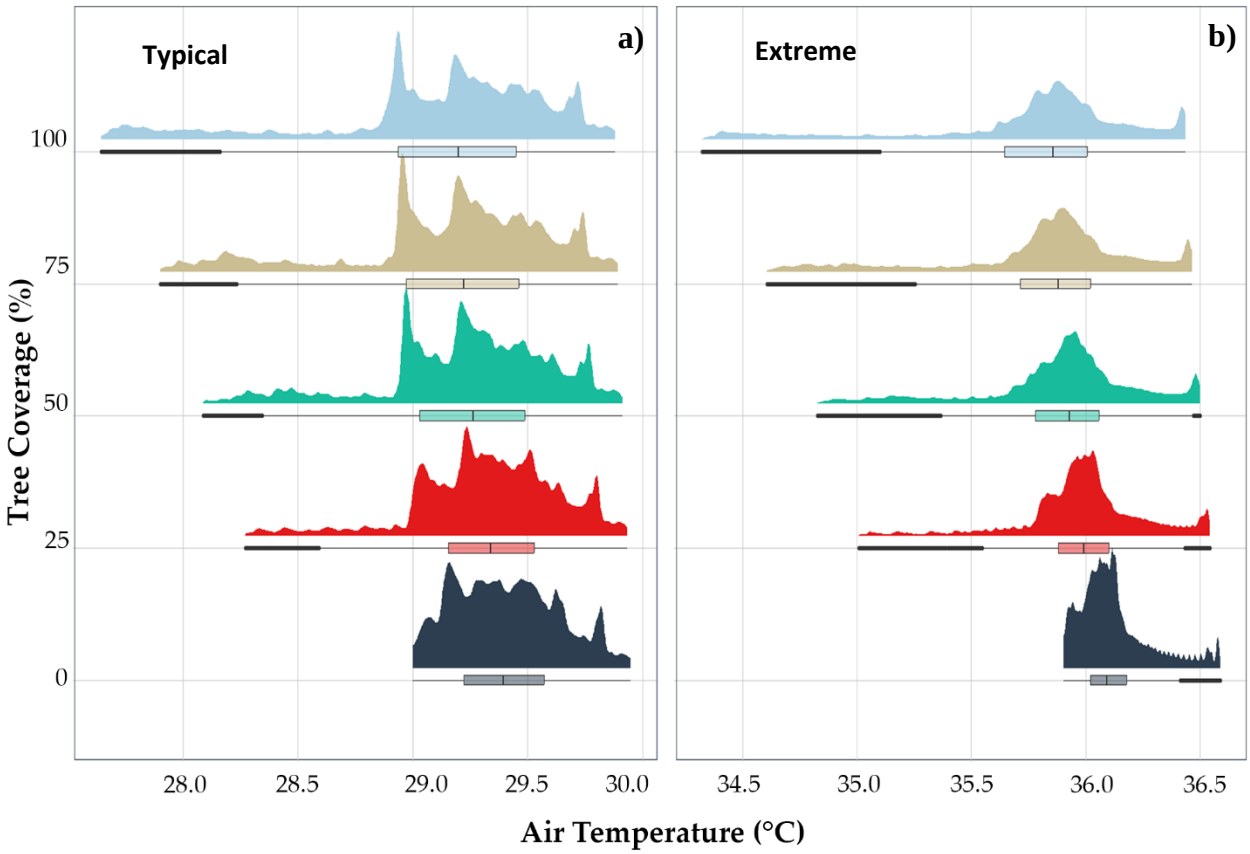

Figure 23. Mean air temperature distributions (°C) at 1800 (LST) for all scenarios during a) typical summer (09 July 2017) and b) extreme heat (01 September 2017) weather conditions.

Spatial distributions of air temperature reductions (Δ) at a 1-meter street level from baseline conditions (Figure 24) show that during typical summer conditions, a 25% tree coverage decreases values along the tree path around -0.86 to -0.70°C, with cooling extending south and reaching values ranging from -0.22 to -0.06°C. Some warming (0.11°C) is also seen along the east, parallel to the tree path. A 50% tree coverage further reduces baseline temperatures by -1.18 to -1.02°C, particularly along tree paths, with cooling extending values (-0.38 to -0.22°C) extending southwards and eastwards. A 75% tree coverage decreases temperatures also along tree paths, but maximum cooling (-1.34°C) is located in the southern parts of the tree paths. A 100% tree coverage decreases temperatures by -1.51 to -1.34°C, with cooling effects reaching the southmost area with

values ranging from -0.54 to -0.38°C. These patterns suggest dominant winds enter from the northern side of the simulated site, decreasing in value along the tree path and then extending the cooling effects to the south towards the Eastridge Mall parking lot and southeast towards residential areas.

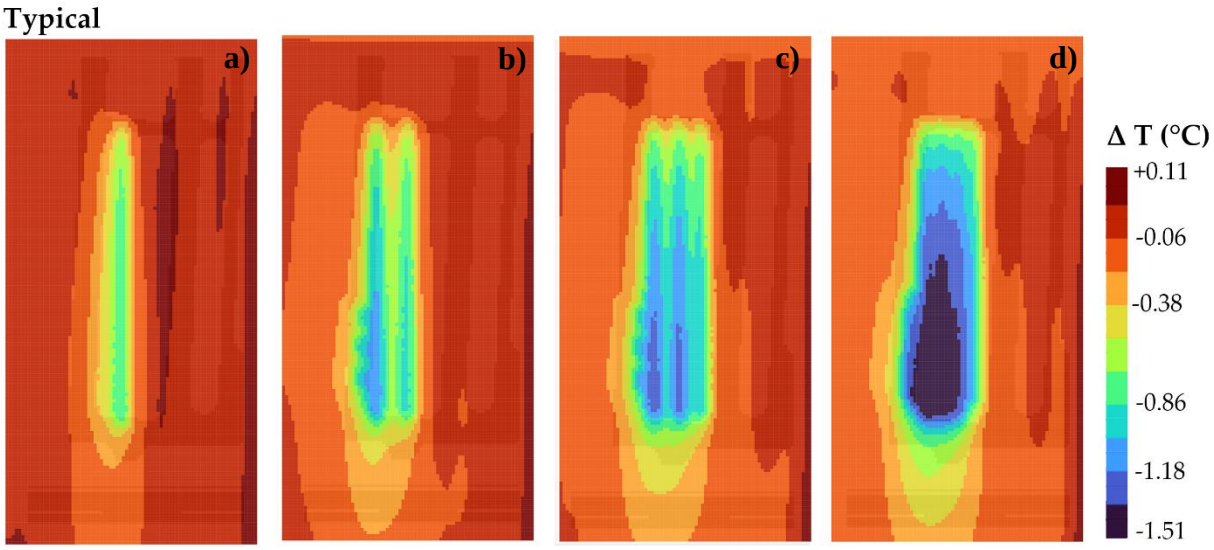

Figure 24. Mean air temperature differences (°C) from the baseline scenario for the entire simulation at 1800 (Local Standard Time; LST) during typical summer (09 July 2017) conditions, with increased tree coverage of a) 25%, b) 50%, c) 75%, and d) 100%.

During extreme heat conditions, spatial distributions of air temperature differences from baseline values (Figure 25) show that the cooling effects of tree planting follow a similar pattern to those in typical summer conditions. The cooling effects, however, are higher than those of typical summer conditions. For a 25% tree coverage, temperature differences from baseline range from -1.00 to -0.86°C, with cooling effects now extending to the southeast by -0.30 to -0.16°C, while a 50% tree coverage results in maximum cooling ranges between -1.14 to -1.00°C along the tree paths and cooling effects further decreasing temperatures by -0.44 to -0.30°C. A 75% tree coverage reduces baseline air temperatures from -1.42 to -1.28°C, with cooling effects extending by -0.58 to -0.44°C. A 100% tree coverage changes baseline temperatures by -1.62 to -1.42°C, with cooling effects extending southerly toward the Eastridge Moll parking lot.

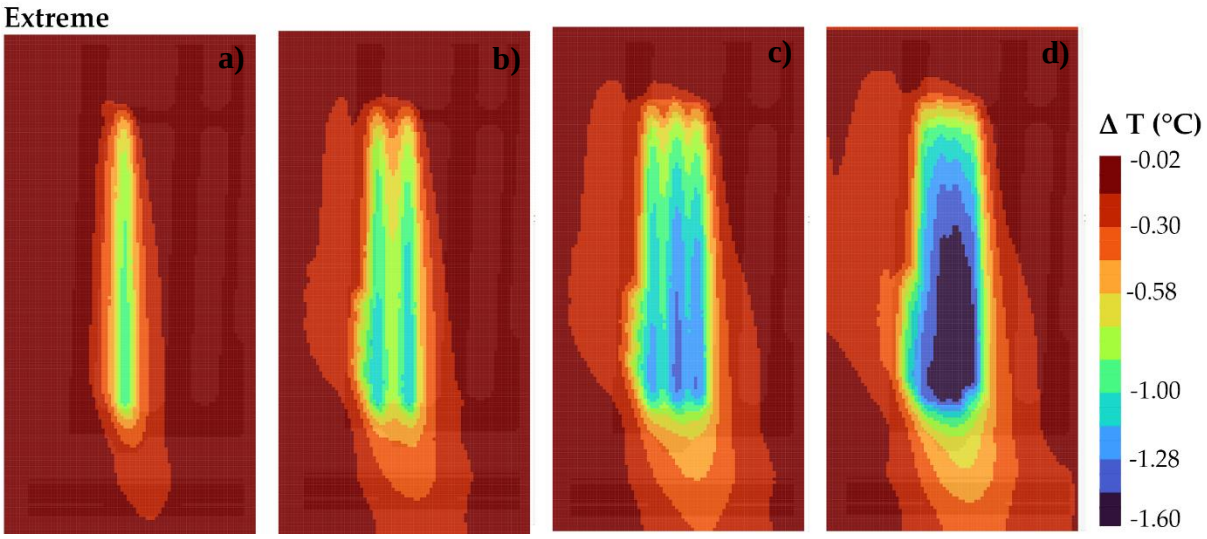

Figure 25. Mean air temperature differences (°C) from the baseline scenario for the entire simulation at 1800 (Local Standard Time; LST) during extreme (01 September 2017) conditions, with increased tree coverage of a) 25%, b) 50%, c) 75%, and d) 100%.

Discussion

Institutionalized racism, in the form of redlining and zoning ordinances, has disproportionately segregated a higher number of low-income and racial/ethnic minorities within green-area deprived neighborhoods, exposing them to higher ambient temperatures (Rivera et al., 2022). Most actions to address green infrastructure inequity are urban reforestation projects, like the Million Trees NYC initiative (Webb, 2017). In Chicago, UHI mitigation measures were part of a landscape ordinance to plant new trees and shrubs. The Arizona Heat Ready project also required shading of at least 75% of sidewalks per the Walkable Urban Code (Phoenix Zoning Ordinance-Chapter 13, 2019; Hammett et al., 2019)

In 2013, the State of California coordinated the Climate Adaptation Strategy to plan for extreme heat and recommend local codes to accelerate the adoption of cooling strategies. California recently adopted residential voluntary measures to reduce the UHI effect: the 2019 California Green Building Standards Code, also known as CalGreen (International Code Council, 2018). CalGreen's "first-in-the-nation mandatory building standards code" was developed by the State's authority to meet Assembly Bill 32 (AB 32). The CalGreen building code contemplates measures to reduce the surface temperatures of nonroof areas. These heat mitigation actions include planting trees that provide shade and mature within 15 years of planting and permeable pavements for at least 20% of parking, walking, or patio surfaces (Commission, n.d.).

These results suggest a threshold of a minimum number of trees coverage to ensure maximum cooling capacity. In the RHVA, under typical summer conditions, a 25% tree coverage minimally reduces the mean air temperature compared to a 50% tree coverage scenario. As the number of trees per area increases, however, more cooling is achieved, as maximum temperature changes result under the 100% tree coverage scenarios. Previous research suggests implementing additional or complementary mitigation strategies, such as cool pavements or roofs in already shaded locations, to improve pedestrian thermal comfort further (Taleghani et al., 2016). The most effective daytime strategy for temperature reduction has been increased vegetation, as it affects the largest area, while changes in albedos provide negligible impacts (McRae et al., 2020).

Trees with a high leaf density can reduce air temperatures by 1.3°C and surface temperatures by 14.7°C and intercept 84% of free horizontal solar direct radiation, thus lowering temperatures by providing shade (Tan et al., 2016). Higher temperature reduction due to tree shade and evapotranspiration are related to greater leaf density, as dense and wide canopies intercept and reflect large amounts of incoming short-wave radiation (Sharmin et al., 2023; C. Wang et al., 2023). Police Departments, however, discourage the placement of dense trees and shrubs that could provide natural shade because their planting obscures the view of open spaces, encouraging criminal activities. In Los Angeles, city officials required the removal of canopy structures, including trees, to comply with the Americans with Disabilities Act (ADA; Bloch, 2019).

Trees that transpire significant volumes of water provide higher cooling effects than trees with low transpiration, as it affects the cooling produced by a tree under its shade (Gupta et al., 2018; Jänicke et al., 2021). Green areas must then be heavily irrigated to increase evapotranspiration (Smith et al., 2023). Irrigated urban green spaces can reduce daily maximum air temperature by 2.5°C (Cheung et al., 2022). Irrigation can enhance evapotranspiration, particularly in arid regions and sites with small amounts of summer precipitation, such as San Francisco, California (May & Oliphant, 2023). There is, however, an increasing concern from public health officials on how the rise in urban green space to reduce temperatures might increase vector-borne diseases by enhancing the survival of mosquitoes and ticks that transmit Malaria, West Nile Virus, and Lyme disease (Huston, 2016).

Urban greening is not a simple affair: it involves major infrastructural, management, maintenance, and watering complexities that impose costs and challenges for low-income communities (Garrison, 2021). As previously discussed, marginalized populations, typically

belonging to minority racial and ethnic groups, have limited resources for neighborhood park maintenance (Sister et al., 2010). Due to decreased government budgets, there are also costs of implementing and maintaining tree planting that may be difficult to fund, and politicians may be willing to spend the money on other issues (e.g., housing education; Pincetl et al., 2013). Some tree species can also be high-allergen or with high volatile organic compounds (VOCs) that could trigger asthma symptoms or contribute to ozone pollution, counteracting some of the benefits of urban green areas (Werbin et al., 2020).

Redressing park deprivation in these communities can also create an urban green space paradox (Wolch et al., 2014). As green space increases, these neighborhoods can become more attractive for non-area residents, leading to rising real estate values and housing costs and exacerbating resident displacement (Sousa-Silva et al., 2023). Improving green areas could result in *green gentrification* (Hoffman et al., 2020), in which low-income residents meant to benefit from greening projects are displaced to similar neighborhoods with a low park provision (Wolch et al., 2014). In Chicago, for example, urban greening initiatives resulted in a lower sense of community, as many residents felt that they did not belong in green space, with communities of color being targeted by community policing, resulting in some youth limiting their visits to green spaces (Harris et al., 2020, 2021). Communities, therefore, do not get the full benefits of greening projects, as access to green infrastructure is often temporary (Jelks et al., 2021).

Conclusion

The increase of urban greenery has become popular among urban planners and policymakers to mitigate the urban heat island effect and reduce green tree inequality. The question of how to maximize the benefits of urban greenery through design remains for most cities. This effort evaluated the cooling effects of green infrastructure at the micro-environment scale, the street level, in SCC. A sensitivity analysis of the thermal conditions of a section of the RHVA after incrementally increasing the percentage of tree coverage was used to evaluate the potential cooling effect of each intervention. Five scenarios, including a baseline, were assessed for daytime hours (1200-1800) under typical summer and extreme heat conditions via ENVI-Met simulations.

Results showed that under both conditions, decreases in mean 1-m air temperature from baseline conditions were maximized under extreme conditions at 1800. After a 25% tree coverage scenario, values changed by -0.14°C, while maximum changes in air temperature were quantified for 50% (-0.24°) and 75% (-0.32°C) of tree coverage scenarios. Slight temperature differences

were observed between the 75 and 100% (-0.39°C) tree coverage scenarios. Non-linear relationships were thus found between changes in air temperature and time for all tree coverage scenarios, suggesting a threshold in the number of trees to maximize cooling capacity, as additional trees would reduce air temperature minimally. A maximum cooling effect was, however, found under the 100% scenario, with 1-m air temperature reductions extending to surrounding residential areas to the west and impervious surfaces to the south.

Future efforts should overcome limitations of the current study, e.g., expand the intervention area to cover a larger extent of the RHVA, evaluate a complete landscape design that includes shrubs and other design elements (e.g., blue spaces), and evaluate interventions in future or projected climates. Additionally, future studies must assess the benefits of increasing urban green areas beyond improving the thermal comfort of trees, such as additional ecological services or social and health impacts. The use of ENVI-Met as the only modeling software is also a limitation since it does not allow the quantification of other benefits, such as carbon sequestration.

Tree planting initiatives require community support to ensure full environmental benefits while contributing to quality of life. Citizen participation in tree-planting initiatives must, therefore, be considered to improve social cohesion among residents, which can create more climate change-resilient communities. Finally, future efforts should address design interventions that meet the cultural needs of minority communities as well as the safety needs of low-income communities. Human and environmental interventions at the micro-scale will lead to sustainable projects in urban areas that meet the unique needs of places and people.

CHAPTER 5. CONCLUSION

Global urbanization accelerates as the world population grows (Chen et al., 2006). Urban land cover transformations produce anthropogenic heat emissions into the atmosphere, which contribute to the formation of UHIs (Mohan et al., 2020). Such areas are found within urban canopy layers (e.g., atmosphere layer at or near the ground surface) and have warmer temperatures than their rural surroundings (Voogt, 2007). The highest temperatures are typically recorded at the city core under calm wind conditions and gradually decrease with distance toward suburban, rural, and wildland areas (Raj et al., 2020). The intensity and magnitude of UHIs are controlled by regional climate conditions and building characteristics (e.g., albedo, emissivity, sky view factor, anthropogenic heat fluxes; Jauregui et al., 1992; Taha et al., 2018). They are also related to seasonal changes in vegetation cover and rural soil moisture (Kim et al., 2016; Park et al., 2017; Li et al., 2020). UHIs negatively impact energy use, air quality, and human thermal comfort and health (He, 2018). Children, the elderly, low-income groups, and people with pre-existing respiratory, cardiovascular, and cerebrovascular conditions are most vulnerable to their adverse effects (McMichael, 2000).

The current methodology evaluated the combined risk of stresses on the SCC population from environmental and socioeconomic factors. This study determined MODIS-derived summer daytime and nighttime LST and NDVI trends from 2000 to 2020, as well as ECOSTRESS-derived LST and ET distributions from 2018 to 2022 in SCC. It then related these results to census tract-level MHHI, the percentage of Hispanic/Latino populations, and the built environment per LCZ classification framework. The level of segregation between Hispanics and non-Hispanic Whites and among Hispanic/Latinos per the Index of Dissimilarity and SES per the Modified Darden-Kamel Composite Socioeconomic Index were calculated and related to health outcomes and temperature exposure. The combination of these assessments comprised a comprehensive human-environment approach to human health exposure evaluation, emphasizing differences among Hispanics by their national origin of birth, thereby exposing them to environmental injustice. In response to the findings from the urban climate and heat vulnerability analyses, urban heat adaptation measures were proposed and evaluated via the ENVI-Met software to measure the potential cooling effect of trees in Reid-Hillview Airport, located in east SCC.

Summary of Dissertation Chapters

Objective 1. Population growth increases urbanization, impacting surface albedo and ET rates. This process results in altered surface energy balances, thus creating distinctive local urban climates, including the formation of SUHIs. The reduction of urban evaporative cooling is an important factor contributing to SUHIs. Urban moisture content is lower than in surrounding areas, allowing them to warm faster than their vegetated counterparts. This exploratory study determined summer daytime and nighttime land surface temperature (LST) and ET trends and distributions in urban Santa Clara County, USA, from 2018 to 2022, as derived from high temporal (diurnal) and spatial (38 by 69-meter pixel) resolution ECOSTRESS data. It then related these results to census tract-level median household income (MHHI).

Results showed downward LST trends in summer area-mean daytime (-0.23°C per year) and nighttime (-0.54°C per year) LST trends. The area-minimum daytime LST increased (1.34°C per year) while its maximum decreased (-0.87°C per year). The corresponding nighttime values were -0.5°C and -1.11°C per year, respectively. Differences between these extremes resulted in a negative daytime (-2.21°C per year) and nighttime (-0.61°C per year) trend of intra-urban SUHI intensity. Spatial distribution showed that LST increased with either decreasing ET or MHHI values. ET values increased with increasing MHHI values. Neighborhoods with very-high MHHI thus experienced slower cooling rates than their very-low-income counterparts (-0.23 vs. -0.32 °C per year), an important finding for future population vulnerability assessments.

Objective 2. In the United States, there is a growing interest in understanding how heat stress in lower-income and racially segregated neighborhoods results in adverse health outcomes. This study spatially identified heat-vulnerable neighborhoods in Santa Clara County (SCC), CA. It evaluated the relationship between temperature exposure, race/ethnicity, and health outcomes of residents in those neighborhoods, emphasizing differences among Hispanics by the origin of birth to capture potential environmental injustices. The current methodology used Landsat 8 via Google Earth Engine to measure the Land Surface Temperature (LST) and Normalized Difference Vegetation Index (NDVI) to assess the potential of heat stress in the physical environment. The human environment was evaluated using the *Modified Darden-Kamel Composite Socioeconomic Index* to determine the spatial variability of socioeconomic status (SES) and the Index of Dissimilarity to assess the level of segregation between Hispanics and non-Hispanic Whites and

among Hispanic/Latinos. Spatial regression models were used to quantify the relationship between these measured assessments and health outcomes.

Results revealed socioeconomic inequalities and uneven residential distributions between Hispanic/Latinos and non-Hispanic Whites. High LST and low NDVI values were found only in Mexican neighborhoods, implying possible environmental racism. Almost half of the Mexican population lived in highly segregated neighborhoods with low and very low SES, mainly located in East San Jose, where, historically, they have been ghettoized. Mexicans reported low health insurance coverage rates and could be at a higher risk of heat stress and heat mortality during heat waves. Future work should examine additional variables (e.g., housing characteristics, crime, social cohesion, and collective behaviors) to comprehensively evaluate the at-risk Mexican population. The combination of these assessments comprised a comprehensive human-environment approach for health exposure evaluation by which to define environmental injustice.

Objective 3. The increase in the number and quality of urban forests has become popular to reduce intra-urban tree-canopy inequality, enhance community well-being, and mitigate urban heat. Previous studies have evaluated the impact of increased vegetation on urban temperature, but the number of trees necessary to effectively improve thermal comfort has been under-explored. This study assessed the cooling efficiency of urban greenery as a heat mitigation measure for a low-income neighborhood in SCC via ENVI-Met software. A series of sensitivity tests were conducted for daytime hours (1200-180) under typical and extreme summer conditions to evaluate the thermal conditions of the area after increasing tree coverage from the baseline scenario (0%) to 25%, 50%, 75%, and 100%.

The results allowed for the quantification of the potential cooling effects of increasing tree coverage. On a 25% tree coverage scenario, values changed by -0.14°C, while maximum changes in air temperature were quantified for 50% (-0.24°) and 75% (-0.32°C) of tree coverage scenarios. Slight temperature differences were observed between the 75 and 100% (-0.39°C) tree coverage scenarios. Similar changes between scenarios were observed under extreme heat conditions, although temperatures decreased faster than under typical summer conditions. Non-linear relationships were found between changes in air temperature and time for all scenarios, suggesting a threshold in the number of trees to maximize cooling capacity, as additional trees would reduce air temperature minimally. As tree coverage increases, differences in mean air temperature between scenarios decrease.

Limitations

Heat vulnerability assessments are necessary for stakeholders to correctly identify vulnerable populations and implement effective mitigation and adaptation strategies. This study proposes the use of the Darden-Kamel CSI, given the lack of consensus among researchers about the variables to measure heat exposure (climatic and built-up environment) and vulnerability (health, demographics, and SES). Different measures of SES, however, would yield different results in the spatial distribution of vulnerable populations. Low-income status is usually associated with racial or ethnic minorities, neighborhoods with less vegetation, and more heat-absorbing surfaces (Gronlund, 2014). High levels of exposure to environmental hazards, including extreme heat weather events, may be related to minorities' lower SES, which limits their access to mitigating resources (e.g., A/C, access to transportation, quality of housing materials) and may also determine acclimatization and adaptation.

SES, however, can be measured using wealth, inherited wealth, occupation, family structure, social networks, and education. Wealth, consequently, can be measured using per capita income, median house value, education levels, or occupational prestige. The most used SES indicator in social science is family income, although it is more likely to be misreported because participants ignore the precise amount of their income or might feel discomfort to report it (Diemer et al., 2013). In the case of the American Community Survey, a recurrent data source for heat vulnerability indices, "the same respondent may give different answers to a question about income or race when interviewed more than once due to random factors, such as how the respondent interprets the question" (National Research Council, 2007, p. 53).

Familial wealth is another indicator that could better represent household economic resources due to their multigenerational nature. Family wealth is the total net worth of a family (stocks, bonds, home equity, businesses owned) minus the family's debt (i.e., mortgage loans, car loans, credit card debt). Finally, SES indicators operate with other individual characteristics like race, ethnicity, age, and gender (Diemer et al., 2013). "Traditional measures of SES are not equivalent across race because, for example, compared to Whites, Blacks may have less purchasing power because the costs of goods and services are higher in Black communities" (Madrigano et al., 2018, p.6).

Distributions of vulnerable populations would also depend on the scale of analysis (e.g., individual-level, zip codes, block groups, census tracts, counties, and metropolitan areas), which

may produce different findings. For example, different segregation patterns may result if they are examined with the use of block groups or census tracts because "block groups tend to be modestly more homogenous than census tracts" (Iceland & Steinmetz, 2003); "the higher the homogeneity, the higher the level of apparent segregation" (Massey & Denton, 1988, p. 262). Additional studies must be performed in other sites at multiple scales for place comparison to uncover other human-environment processes occurring within other administrative boundaries. Results of these studies would allow a better understanding of Hispanic/Latino experiences in the US, as the population is expected to double by 2050.

Future Research

Accounting for race in heat vulnerability studies can be complicated because 1) structural racism influences the production of knowledge (literature characterized by stereotypes) that reflect uncritical, popular understandings of race (Pulido, 2000) and 2) the concept and measure of race, and the subsequent racial groupings, has varied over time in the history of the United States, mainly shaped by political forces (Ford & Airhihenbuwa, 2010; Hamilton et al., 1988). Race is a social construct, not biological, and therefore, future discussion of racial differences in heat vulnerability should focus on this social aspect, recognizing that all people may be susceptible to heat, but some people are more or less vulnerable to heat because of where they live. Culture also plays an important role in the adaptation to heat and whether heat contributes to poorer health outcomes. Heat vulnerability indices can be characterized by stereotypes that reflect an uncritical understanding of an ethnic or racial group. For example, when constructing heat vulnerability indices, researchers suggest that Hispanics tend to be more vulnerable during extreme heat events, but this could be a social construct. Hispanics could be at higher exposure but could also have become more resilient. Low-income Hispanics are exposed to cumulative hazards, but their ability to cope with adversity will determine their vulnerability, which includes intangible resources such as cultural, social, or religious groups (Williams et al., 2010).

Immigration status and duration of residence in the United States may also influence health outcomes. For example, the health outcomes of US-born Hispanics are comparable to Black/African Americans, while highly segregated foreign-born Hispanics report better health outcomes (Do et al., 2017). The findings suggest that segregation can have deleterious effects on US-born Hispanics but may offer a protective health benefit for newcomers, also referred to as the ethnic density effect (Grady, 2006). Future efforts in heat vulnerability analysis must, therefore,

evaluate the capacities of vulnerable groups with the use of quantitative (secondary data sources) and qualitative (primary data sources) measures. Heat-adapted building codes are further needed as risks rise under climate change. Qualitative methods are vital in identifying coping and adaptation strategies, including social capital via networks and institutions, while quantitative methods could be used to compare the vulnerability of places and trends over time (Tate, 2012).

Heat vulnerability studies have documented that minorities are overexposed to environmental hazards, including extreme heat. In California, communities of color have lower MHHI and home values, and fewer are homeowners while also being exposed to higher toxic release facilities (Morello-Frosch et al., 2002). Inequities can be explained from an institutional racism lens, which is reflected in the social and geographic characteristics of minorities (Chow et al., 2012). Future studies that attempt to explain the geographical distribution of heat risk must, therefore, emphasize the historical roots that contribute to today's health disparities and the poor health outcomes among communities of color (Ford & Airhihenbuwa, 2010).

Vulnerability is not a time-fixed variable as it varies with socioeconomic, political, and cultural dynamics. As with this study, heat vulnerability is presented as a cross-sectional measure, exploring risk exposure at one period in time. Future efforts could benefit from a longitudinal evaluation (Morello-Frosch & Shenassa, 2006), considering additional variables such as the generational effect of populations, economic downturns, and other policies in mediating heat vulnerability. Vulnerability indices need to transition from an academic construct to a decision-making tool (Tate, 2012). Heat vulnerability indices should consider the nuances of an urban area, including its historical and institutional context, to make cities and their people resilient to current and future extreme heat weather events.

Policy Implications

The results of this study provide a methodology for local governments to evaluate high-temperature distributions and implement mitigation/adaptation strategies to reduce heat risks (heat warning systems and urban greenery projects, zoning codes, and air quality standards), particularly in low-income communities whose residents are most vulnerable. Heat syndromic surveillance can be implemented with the analysis of diagnostic codes beyond those related to heat-related illnesses (e.g., sunstroke), such as cardiovascular disorders. Additional health programs can be implemented during summer and heat waves, particularly in areas where populations report not having access to health insurance.

Heat mitigation actions are important, but they are not the definite solution if unequal heat exposure continues disadvantaging groups based on income, race, or color. Government agencies must identify areas where human health and the environment are disproportionately affected by heat and other noxious facilities. Programs, policies, and zoning ordinances must then be placed to redress inequities and allocate resources and actions where the environmental and health needs are the greatest. Even if green areas are required by building and construction codes, evidence suggests that zoning ordinance enforcement is low within low-income communities, especially in areas where homeownership is low.

Although green redevelopment can mitigate the increasing urban heat effects, it can also exclude those whose need for access is most acute. As access to green space is recognized as environmental justice, cities have implemented the supply of urban green areas in low-income areas, which has made them attractive to a population of higher status, encouraging gentrification. Access to credits for landlords to upgrade housing materials in low-income communities could decrease the negative impacts of high summer temperatures without promoting green gentrification.

BIBLIOGRAPHY

Ali-Toudert, F., & Mayer, H. (2007). Effects of asymmetry, galleries, overhanging façades, and vegetation on thermal comfort in urban street canyons. Solar Energy, 81(6), 742–754. https://doi.org/10.1016/j.solener.2006.10.007

Allen, M. A., Roberts, D. A., & McFadden, J. P. (2021). Reduced urban green cover and daytime cooling capacity during the 2012–2016 California drought. Urban Climate, 36 (December 2020), 100768. https://doi.org/10.1016/j.uclim.2020.100768

Almaguer, T. (2009). Racial fault lines: the historical origins of White supremacy in California. University of California Press.

Ambrosini, D., Galli, G., Mancini, B., Nardi, I., & Sfarra, S. (2014). Evaluating mitigation effects of urban heat islands in a historical small center with the ENVI-Met® climate model. Sustainability (Switzerland), 6(10), 7013–7029. https://doi.org/10.3390/su6107013

Anselin, L. (1995). Local Indicators of Spatial Association—LISA. Geographical Analysis, 27(2), 93–115. https://doi.org/10.1111/j.1538-4632.1995.tb00338.x

Anselin, L., & Rey, S. J. (2014). Modern Spatial Econometrics in Practice: A Guide to GeoDa, GeoDaSpace and PySAL. In GeoDa Press LLC. GeoDa Press LLC.

Anselin, L., Syabri, I., & Smirnov, O. (2002). Visualizing multivariate spatial correlation with dynamically linked windows. New Tools for Spatial Data Analysis: Proceedings of the Specialist Meeting, 1–20. http://geodacenter.asu.edu/pdf/multi_lisa.pdf

Applied Survey Research. (2017). City of San Jose, Homeless Census and Survey Report 2017. http://www.sanjoseca.gov/DocumentCenter/View/70076

Arnfield, A. J. (2003). Review Two Decades Of Urban Climate Research: A Review Of Turbulence, Exchanges Of Energy And Water, And The Urban Heat Island. International Journal of Climatology, 23(1), 1–26. https://doi.org/10.1002/joc.859

Aspinall, R. (2010). A century of physical geography research in the Annals. Annals of the Association of American Geographers, 100(5), 1049-1059.

Avdan, U., & Jovanovska, G. (2016). Algorithm for Automated Mapping of Land Surface Temperature Using LANDSAT 8 Satellite Data. Journal of Sensors, 2016, 1–8. https://doi.org/10.1155/2016/1480307

Balchin, W. G. V, & Pye, N. (1947). A micro-climatological investigation of bath and the surrounding district. Quarterly Journal of the Royal Meteorological Society, 73(317–318), 297–323. https://doi.org/10.1002/qj.49707331706

Ballinas, M., & Barradas, V. L. (2015). The Urban Tree as a Tool to Mitigate the Urban Heat Island in Mexico City: A Simple Phenomenological Model. Journal of Environment Quality, 45(1), 157. https://doi.org/10.2134/jeq2015.01.0056

Bassil, K. L., Cole, D. C., Moineddin, R., Lou, W., Craig, A. M., Schwartz, B., & Rea, E. (2011). The relationship between temperature and ambulance response calls for heat-related illness in Toronto, Ontario, 2005. Journal of Epidemiology and Community Health, 65(9), 829–831. https://doi.org/10.1136/jech.2009.101485

Basu, R., & Malig, B. (2011). High ambient temperature and mortality in California: exploring the roles of age, disease, and mortality displacement. Environmental Research, 111(8), 1286-1292.

Basu, R., & Samet, J. M. (2002). Relation between elevated ambient temperature and mortality: A review of the epidemiologic evidence. Epidemiologic Reviews, 24(2), 190–202. https://doi.org/10.1093/epirev/mxf007

Baxter, V. (2010). Prosperity, Immigration, and Neighborhood Change in Silicon Valley: 1990-2000. Sociological Spectrum, 30(3), 338–364. https://doi.org/10.1080/02732171003635554

Bean, F. D., & Tienda, M. (1987). Hispanic Population of the United States, The. Russell Sage Foundation. http://www.jstor.org/stable/10.7758/9781610440370

Bechtel, B., Alexander, P., Böhner, J., Ching, J., Conrad, O., Feddema, J., Mills, G., See, L., & Stewart, I. (2015). Mapping Local Climate Zones for a Worldwide Database of the Form and Function of Cities. ISPRS International Journal of Geo-Information, 4(1), 199–219. https://doi.org/10.3390/ijgi4010199

Benmarhnia, T., Alexander, S., Price, K., Smargiassi, A., King, N., & Kaufman, J. S. (2018). The heterogeneity of vulnerability in public health: a heat wave action plan as a case study. Critical Public Health, 28(5), 619–625. https://doi.org/10.1080/09581596.2017.1322176

Bloch, S. (2019). Shade. Places Journal, 2019. https://doi.org/10.22269/190423

Boessen, A., & Hipp, J. R. (2018). Parks as crime inhibitors or generators: Examining parks and the role of their nearby context. Social Science Research, 76, 186–201. https://doi.org/10.1016/j.ssresearch.2018.08.008

Boone, C. G., Buckley, G. L., Grove, J. M., & Sister, C. (2009). Parks and People: An Environmental Justice Inquiry in Baltimore, Maryland.: Start here for books, articles & more. 99(June 2008), 767–787. http://eds.b.ebscohost.com.libproxy.smith.edu:2048/eds/pdfviewer/pdfviewer?sid=9d889308-036e-4fd7-a1e1-3324503d4446%40sessionmgr114&vid=7&hid=116

Bornstein, R. D. (1968). Observations of the Urban Heat Island Effect in New York City. Journal of Applied Meteorology, 7(4), 575–582. https://doi.org/10.1175/1520-0450(1968)007<0575:OOTUHI>2.0.CO;2

Bornstein, R., Styrbicki-Imamura, R., González, J. E., & Lebassi, B. (2012). Interactions of Global-Warming and Urban Heat Islands in Different Climate-Zones. In H. J. S. Fernando, Z. Klaić, & J. L. McCulley (Eds.), National Security and Human Health Implications of Climate Change (pp. 49–60). Springer Netherlands.

Bowleg, L. (2012). The problem with the phrase women and minorities: Intersectionality-an important theoretical framework for public health. American Journal of Public Health, 102(7), 1267–1273. https://doi.org/10.2105/AJPH.2012.300750

Bradford, K., Abrahams, L., Hegglin, M., & Klima, K. (2015). A Heat Vulnerability Index and Adaptation Solutions for Pittsburgh, Pennsylvania. Environmental Science & Technology, 49(19), 11303–11311. https://doi.org/10.1021/acs.est.5b03127

Browning, C. R., Wallace, D., Feinberg, S. L., & Cagney, K. A. (2006). Neighborhood Social Processes, Physical Conditions, and Disaster-Related Mortality: The Case of the 1995 Chicago Heat Wave. American Sociological Review, 71(4), 661–678. https://doi.org/10.1177/000312240607100407

Budhiraja, B., Agrawal, G., & Pathak, P. (2020). Urban heat island effect of a polynuclear megacity Delhi – Compactness and thermal evaluation of four sub-cities. Urban Climate, 32(May 2019), 100634. https://doi.org/10.1016/j.uclim.2020.100634

Cai, M., Ren, C., Xu, Y., Lau, K., & Wang, R. (2018). Investigating the relationship between local climate zone and land surface temperature using an improved WUDAPT methodology – A case study of Yangtze River Delta, China. Urban Climate, 24, 485–502. https://doi.org/10.1016/j.uclim.2017.05.010

CalEPA. (2018). Indicators of Climate Change in California. https://oehha.ca.gov/media/downloads/climate-change/report/2018caindicatorsreportmay2018.pdf

Casey, J. A., Morello-Frosch, R., Mennitt, D. J., Fristrup, K., Ogburn, E. L., & James, P. (2017). Race/Ethnicity, Socioeconomic Status, Residential Segregation, and Spatial Variation in Noise Exposure in the Contiguous United States. Environmental Health Perspectives, 125(7), 077017. https://doi.org/10.1289/EHP898

Cawse-Nicholson, K., Anderson, M. C., Yang, Y., Yang, Y., Hook, S. J., Fisher, J. B., Halverson, G., Hulley, G. C., Hain, C., Baldocchi, D. D., Brunsell, N. A., Desai, A. R., Griffis, T. J., & Novick, K. A. (2021). Evaluation of a CONUS-Wide ECOSTRESS DisALEXI Evapotranspiration Product. IEEE Journal of Selected Topics in Applied Earth Observations and Remote Sensing, 14, 10117–10133. https://doi.org/10.1109/JSTARS.2021.3111867

CDC. (2013). Climate Change and Extreme Heat Events. https://www.cdc.gov/climateandhealth/pubs/climatechangeandextremeheatevents.pdf

Chakraborty, T., Hsu, A., Manya, D., & Sheriff, G. (2020). A spatially explicit surface urban heat island database for the United States: Characterization, uncertainties, and possible applications. ISPRS Journal of Photogrammetry and Remote Sensing, 168(April), 74–88. https://doi.org/10.1016/j.isprsjprs.2020.07.021

Chakraborty, T., & Lee, X. (2019). A simplified urban-extent algorithm to characterize surface urban heat islands on a global scale and examine vegetation control on their spatiotemporal variability. International Journal of Applied Earth Observation and Geoinformation, 74(May 2018), 269–280. https://doi.org/10.1016/j.jag.2018.09.015

Chambers, B. D., Baer, R. J., McLemore, M. R., & Jelliffe-Pawlowski, L. L. (2019). Using Index of Concentration at the Extremes as Indicators of Structural Racism to Evaluate the Association with Preterm Birth and Infant Mortality—California, 2011–2012. Journal of Urban Health, 96(2), 159–170. https://doi.org/10.1007/s11524-018-0272-4

Chang, Y., Xiao, J., Li, X., Zhou, D., & Wu, Y. (2022). Combining GOES-R and ECOSTRESS land surface temperature data to investigate diurnal variations of surface urban heat island. Science of the Total Environment, 823, 153652. https://doi.org/10.1016/j.scitotenv.2022.153652

Cheung, P. K., Nice, K. A., & Livesley, S. J. (2022). Irrigating urban green space for cooling benefits: the mechanisms and management considerations. Environmental Research: Climate, 1(1), 015001. https://doi.org/10.1088/2752-5295/ac6e7c

Cheyre, C., Kowalski, J., & Veloso, F. M. (2015). Spinoffs and the ascension of Silicon Valley. Industrial and Corporate Change, 24(4), 837–858. https://doi.org/10.1093/icc/dtv025

Ching, J., Mills, G., Bechtel, B., See, L., Feddema, J., Wang, X., Ren, C., Brorousse, O., Martilli, A., Neophytou, M., Mouzourides, P., Stewart, I., Hanna, A., Ng, E., Foley, M., Alexander, P., Aliaga, D., Niyogi, D., Shreevastava, A., … Theeuwesits, N. (2018). WUDAPT: An urban weather, climate, and environmental modeling infrastructure for the anthropocene. Bulletin of the American Meteorological Society, 99(9), 1907–1924. https://doi.org/10.1175/BAMS-D-16-0236.1

Chow, W. T. L., Chuang, W. C., & Gober, P. (2012). Vulnerability to Extreme Heat in Metropolitan Phoenix: Spatial, Temporal, and Demographic Dimensions. Professional Geographer, 64(2), 286–302. https://doi.org/10.1080/00330124.2011.600225

Coleman, R. W., Stavros, N., Hulley, G., & Parazoo, N. (2020). Comparison of thermal infrared-derived maps of irrigated and non-irrigated vegetation in urban and non-urban areas of southern California. Remote Sensing, 12(24), 1–19. https://doi.org/10.3390/rs12244102

Comission, C. B. S. (n.d.). 2019 California Green Building Standards Code, Title 24, Part 11 with Jan 2020 Errata | ICC Digital Codes. https://codes.iccsafe.org/content/CGBC2019P3

Dalenius, T., & Hodges, J. L. (1959). Minimum Variance Stratification. Journal of the American Statistical Association, 54(285), 88. https://doi.org/10.2307/2282141

Darden, J. T., & Rubalcava, L. (2018). The Measurement of Neighborhood Socioeconomic Characteristics and Hispanic and Non-Hispanic White Residential Segregation in Metropolitan Detroit. Hispanic Journal of Behavioral Sciences, 40(3), 312–329. https://doi.org/10.1177/0739986318769316

De Munck, C., Pigeon, G., Masson, V., Meunier, F., Bousquet, P., Tréméac, B., Merchat, M., Poeuf, P., & Marchadier, C. (2013). How much can air conditioning increase air temperatures for a city like Paris, France? International Journal of Climatology, 33(1), 210–227. https://doi.org/10.1002/joc.3415

Declet-Barreto, J., Brazel, A. J., Martin, C. A., Chow, W. T. L., & Harlan, S. L. (2013). Creating the park cool island in an inner-city neighborhood: Heat mitigation strategy for Phoenix, AZ. Urban Ecosystems, 16(3), 617–635. https://doi.org/10.1007/s11252-012-0278-8

Deilami, K., Kamruzzaman, M., & Liu, Y. (2018). Urban heat island e ff ect : A systematic review of spatio-temporal factors , data , methods , and mitigation measures. International Journal of Applied Earth Observation and Geoinformation, 67, 30–42. https://doi.org/10.1016/J.JAG.2017.12.009

Diemer, M. A., Mistry, R. S., Wadsworth, M. E., López, I., & Reimers, F. (2013). Best practices in conceptualizing and measuring social class in psychological research. Analyses of Social Issues and Public Policy, 13(1), 77–113. https://doi.org/10.1111/asap.12001

Do, D. P., Frank, R., Zheng, C., & Iceland, J. (2017). Hispanic Segregation and Poor Health: It's Not Just Black and White. American Journal of Epidemiology, 186(8), 990–999. https://doi.org/10.1093/aje/kwx172

Dong, L., Mitra, C., Greer, S., & Burt, E. (2018). The dynamical linkage of atmospheric blocking to drought, heatwave and urban heat island in southeastern US: A multi-scale case study. Atmosphere, 9(1). https://doi.org/10.3390/ATMOS9010033

Dou, J., Wang, Y., Bornstein, R., & Miao, S. (2015). Observed spatial characteristics of Beijing urban climate impacts on summer thunderstorms. Journal of Applied Meteorology and Climatology, 54(1), 94–105. https://doi.org/10.1175/JAMC-D-13-0355.1

Duckworth, F. S., & Sandberg, J. S. (1954). The effect of cities upon horizontal and vertical temperature gradients. Bulletin of the American Meteorological Society, 35(5), 198–207. http://www.jstor.org/stable/26242101

Emch, M., Root, E. D., & Carrel, M. (2017). Health and medical geography (4th Editio). Giuldford Press.

EPA. (2021). Heat Island Impacts. Heat Islands. https://www.epa.gov/heatislands/heat-island-impacts

Ermida, S. L., Soares, P., Mantas, V., Göttsche, F. M., & Trigo, I. F. (2020). Google earth engine open-source code for land surface temperature estimation from the landsat series. Remote Sensing, 12(9), 1–21. https://doi.org/10.3390/RS12091471

Ford, C. L., & Airhihenbuwa, C. O. (2010). Critical Race Theory, Race Equity, and Public Health: Toward Antiracism Praxis. American Journal of Public Health, 100(S1), S30–S35. https://doi.org/10.2105/AJPH.2009.171058

Fotheringham, A. S., & Wong, D. W. (1991). The modifiable areal unit problem in multivariate statistical analysis. Environment and Planning A, 23(7), 1025-1044.

Gaitani, N., Mihalakakou, G., & Santamouris, M. (2007). On the use of bioclimatic architecture principles in order to improve thermal comfort conditions in outdoor spaces. Building and Environment, 42(1), 317–324. https://doi.org/10.1016/j.buildenv.2005.08.018

Garrison, J. D. (2021). Environmental Justice in Theory and Practice: Measuring the Equity Outcomes of Los Angeles and New York's "Million Trees" Campaigns. Journal of Planning Education and Research, 41(1), 6–17. https://doi.org/10.1177/0739456X18772072

Gershunov, A., & Guirguis, K. (2012). California heat waves in the present and future. Geophysical Research Letters, 39(18).

Giovannini, L., Zardi, D., & de Franceschi, M. (2013). Characterization of the Thermal Structure inside an Urban Canyon: Field Measurements and Validation of a Simple Model. Journal of Applied Meteorology and Climatology, 52(1), 64–81. https://doi.org/10.1175/JAMC-D-12-06.1

Gorelick, N., Hancher, M., Dixon, M., Ilyushchenko, S., Thau, D., & Moore, R. (2017). Google Earth Engine: Planetary-scale geospatial analysis for everyone. Remote Sensing of Environment, 202, 18–27. https://doi.org/10.1016/j.rse.2017.06.031

Grady, S. C. (2012). Climate change vulnerability and impacts on human health. Climate Change in the Midwest: Impacts, Risks, Vulnerability, and Adaptation, 117–133.

Green, R. S., Basu, R., Malig, B., Broadwin, R., Kim, J. J., & Ostro, B. (2010). The effect of temperature on hospital admissions in nine California counties. International Journal of Public Health, 55(2), 113–121. https://doi.org/10.1007/s00038-009-0076-0

Grineski, S. E., Collins, T. W., McDonald, Y. J., Aldouri, R., Aboargob, F., Eldeb, A., Romo Aguilar, M. de L., & Velázquez-Angulo, G. (2015). Double exposure and the climate gap: changing demographics and extreme heat in Ciudad Juárez, Mexico. Local Environment, 20(2), 180–201. https://doi.org/10.1080/13549839.2013.839644

Gronlund, C. J. (2014). Racial and Socioeconomic Disparities in Heat-Related Health Effects and Their Mechanisms: a Review. Current Epidemiology Reports, 1(3), 165–173. https://doi.org/10.1007/s40471-014-0014-4

Gunawardena, K. R., Wells, M. J., & Kershaw, T. (2017). Utilising green and bluespace to mitigate urban heat island intensity. Science of the Total Environment, 584–585, 1040–1055. https://doi.org/10.1016/j.scitotenv.2017.01.158

Gupta, S. K., Ram, J., & Singh, H. (2018). Comparative Study of Transpiration in Cooling Effect of Tree Species in the Atmosphere. Journal of Geoscience and Environment Protection, 06(08), 151–166. https://doi.org/10.4236/gep.2018.68011

Hajat, S., & Kosatky, T. (2010). Heat-related mortality: A review and exploration of heterogeneity. Journal of Epidemiology and Community Health, 64(9), 753–760. https://doi.org/10.1136/jech.2009.087999

Hamilton, C. V., Omi, M., & Winant, H. (1988). Racial Formation in the United States from the 1960s to the 1980s. Political Science Quarterly, 103(1), 158. https://doi.org/10.2307/2151151

Hammett, M., Hondula, D., Chakalian P., Guardaro, M., Hartman M., Kurtz, L., Peters, K., Quay, R., Redman, C., Stotler, C., Waller, K., and Zafaranlou, A. Hammett, M., Hondula, D., Chakalian P., Guardaro, M., Hartman M., Kurtz, L., Peters, K., Quay, R., R, A. (2019). Heatready Phoenix: A Comprehensive Framework for Addressing Extreme Heat. AMS, 99th Annual Meeting. https://ams.confex.com/ams/2019Annual/webprogram/Paper354868.html

Harlan, S. L., Declet-Barreto, J. H., Stefanov, W. L., & Petitti, D. B. (2013). Neighborhood effects on heat deaths: social and environmental predictors of vulnerability in Maricopa County, Arizona. Environmental Health Perspectives, 121(2), 197–204. https://doi.org/10.1289/ehp.1104625

Harris, B., Schmalz, D., Larson, L., & Fernandez, M. (2021). Fear of the Unknown: Examining Neighborhood Stigma's Effect on Urban Greenway Use and Surrounding Communities. Urban Affairs Review, 57(4), 1015–1048. https://doi.org/10.1177/1078087420909529

Harris, B., Schmalz, D., Larson, L., Fernandez, M., & Griffin, S. (2020). Contested Spaces: Intimate Segregation and Environmental Gentrification on Chicago's 606 Trail. City and Community, 19(4), 933–962. https://doi.org/10.1111/cico.12422

Hattis, D., Ogneva-Himmelberger, Y., & Ratick, S. (2012). The spatial variability of heat-related mortality in Massachusetts. Applied Geography, 33(1), 45–52. https://doi.org/10.1016/j.apgeog.2011.07.008

He, B. J. (2018). Potentials of meteorological characteristics and synoptic conditions to mitigate urban heat island effects. Urban Climate, 24(November 2017), 26–33. https://doi.org/10.1016/j.uclim.2018.01.004

Hebbert, M., & Jankovic, V. (2013). Cities and Climate Change: The Precedents and Why They Matter. Urban Studies, 50(7), 1332–1347. https://doi.org/10.1177/0042098013480970

Heppler, J. (2018). Sal si Puedes. Silicon Valley Historical. http://svhistorical.org/items/show/9

Hoffman, J. S., Shandas, V., & Pendleton, N. (2020). The Effects of Historical Housing Policies on Resident Urban Areas. Climate, 8(12), 1–15. https://www.mdpi.com/2225-1154/8/1/12/htm

Hsu, A., Sheriff, G., Chakraborty, T., & Manya, D. (2021). Disproportionate exposure to urban heat island intensity across major US cities. Nature Communications, 12(1), 1–11. https://doi.org/10.1038/s41467-021-22799-5

Huang, G., Zhou, W., & Cadenasso, M. L. (2011). Is everyone hot in the city? Spatial pattern of land surface temperatures, land cover and neighborhood socioeconomic characteristics in Baltimore, MD. Journal of Environmental Management, 92(7), 1753–1759. https://doi.org/10.1016/j.jenvman.2011.02.006

Huston, P. (2016). Vector-borne disease, cities, and climate change. Canada Communicable Disease Report, 62(10), 818. http://www.ncbi.nlm.nih.gov/pubmed/27737979

Iceland, J., & Steinmetz, E. (2003). The Effects of Using Census Block Groups Instead of Census Tracts When Examining Residential Housing Patterns. Social Forces, July, 1–8. www.census.gov/hhes/www/housing/resseg/pdf/unit_of_analysis.pdf

Imhoff, M. L., Zhang, P., Wolfe, R. E., & Bounoua, L. (2010). Remote sensing of the urban heat island effect across biomes in the continental USA. Remote Sensing of Environment, 114(3), 504–513. https://doi.org/10.1016/j.rse.2009.10.008

International Code Council. (2018). California Green Building Standards Code. https://www.dgs.ca.gov/BSC/Resources/Page-Content/Building-Standards-Commission-Resources-List-Folder/CALGreen

Jänicke, B., Milošević, D., & Manavvi, S. (2021). Review of user-friendly models to improve the urban micro-climate. Atmosphere, 12(10), 1–22. https://doi.org/10.3390/atmos12101291

Jauregui, E. (1997). Heat Island Development in Mexico City. Atmospheric Environment, 31(22), 3821–3831. https://doi.org/http://dx.doi.org/10.1016/S1352-2310(97)00136-2

Jelks, N. O., Jennings, V., & Rigolon, A. (2021). Green gentrification and health: A scoping review. International Journal of Environmental Research and Public Health, 18(3), 1–23. https://doi.org/10.3390/ijerph18030907

Jenerette, G. D., Harlan, S. L., Brazel, A., Jones, N., Larsen, L., & Stefanov, W. L. (2007). Regional relationships between surface temperature, vegetation, and human settlement in

a rapidly urbanizing ecosystem. Landscape Ecology, 22(3), 353–365. https://doi.org/10.1007/s10980-006-9032-z

Jesdale, B. M., Morello-Frosch, R., & Cushing, L. (2013). The Racial/Ethnic Distribution of Heat Risk–Related Land Cover in Relation to Residential Segregation. Environmental Health Perspectives, 121(7), 811–817. https://doi.org/10.1289/ehp.1205919

Johnson, D. P., & Wilson, J. S. (2009). The socio-spatial dynamics of extreme urban heat events: The case of heat-related deaths in Philadelphia. Applied Geography, 29(3), 419–434. https://doi.org/10.1016/j.apgeog.2008.11.004

Johnson, D. P., Wilson, J. S., & Luber, G. C. (2009). Socioeconomic indicators of heat-related health risk supplemented with remotely sensed data. International Journal of Health Geographics, 8(1), 57. https://doi.org/10.1186/1476-072X-8-57

Johnson, R. (2013, September 7). Homeless in Silicon Valley. Business Insider. https://www.businessinsider.com/homeless-in-silicon-valley-infographic-2013-8

Kim, J. H., Gu, D., Sohn, W., Kil, S. H., Kim, H., & Lee, D. K. (2016). Neighborhood landscape spatial patterns and land surface temperature: An empirical study on single-family residential areas in Austin, Texas. International Journal of Environmental Research and Public Health, 13(9). https://doi.org/10.3390/ijerph13090880

Kim, Y. A., Collins, T. W., & Grineski, S. E. (2014). Neighborhood context and the Hispanic health paradox: Differential effects of immigrant density on children's wheezing by poverty, nativity and medical history. Health and Place, 27, 1–8. https://doi.org/10.1016/j.healthplace.2014.01.006

Klinenberg, E. (2002). Heat Wave: A Social Autopsy of the Disaster in Chicago. In Sociology of Health & Illness (Vol. 8, Issue 3, pp. 376–378). https://doi.org/doi: 10.2708/Chicago/9780226276212.001.0001

Kruskal, W. H., & Wallis, W. A. (1952). Use of Ranks in One-Criterion Variance Analysis. Journal of the American Statistical Association, 47(260), 583–621. https://doi.org/10.1080/01621459.1952.10483441

Kueppers, L. M., Snyder, M. A., & Sloan, L. C. (2007). Irrigation cooling effect: Regional climate forcing by land-use change. Geophysical Research Letters, 34(3), 1–5. https://doi.org/10.1029/2006GL028679

Lebassi, B., Gonzalez, J., Fabris, D., Maurer, E., Miller, N., Milesi, C., Switzer, P., & Bornstein, R. (2009). Observed 1970-2005 cooling of summer daytime temperatures in coastal California. Journal of Climate, 22(13), 3558–3573. https://doi.org/10.1175/2008JCLI2111.1

Li, H., Zhou, Y., Li, X., Meng, L., Wang, X., Wu, S., & Sodoudi, S. (2018). A new method to quantify surface urban heat island intensity. Science of The Total Environment, 624, 262–272. https://doi.org/10.1016/j.scitotenv.2017.11.360

Li, L., Zha, Y., & Zhang, J. (2020). Spatial and dynamic perspectives on surface urban heat island and their relationships with vegetation activity in Beijing, China, based on Moderate Resolution Imaging Spectroradiometer data. International Journal of Remote Sensing, 41(3), 882–896. https://doi.org/10.1080/01431161.2019.1650985

Li, X., Zhou, Y., Asrar, G. R., Imhoff, M., & Li, X. (2017). Science of the Total Environment The surface urban heat island response to urban expansion : A panel analysis for the conterminous United States. Science of the Total Environment, 605–606, 426–435. https://doi.org/10.1016/j.scitotenv.2017.06.229

Makido, Y., Hellman, D., & Shandas, V. (2019). Nature-Based Designs to Mitigate Urban Heat: The Efficacy of Green Infrastructure Treatments in Portland, Oregon. Atmosphere, 10(5), 282. https://doi.org/10.3390/atmos10050282

Manoli, G., Fatichi, S., Bou-Zeid, E., & Katul, G. G. (2020). Seasonal hysteresis of surface urban heat islands. Proceedings of the National Academy of Sciences of the United States of America, 117(13), 7082–7089. https://doi.org/10.1073/pnas.1917554117

Martínez-Austria, P. F., Bandala, E. R., & Patiño-Gómez, C. (2016). Temperature and heat wave trends in northwest Mexico. Physics and Chemistry of the Earth, 91, 20–26. https://doi.org/10.1016/j.pce.2015.07.005

Marzban, F., Sodoudi, S., & Preusker, R. (2018). The influence of land-cover type on the relationship between NDVI–LST and LST-T air. International Journal of Remote Sensing, 39(5), 1377-1398.

Massey, D. S., & Denton, N. A. (1988). The Dimensions of Residential Segregation. Social Foreces, 67, 281–315.

Massey, D. S., & Denton, N. A. (1989). Hypersegregation in U.S. Metropolitan Areas: Black and Hispanic Segregation Along Five Dimensions. Demography, 26(3), 373–391. https://doi.org/10.2307/2061599

May, S., & Oliphant, A. J. (2023). Characteristics of the Park Cool Island in Golden Gate Park, San Francisco. Theoretical and Applied Climatology, 151(3–4), 1269–1282. https://doi.org/10.1007/s00704-022-04296-x

Mballo, S., Herpin, S., Manteau, M., Demotes-Mainard, S., & Bournet, P. E. (2021). Impact of well-watered trees on the microclimate inside a canyon street scale model in outdoor environment. Urban Climate, 37(November 2020). https://doi.org/10.1016/j.uclim.2021.100844

McMichael, A. J. (2000). The urban environment and health in a world of increasing globalization: issues for developing countries. Bulletin of the World Health Organization, 78(9), 1117–1126. https://doi.org/10.1590/S0042-96862000000900007

Mehrens, D. (2015). Inequality in Silicon Valley. In Working Partnerships USA. (Ed.), Let's Get Moving Summit. TransformCa. http://www.transformca.org/sites/default/files/Summit Plenary Slides - WPUSA Derecka Mehrens.pdf

Memon, R. A., Leung, D. Y. C., & Chunho, L. (2008). A review on the generation, determination, and mitigation of urban heat island. Journal of Environmental Sciences (China), 20(1), 120–128. https://doi.org/10.1016/S1001-0742(08)60019-4

Menendian, S., & Gambhir, S. (2018). Racial Segregation in the San Francisco Bay Area. Haas Institute, UC Berkeley. https://haasinstitute.berkeley.edu/racial-segregation-san-francisco-bay-area#bay-area

Miller, D. L., Wetherley, E. B., Roberts, D. A., Tague, C. L., & McFadden, J. P. (2022). Vegetation cover change during a multi-year drought in Los Angeles. Urban Climate, 43(February), 101157. https://doi.org/10.1016/j.uclim.2022.101157

Mills, G., Cleugh, H., Emmanuel, R., Endlicher, W., Erell, E., McGranahan, G., Ng, E., Nickson, A., Rosenthal, J., & Steemer, K. (2010). Climate information for improved planning and management of mega cities (Needs Perspective). Procedia Environmental Sciences, 1(1), 228–246. https://doi.org/10.1016/j.proenv.2010.09.015

Mini, C., Hogue, T. S., & Pincetl, S. (2014). Estimation of residential outdoor water use in Los Angeles, California. Landscape and Urban Planning, 127, 124–135. https://doi.org/10.1016/j.landurbplan.2014.04.007

Mirzaei, P. A. (2015). Recent challenges in modeling of urban heat island. Sustainable Cities and Society, 1–7. https://doi.org/10.1016/j.scs.2015.04.001

Mitchell, Bruce C., & Chakraborty, J. (2015). Landscapes of thermal inequity: Disproportionate exposure to urban heat in the three largest US cities. Environmental Research Letters, 10(11). https://doi.org/10.1088/1748-9326/10/11/115005

Mitchell, Bruce Coffyn, & Chakraborty, J. (2018). Exploring the relationship between residential segregation and thermal inequity in 20 U.S. cities. Local Environment, 23(8), 796–813. https://doi.org/10.1080/13549839.2018.1474861

Morakinyo, T. E., Kong, L., Lau, K. K. L., Yuan, C., & Ng, E. (2017). A study on the impact of shadow-cast and tree species on in-canyon and neighborhood's thermal comfort. Building and Environment, 115, 1–17. https://doi.org/10.1016/j.buildenv.2017.01.005

Morello-Frosch, R., & Lopez, R. (2006). The riskscape and the color line: Examining the role of segregation in environmental health disparities. Environmental Research, 102(2), 181–196. https://doi.org/10.1016/j.envres.2006.05.007

Morello-Frosch, R., Pastor, M., Porras, C., & Sadd, J. (2002). Environmental justice and regional inequality in southern California: implications for future research. Environmental Health Perspectives, 110(2), 149–154. https://doi.org/10.1289/ehp.02110s2149

Morello-Frosch, R., & Shenassa, E. D. (2006). The environmental "Riskscape" and social inequality: Implications for explaining maternal and child health disparities. Environmental Health Perspectives, 114(8), 1150–1153. https://doi.org/10.1289/ehp.8930

Moseley, W. G., Perramond, E., Hapke, H. M., Laris, P. (2013). An Introduction to Human-Environment Geography: Local Dynamics and Global Processes. Germany: Wiley.

National Research Council. (2001). America Becoming. In America Becoming (Volume I). National Academies Press. https://doi.org/10.17226/9599

Ng, E., Chen, L., Wang, Y., & Yuan, C. (2012). A study on the cooling effects of greening in a high-density city: An experience from Hong Kong. Building and Environment, 47(1), 256–271. https://doi.org/10.1016/j.buildenv.2011.07.014

Ng, S. C., Low, K. S., & Tioh, N. H. (2011). Newspaper sandwiched aerated lightweight concrete wall panels - Thermal inertia, transient thermal behavior and surface temperature prediction. Energy and Buildings, 43(7), 1636–1645. https://doi.org/10.1016/j.enbuild.2011.03.007

Nicolay, M., Brown, L. M., Johns, R., & Ialynytchev, A. (2016). A study of heat related illness preparedness in homeless veterans. International Journal of Disaster Risk Reduction, 18, 72–74. https://doi.org/10.1016/j.ijdrr.2016.05.009

New York City (2023). NYC CoolRoofs: Helping the Environment and Saving Energy. New York City Business. https://nyc-business.nyc.gov/nycbusiness/article/nyc-coolroofs

O'Neill, M. S. (2005). Disparities by Race in Heat-Related Mortality in Four US Cities: The Role of Air Conditioning Prevalence. Journal of Urban Health: Bulletin of the New York Academy of Medicine, 82(2), 191–197. https://doi.org/10.1093/jurban/jti043

Oke, T., Mills, G., Christen, A., & Voogt, J. (2017). Urban Climates. In Urban Climates. Cambridge University Press. https://doi.org/10.1017/9781139016476

Oke, T. R. (1982). The energetic basis of the urban heat island. Quarterly Journal of the Royal Meteorological Society, 108(455), 1–24. https://doi.org/10.1002/qj.49710845502

Oke, T. R. (1987). Boundary Layer Climates. Routledge. https://doi.org/10.4324/9780203407219

Oke, T. R., Crowther, J. M., McNaughton, K. G., Monteith, J. L., & Gardiner, B. (1989). The Micrometeorology of the Urban Forest [and Discussion]. Philosophical Transactions - Royal Society of London, 324(1223), 335–349. https://www.jstor.org/stable/2990186

Park, J., Kim, J. H., Lee, D. K., Park, C. Y., & Jeong, S. G. (2017). The influence of small green space type and structure at the street level on urban heat island mitigation. Urban Forestry and Urban Greening, 21, 203–212. https://doi.org/10.1016/j.ufug.2016.12.005

Pearl, J. (2022). Comment: understanding Simpson's paradox. In Probabilistic and causal inference: The works of judea Pearl (pp. 399-412).

Pellow, D., & Park, L. (2002). The Silicon Valley of Dreams. New York, New York. https://doi.org/10.1017/CBO9781107415324.004

Peng, S., Piao, S., Ciais, P., Friedlingstein, P., Ottle, C., Bréon, F. M., Nan, H., Zhou, L., & Myneni, R. B. (2012). Surface urban heat island across 419 global big cities. Environmental Science and Technology, 46(2), 696–703. https://doi.org/10.1021/es2030438

Peterson, J. T. (1969). The climate of cities : a survey of recent literature. In National Air Pollution Control Administration publication (3rd ed., Issue no AP-59). Environmental Protection Agency: Office of Air Programs.

Pincetl, S., Gillespie, T., Pataki, D. E., Saatchi, S., & Saphores, J. D. (2013). Urban tree planting programs, function or fashion? Los Angeles and urban tree planting campaigns. GeoJournal, 78(3), 475–493. https://doi.org/10.1007/s10708-012-9446-x

Pitti, S. J. (2004). The Devil in Silicon Valley: Norhtern California, Race, and Mexican Americans. Princeton University Press.

Plumer, B., & Popovich, N. (2020, August 24). How Decades of Racist Housing Policy Left Neighborhoods Sweltering. The New York Times. https://www.nytimes.com/interactive/2020/08/24/climate/racism-redlining-cities-global-warming.html

Priyadarsini, R., Hien, W. N., & Wai David, C. K. (2008). Microclimatic modeling of the urban thermal environment of Singapore to mitigate urban heat island. Solar Energy, 82(8), 727–745. https://doi.org/10.1016/j.solener.2008.02.008

Pulido, L. (2000). Rethinking Environmental Racism: White Privilege and Urban Development in Southern California. Annals of the Association of American Geographers, 90(1), 12–40. https://doi.org/10.1111/0004-5608.00182

Putnam, H., Hondula, D. M., Urban, A., Berisha, V., Iniguez, P., & Roach, M. (2018). It's not the heat, it's the vulnerability: Attribution of the 2016 spike in heat-associated deaths in Maricopa County, Arizona. Environmental Research Letters, 13(9). https://doi.org/10.1088/1748-9326/aadb44

Raj, S., Paul, S. K., Chakraborty, A., & Kuttippurath, J. (2020). Anthropogenic forcing exacerbating the urban heat islands in India. Journal of Environmental Management, 257(August 2019), 110006. https://doi.org/10.1016/j.jenvman.2019.110006

Ramin, B., & Svoboda, T. (2009). Health of the homeless and climate change. Journal of Urban Health, 86(4), 654–664. https://doi.org/10.1007/s11524-009-9354-7

Ren, C., Cai, M., Li, X., Zhang, L., Wang, R., Xu, Y., & Ng, E. (2019). Assessment of Local Climate Zone Classification Maps of Cities in China and Feasible Refinements. Scientific Reports, 9(1), 1–11. https://doi.org/10.1038/s41598-019-55444-9

Rivera, A., Darden, J. T., Dear, N., & Grady, S. C. (2022). Environmental injustice among Hispanics in Santa Clara, California: a human–environment heat vulnerability assessment. GeoJournal. https://doi.org/10.1007/s10708-022-10768-4

Rivera, E., Antonio-Némiga, X., Origel-Gutiérrez, G., Sarricolea, P., & Adame-Martínez, S. (2017). Spatiotemporal analysis of the atmospheric and surface urban heat islands of the Metropolitan Area of Toluca, Mexico. Environmental Earth Sciences, 76(5), 225. https://doi.org/10.1007/s12665-017-6538-4

Robine, J. M., Cheung, S. L. K., Le Roy, S., Van Oyen, H., Griffiths, C., Michel, J. P., & Herrmann, F. R. (2008). Death toll exceeded 70,000 in Europe during the summer of 2003. Comptes Rendus - Biologies, 331(2), 171–178. https://doi.org/10.1016/j.crvi.2007.12.001

Rodriquez, M., & Chapman, R. (2013). Preparing California for Extreme Heat : Guidance and Recommendations (Issue October).

Rosenberg, M. (2017). Health geography III: Old ideas, new ideas or new determinisms? Progress in Human Geography, 41(6), 832–842. https://doi.org/10.1177/0309132516670054

Rosenfeld, A. H., Akbari, H., Bretz, S., Fishman, B. L., Kurn, D. M., Sailor, D., & Taha, H. (1995). Mitigation of urban heat islands: materials, utility programs, updates. Energy and Buildings, 22(3), 255–265. https://doi.org/10.1016/0378-7788(95)00927-P

Rosenthal, J. K., Kinney, P. L., & Metzger, K. B. (2014). Intra-urban vulnerability to heat-related mortality in New York City, 1997-2006. Health and Place, 30, 45–60. https://doi.org/10.1016/j.healthplace.2014.07.014

Rosenzweig, C., Solecki, W., & Slosberg, R. (2006). Mitigating New York City's heat island with urban forestry, living roofs, and light surfaces. 86th AMS Annual Meeting. In A report to the New York State Energy Research and Development Authority. Retrieved from

https://www.coolrooftoolkit.org/wp-content/uploads/2012/04/Mitigating-New-York-Citys-Heat-Island-with-Urban-Forestry-Living-Roofs-and-Light-Surfaces.pdf

Santos Nouri, A., & Costa, J. P. (2017). Placemaking and climate change adaptation: new qualitative and quantitative considerations for the "Place Diagram." Journal of Urbanism, 10(3), 356–382. https://doi.org/10.1080/17549175.2017.1295096

Santos Nouri, Andre, Costa, J., Santamouris, M., & Matzarakis, A. (2018). Approaches to Outdoor Thermal Comfort Thresholds through Public Space Design: A Review. Atmosphere, 9(3), 108. https://doi.org/10.3390/atmos9030108

Semenza, J. C., Rubin, C. H., Falter, K. H., Selanikio, J. D., Flanders, W. D., Howe, H. L., & Wilhelm, J. L. (1996). Heat-Related Deaths during the July 1995 Heat Wave in Chicago. New England Journal of Medicine, 335(2), 84–90. https://doi.org/10.1056/NEJM199607113350203

Shapiro, S. S., & Wilk, M. B. (1965). An analysis of variance test for normality (complete samples). Biometrika, 52(3–4), 591–611. https://doi.org/10.1093/biomet/52.3-4.591

Sharmin, M., Tjoelker, M. G., Pfautsch, S., Esperon-Rodriguez, M., Rymer, P. D., & Power, S. A. (2023). Tree crown traits and planting context contribute to reducing urban heat. Urban Forestry and Urban Greening, 83(March), 127913. https://doi.org/10.1016/j.ufug.2023.127913

Shonkoff, S. B., Morello-Frosch, R., Pastor, M., & Sadd, J. (2011). The climate gap: environmental health and equity implications of climate change and mitigation policies in California—a review of the literature. Climatic Change, 109(S1), 485–503. https://doi.org/10.1007/s10584-011-0310-7

Shrider, E. A., Kollar, M., Chen, F., & Semega, J. (2021). Income and Poverty in the United States : 2020. In Current Population Reports. https://www.census.gov/content/dam/Census/library/publications/2021/demo/p60-273.pdf

Siddiqui, A., Kushwaha, G., Nikam, B., Srivastav, S. K., Shelar, A., & Kumar, P. (2021). Analysing the day/night seasonal and annual changes and trends in land surface temperature and surface urban heat island intensity (SUHII) for Indian cities. Sustainable Cities and Society, 75(August), 103374. https://doi.org/10.1016/j.scs.2021.103374

Siegel, L. (1995). Case Study: Comparing Apples and Supercomputers: Evaluating Environmental Risk in Silicon Valley. In W. Ik (Ed.), Community risk profiles: A tool to improve environment community health. The Rockefeller University. http://phe.rockefeller.edu/comm_risk/

Sismanidis, P., Bechtel, B., Perry, M., & Ghent, D. (2022). The Seasonality of Surface Urban Heat Islands across Climates. Remote Sensing, 14(10), 1–21. https://doi.org/10.3390/rs14102318

Sister, C., Wolch, J., & Wilson, J. (2010). Got green? addressing environmental justice in park provision. GeoJournal, 75(3), 229–248. https://doi.org/10.1007/s10708-009-9303-8

Smith, I. A., Fabian, M. P., & Hutyra, L. R. (2023). Urban green space and albedo impacts on surface temperature across seven United States cities. Science of the Total Environment, 857(July 2022), 159663. https://doi.org/10.1016/j.scitotenv.2022.159663

Smoyer, K. E. (1998). Putting risk in its place: Methodological considerations for investigating extreme event health risk. Social Science and Medicine, 47(11), 1809–1824. https://doi.org/10.1016/S0277-9536(98)00237-8

Sousa-Silva, R., Duflos, M., Ordóñez Barona, C., & Paquette, A. (2023). Keys to better planning and integrating urban tree planting initiatives. Landscape and Urban Planning, 231(March 2022). https://doi.org/10.1016/j.landurbplan.2022.104649

Stewart, I. D., & Oke, T. R. (2012). Local Climate Zones for Urban Temperature Studies. Bulletin of the American Meteorological Society, 93(12), 1879–1900. https://doi.org/10.1175/BAMS-D-11-00019.1

Su, J. G., Jerrett, M., de Nazelle, A., & Wolch, J. (2011). Does exposure to air pollution in urban parks have socioeconomic, racial or ethnic gradients? Environmental Research, 111(3), 319–328. https://doi.org/10.1016/j.envres.2011.01.002

Sundborg, Ã. (1950). Local Climatological Studies of the Temperature Conditions in an Urban Area. Tellus A, 2(3). https://doi.org/10.3402/tellusa.v2i3.8544

Swaid, H. (1991). Nocturnal variation of air-surface temperature gradients for typical urban and rural surfaces. Atmospheric Environment. Part B, Urban Atmosphere, 25(3), 333–341. https://doi.org/10.1016/0957-1272(91)90005-Y

Taha, H. (2004). Heat Islands and Energy. In Encyclopedia of Energy (pp. 133–143). Elsevier. https://doi.org/10.1016/B0-12-176480-X/00394-6

Taha, H. (2017). Characterization of Urban Heat and Exacerbation: Development of a Heat Island Index for California. Climate, 5(3), 59. https://doi.org/10.3390/cli5030059

Taleghani, M. (2018). The impact of increasing urban surface albedo on outdoor summer thermal comfort within a university campus. Urban Climate, 24(October 2017), 175–184. https://doi.org/10.1016/j.uclim.2018.03.001

Taleghani, M., Sailor, D., & Ban-Weiss, G. A. (2016). Micrometeorological simulations to predict the impacts of heat mitigation strategies on pedestrian thermal comfort in a Los Angeles neighborhood. Environmental Research Letters, 11(2), 024003. https://doi.org/10.1088/1748-9326/11/2/024003

Tan, Z., Lau, K. K. L., & Ng, E. (2016). Urban tree design approaches for mitigating daytime urban heat island effects in a high-density urban environment. Energy and Buildings, 114, 265–274. https://doi.org/10.1016/j.enbuild.2015.06.031

Tate, E. (2012). Social vulnerability indices: A comparative assessment using uncertainty and sensitivity analysis. Natural Hazards, 63(2), 325–347. https://doi.org/10.1007/s11069-012-0152-2

Tayyebi, A., & Darrel Jenerette, G. (2016). Increases in the climate change adaption effectiveness and availability of vegetation across a coastal to desert climate gradient in metropolitan Los Angeles, CA, USA. Science of the Total Environment, 548–549, 60–71. https://doi.org/10.1016/j.scitotenv.2016.01.049

Thanabalan, P., Vidhya, R., Kankara, R. S., & Manonmani, R. (2023). Time-series analysis of MODIS (LST and NDVI) and TRMM rainfall for drought assessment over India. Applied Geomatics, 383–405. https://doi.org/10.1007/s12518-023-00505-y

Tomlinson, C. J., Chapman, L., Thornes, J. E., & Baker, C. J. (2011). Including the urban heat island in spatial heat health risk assessment strategies: a case study for Birmingham, UK. International Journal of Health Geographics, 10(1), 42. https://doi.org/10.1186/1476-072X-10-42

Tran, H., Uchihama, D., Ochi, S., & Yasuoka, Y. (2006). Assessment with satellite data of the urban heat island effects in Asian mega cities. International Journal of Applied Earth Observation and Geoinformation, 8(1), 34–48. https://doi.org/10.1016/j.jag.2005.05.003

Turner-Skoff, J. B., & Cavender, N. (2019). The benefits of trees for livable and sustainable communities. Plants People Planet, 1(4), 323–335. https://doi.org/10.1002/ppp3.39

Uejio, C. K., Wilhelmi, O. V., Golden, J. S., Mills, D. M., Gulino, S. P., & Samenow, J. P. (2011). Intra-urban societal vulnerability to extreme heat: The role of heat exposure and the built environment, socioeconomics, and neighborhood stability. Health and Place, 17(2), 498–507. https://doi.org/10.1016/j.healthplace.2010.12.005

UN-Habitat. (2020). The Value of Sustainable Urbanization. https://unhabitat.org/sites/default/files/2020/10/wcr_2020_report.pdf

USGS (2019). NLCD 2011 Land Cover. National Geospatial Data Asset (NGDA) Land Use Land Cover: U.S. Geological Survey. Retrieved from https://www.mrlc.gov/data

US Census Bureau. (2000). Appendix B. Measures of residential segregation. Racial and Ethnic Residential Segregation in the United States: 1980-2000, 1988, 119–123.

US Census Bureau (2018). 2013 – 2017 American Community Survey, 5-Year Estimates. Table DP02, DP03, DP04, DP05; generated by Ana Rivera; using American Fact Finder; http://factfinder2.census.gov; (February 26 2019).

US Census Bureau (2020). 2015 – 2019 American Community Survey, 5-Year Estimates. Table DP02, DP03, DP04, DP05; generated by Ana Rivera; using American FactFinder; http://factfinder2.census.gov; (February 26 2022).

Vaidyanathan, A., Malilay, J., Schramm, P., & Saha, S. (2020). MMWR - Heat-Related Deaths — United States, 2004–2018. 69(24), 730–734. https://www.cdc.gov/nchs/data/dvs/2e_volume1_2017.pdf.

Vandentorren, S., Bretin, P., Zeghnoun, A., Mandereau-Bruno, L., Croisier, A., Cochet, C., Ribéron, J., Siberan, I., Declercq, B., & Ledrans, M. (2006). August 2003 Heat Wave in France: Risk Factors for Death of Elderly People Living at Home. European Journal of Public Health, 16(6), 583–591. https://doi.org/10.1093/eurpub/ckl063

Verdonck, M. L., Demuzere, M., Hooyberghs, H., Beck, C., Cyrys, J., Schneider, A., Dewulf, R., & Van Coillie, F. (2018). The potential of local climate zones maps as a heat stress assessment tool, supported by simulated air temperature data. Landscape and Urban Planning, 178(July 2017), 183–197. https://doi.org/10.1016/j.landurbplan.2018.06.004

Vespa, J., Medina, L., & Armstrong, D. (2020). Demographic turning points for the United States: Population projections for 2020 to 2060. In Population Estimates and Projections. https://www.census.gov/content/dam/Census/library/publications/2020/demo/p25-1144.pdf

Voelkel, J., Hellman, D., Sakuma, R., & Shandas, V. (2018). Assessing vulnerability to urban heat: A study of disproportionate heat exposure and access to refuge by socio-demographic status in Portland, Oregon. International Journal of Environmental Research and Public Health, 15(4). https://doi.org/10.3390/ijerph15040640

Voogt, J. (2007). How researchers measure urban heat islands. United States Environmental Protection Agency (EPA), State and Local Climate and Energy Program, Heat Island Effect, Urban Heat Island Webcasts and Conference Calls, 34. http://epa.gov/heatisland/resources/pdf/EPA_How_to_measure_a_UHI.pdf

Wang, C., Ren, Z., Chang, X., Wang, G., Hong, X., Dong, Y., Guo, Y., Zhang, P., Ma, Z., & Wang, W. (2023). Understanding the cooling capacity and its potential drivers in urban forests at the single tree and cluster scales. Sustainable Cities and Society, 93(March), 104531. https://doi.org/10.1016/j.scs.2023.104531

Wang, M., Zhang, Z., Hu, T., Wang, G., He, G., Zhang, Z., Li, H., Wu, Z., & Liu, X. (2020). An Efficient Framework for Producing Landsat-Based Land Surface Temperature Data Using Google Earth Engine. IEEE Journal of Selected Topics in Applied Earth Observations and Remote Sensing, 13, 4689–4701. https://doi.org/10.1109/JSTARS.2020.3014586

Webb, B. (2017). The use of urban climatology in local climate change strategies: a comparative perspective. International Planning Studies, 22(2), 68–84. https://doi.org/10.1080/13563475.2016.1169916

Weber, S., Sadoff, N., Zell, E., & de Sherbinin, A. (2015). Policy-relevant indicators for mapping the vulnerability of urban populations to extreme heat events: A case study of Philadelphia. Applied Geography, 63, 231–243. https://doi.org/10.1016/j.apgeog.2015.07.006

Weinick, R. M., Jacobs, E. A., Stone, L. C., Ortega, A. N., & Burstin, H. (2004). Hispanic healthcare disparities: challenging the myth of a monolithic Hispanic population. Medical Care, 42(4), 313–320. https://doi.org/10.1097/01.mlr.0000118705.27241.7c

Weng, Q., Lu, D., & Schubring, J. (2004). Estimation of land surface temperature-vegetation abundance relationship for urban heat island studies. Remote Sensing of Environment, 89(4), 467–483. https://doi.org/10.1016/j.rse.2003.11.005

Werbin, Z. R., Heidari, L., Buckley, S., Brochu, P., Butler, L. J., Connolly, C., Bloemendaal, L. H., McCabe, T. D., Miller, T. K., & Hutyra, L. R. (2020). A tree-planting decision support tool for urban heat mitigation. PLoS ONE, 15(10 October), 1–13. https://doi.org/10.1371/journal.pone.0224959

Widerynski, S., Schramm, P. J., Conlon, K. C., Noe, R. S., Grossman, E., Hawkins, M., Nayak, S. U., Roach, M., & Hilts, A. S. (2017). Use of cooling centers to prevent heat-related illness : summary of evidence and strategies for implementation. https://stacks.cdc.gov/view/cdc/47657

Wilhelmi, O. V. & Hayden, M. H. (2010). Connecting people and place: a new framework for reducing urban vulnerability to extreme heat. Environmental Research Letters, 5(1), 1–7. https://doi.org/10.1088/1748-9326/5/1/014021

Williams, D. R., Mohammed, S. A., Leavell, J., & Collins, C. (2010). Race, socioeconomic status, and health: Complexities, ongoing challenges, and research opportunities. Annals of the New York Academy of Sciences, 1186(1), 69–101. https://doi.org/10.1111/j.1749-6632.2009.05339.x

Wilson, J. P., & Belonis, A. (2016). The Distribution of Nature's Services : Geographic Patterns of Green Cover in Los Angeles County MAPPING THE DISTRIBUTION AND DENSITY OF GREEN COVER IN LOS ANGELES COUNTY. September.

Wolch, J. R., Byrne, J., & Newell, J. P. (2014). Urban green space, public health, and environmental justice: The challenge of making cities "just green enough." Landscape and Urban Planning, 125, 234–244. https://doi.org/10.1016/j.landurbplan.2014.01.017

Wolch, J., Wilson, J. P., & Fehrenbach, J. (2005). Parks and Park Funding in Los Angeles: An Equity-Mapping Analysis. Urban Geography, 26(1), 4–35. https://doi.org/10.2747/0272-3638.26.1.4

Wolf, T., & McGregor, G. (2013). The development of a heat wave vulnerability index for London, United Kingdom. Weather and Climate Extremes, 1(August 2003), 59–68. https://doi.org/10.1016/j.wace.2013.07.004

Wu, X., Wang, G., Yao, R., Wang, L., Yu, D., & Gui, X. (2019). Investigating surface urban heat islands in South America based on MODIS data from 2003-2016. In Remote Sensing (Vol. 11, Issue 10). https://doi.org/10.3390/rs11101212

Xu, Y., Dadvand, P., Barrera-Gómez, J., Sartini, C., Marí-Dell'Olmo, M., Borrell, C., Medina-Ramón, M., Sunyer, J., & Basagaña, X. (2013). Differences on the effect of heat waves on mortality by sociodemographic and urban landscape characteristics. Journal of Epidemiology and Community Health, 67(6), 519–525. https://doi.org/10.1136/jech-2012-201899

Yu, Q., Acheampong, M., Pu, R., Landry, S. M., Ji, W., & Dahigamuwa, T. (2018). Assessing effects of urban vegetation height on land surface temperature in the City of Tampa, Florida, USA. International Journal of Applied Earth Observation and Geoinformation, 73(April), 712–720. https://doi.org/10.1016/j.jag.2018.08.016

Yuan, C., Norford, L., & Ng, E. (2017). A semi-empirical model for the effect of trees on the urban wind environment. Landscape and Urban Planning, 168(September), 84–93. https://doi.org/10.1016/j.landurbplan.2017.09.029

Zhao, L., Oppenheimer, M., Zhu, Q., Baldwin, J. W., Ebi, K. L., Bou-Zeid, E., Guan, K., & Liu, X. (2018). Interactions between urban heat islands and heat waves. Environmental Research Letters, 13(3), 034003. https://doi.org/10.1088/1748-9326/aa9f73